

Diss. ETH No. 12878

Coupled Flow and SST Patterns of the North Atlantic: A Statistical and Dynamical Study

A dissertation submitted to the
SWISS FEDERAL INSTITUTE OF TECHNOLOGY (ETH)
ZÜRICH

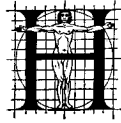
for the degree of
DOCTOR OF NATURAL SCIENCE

presented by
DAVID N. BRESCH
Dipl. Phys. ETH
born 9 April 1970
citizen of Zürich (ZH)

accepted on the recommendation of
Prof. Dr. H. C. Davies, examiner
Prof. Dr. K. Fraedrich, co-examiner
Prof. Dr. C. Schär, co-examiner

1998

Leer - Vide - Empty



oc opus tractat de coniuncta et disiuncta
variabilitatibus oceani aerisque in regionibus
maris externi spatiis temporis ab nonnullis
diebus usque ad tres menses. Systema con-
iunctum enim multum interest et tempori climaticae
regionum septentrionalium et praevidendo tempus ad
longum spatium. Intuitus revelat qualitates temperiei
aequoris pressusque aeris cursusque tempestatis tem-
pore hibernali coniunctas esse. Insuper demonstratur
aerem oceanum lineariter variare nec excludendos esse
effectus oceani. Experimento simplicitate investigan-
tur effectus potentiales conditionum electarum temperiei
aequoris. Item posteriores investigationes experimento
vero amplificationem cursus tempestatis depressionisque
revelant. Dicti intuitus experimentaque sequentem hy-
pothesim suggerunt: Structura systematis coniuncti
oceani et aeris in regionibus maris externi spatiis tem-
poris ab nonnullis diebus usque ad tres menses regi-
tur circulatione aeris. Ipsa conditio temperiei aequoris
regit tempestates singulares latentibus sensibilibusque
fluxibus caloris. Haec videri possunt in structura am-
plitudineque cursus tempestatis, qui sponte sua regit
fluxus aeris. Tractatus ipse demonstrat coniunctio-
nem methodi intuitus experimentorumque contribuere
ad comprehensionem problematis coniunctae variabili-
tatis oceani aerisque in regionibus septentrionalibus.

Leer - Vide - Empty

Contents

Abstract	vii
Zusammenfassung	ix
1 Introduction	1
2 Basic Notions and Tools	13
2.1 Theory of Singular Value Decomposition	13
2.1.1 The Matrix Decomposition	14
2.1.2 SVD of a Cross-Covariance Matrix	14
2.1.3 The Linkage between PCA and SVD	15
2.1.4 Reconstruction	17
2.1.5 Explained (Cross-) Covariance and Selection Rules	18
2.1.6 Comparison to Canonical Correlation Analysis and Caveats	19
2.2 Storm Track Identification	20
2.2.1 Variance Filtering	20
2.2.2 Objective Identification of Cyclones	21
2.3 The Models	21
2.3.1 The Limited Area NWP Model	21
2.3.2 The Idealised Model	22
2.3.3 Model Comparison in Terms of EOFs	25
3 Statistical Analysis	27
3.1 Data	27
3.2 Coupled Patterns	28
3.2.1 SST – Geopotential Height	29
3.2.2 SST – Storm Track	31
3.2.3 Geopotential Height – Storm Track	33
3.3 Temporal Interaction	35
3.4 Trends	39
3.4.1 Observed Decadal Trends	40
3.4.2 (Re-) construction of the Trend Patterns	42
3.5 Discussion	44

4	Idealised Study	47
4.1	Control Simulation	48
4.2	Experiments	50
4.2.1	SST Dipole Anomaly	51
4.2.2	Decomposition, Shift and Reversal of Anomaly Pattern	54
4.3	Comparison of Surface Fluxes	59
4.4	Summary and Discussion	61
5	Case Studies	63
5.0.1	Case Selection	64
5.1	Filtered-out SST	65
5.1.1	December 1981	65
5.1.2	December 1986	68
5.2	Imposition of SST Anomalies	70
5.2.1	Control Simulation	71
5.2.2	Experiments	71
5.2.3	Comparison of Surface Fluxes	79
5.2.4	Growth and Decay Rates of Synoptic Systems	82
5.2.5	Moisture Distribution	82
5.2.6	Vertical Structure	83
5.2.7	Phase Space: Coupled Patterns	85
5.3	Summary and Discussion	89
6	Further Remarks	93
A	Another Application of PCA	97
B	Overview of Model Experiments	99
	References	101
	Acknowledgments	117
	Curriculum Vitae	119

Abstract

Coupled and uncoupled variability of ocean and atmosphere in the North Atlantic region on time scales ranging from several days to months forms the centerpiece of this thesis. The contrasting properties of ocean and atmosphere render the coupled system of significant importance for the understanding of midlatitude climate variability. Indeed the linkage between oceanic and atmospheric fluctuations is an important component of the climate system, and has far-reaching practical implications, particularly in the realm of extended-range prediction of weather and climate. To assess these issues, a twofold approach has been followed and it involves both statistical and modelling tools.

The leading coupled modes of SST, geopotential height and storm track at 500 hPa of the wintertime circulation over the North Atlantic sector are identified by multivariate statistical (SVD) analysis of the monthly mean fields. The dipole signature of the first geopotential height pattern and the concomitant structure of the North Atlantic storm track is observed to be coupled to a dipole pattern in the SST field. This mode explains over 30% of the intraseasonal variability of the observed fields and is a reflection of its two extremes of strong and weak zonal flow regimes. Investigation of the last 30 years' trends in the aforementioned fields suggests that the dominant coupled modes do represent a significant part of both the intraseasonal variability and the decadal trends. The concomitant inference is that the latest strengthening phase of the North Atlantic Oscillation (NAO) was characterised by changes in amplitude (and/or frequency) of recurrent weather modes rather than involving a transition towards a new regime. It is shown that the atmosphere dominates the linear coupling between ocean and atmosphere on monthly time scales, but a feedback of the ocean to the atmosphere can not be ruled out.

An examination of the possible effect of the distinctive SST patterns (identified using the statistical analysis) formed the basis for a sequence of simulations with an idealised primitive equation model. The imposition of the SST dipole does not yield atmospheric anomalies that project on the corresponding statistically derived coupled patterns, but particular features of the idealised model results do relate to the overall structure of the first coupled mode. In effect the simulated intensification of the storm track and the concomitant strengthening of the trough in the geopotential height indicate that the SST dipole forces only limited features of the whole coupled atmospheric patterns. Furthermore, the modelled atmospheric response has been shown to be both nonlinear and highly sensitive to the precise location of the SST anomaly. An inference is that the atmosphere dominates the linear coupling and the ocean configuration feeds back onto the atmosphere in a way difficult to isolate in the framework of linear statistical analysis.

To address the effect of SST anomalies in a more realistic set up, sensitivity experiments are conducted for selected months and seasons with a limited area NWP model of the North Atlantic region. Two kinds of experiments are performed that differed in the way the SST fields are modified (either by suppressing or imposing the dominant statistically derived SST mode). Imposition of SST anomalies provided more reliable results than simulations with filtered SST patterns. The response to a dipole SST anomaly consisted of a strengthening of the trough in the geopotential height field over southern Greenland and a strengthening of the storm track. It was shown that the warm pole of the SST dipole is responsible for a major part of the response. The pattern of the geopotential height response projects significantly on the first *model* geopotential height EOF, and also on the statistically derived leading *climatological* geopotential height pattern. In addition, the storm track signal projects on the dominant climatological storm track pattern. The atmospheric response appears to be strongly dependent on the polarity, shape and precise location of the SST anomaly and on the large-scale time-mean atmospheric flow itself.

The results of both the statistical analysis and model simulations are in harmony with the following hypothesis: The large scale structure of the coupled system is set predominantly by the atmospheric circulation. To a measure the dipole-mode in geopotential height replicates the eigenmode of the North Atlantic sector, whereas the SST pattern is shaped by atmospheric influence to the observed dipole structure. In turn the anomalous SST configuration affects the life cycle of individual cyclones via the fluxes of latent and sensible heat. These recurrent effects on single cyclones in turn alter the storm track's position and intensity, and the latter effects feed back on the atmospheric mean flow.

Taken together, the twofold approach involving both statistical and modelling techniques proves to be helpful for gaining insight in the nature and dynamics of midlatitude variability of the ocean and atmosphere. The observational data analysis reveals the dominant coupled modes of variability and prompts the formulation of hypotheses of air-sea interaction and their preliminary testing. It also provides a basis for model validation and the choice of suitable simulations. The models themselves enable an investigation of the previously formulated hypotheses to be undertaken and provide further insight on the physical mechanisms.

Zusammenfassung

Die vorliegende Arbeit befasst sich mit der gekoppelten und ungekoppelten Variabilität von Ozean und Atmosphäre im Nordatlantik auf Zeitskalen von einigen Tagen bis Monaten. Aufgrund der unterschiedlichen Eigenschaften von Ozean und Atmosphäre ist das gekoppelte System ein wichtiger Faktor in Bezug auf Wetter und Klima der mittleren Breiten mit weitreichenden Konsequenzen für die längerfristige Vorhersage. Die dominanten Muster der (gekoppelten) Variabilität von Ozean und Atmosphäre werden in dieser Studie sowohl mit statistischen Analysemethoden als auch mit dynamischen Modellen untersucht.

Mit Hilfe multivariater statistischer Analysen werden die dominanten gekoppelten Moden von Meeresoberflächentemperatur (SST), Geopotential und Sturmbahn auf 500 hPa während der Wintersaison im Nordatlantik identifiziert. Die Dipolstruktur im ersten Muster von Geopotential und Sturmbahn findet sich auch im führenden Muster der Meeresoberflächentemperatur. Dieser Mode erklärt über 30% der intrasaisonalen Variabilität und stellt in seinen beiden Extremen stark und schwach zonale Strömungsregimes dar. Eine Untersuchung des linearen Trends der letzten 30 Jahre in den erwähnten Variablen weist darauf hin, dass die dominanten gekoppelten Muster zudem einen signifikanten Anteil der dekadischen Trends repräsentieren. Dies weist darauf hin, dass die letzte Verstärkungsphase der Nordatlantischen Oszillation durch eine Zunahme der Amplitude (und/oder Frequenz) von wiederkehrenden Strömungsregimes und nicht durch den Übergang zu einem neuen Regime charakterisiert wird. Es wird weiter gezeigt, dass die Atmosphäre die lineare Kopplung zwischen Ozean und Atmosphäre dominiert, was aber eine Rückkoppelung vom Ozean auf die Atmosphäre nicht ausschließt.

Unter Zuhilfenahme eines idealisierten Modells basierend auf den primitiven Gleichungen wird der mögliche Einfluss ausgewählter Muster der Meeresoberflächentemperatur auf die atmosphärische Strömung untersucht. Eine Simulation mit einer durch das – mit Hilfe statistischer Methoden eruierte – Dipolmuster veränderten Meeresoberflächentemperatur zeigt im Vergleich zur Simulation mit unveränderter Meeresoberflächentemperatur eine Verstärkung der Sturmbahn sowie des stationären Trogens im Geopotential, nicht aber die komplette, aufgrund der statistischen Resultate zu erwartende anomale Struktur der atmosphärischen Strömung. Die Simulationen weisen darauf hin, dass die durch die Dipol-Anomalie der Meeresoberflächentemperatur hervorgerufene Strömungsanomalie in nichtlinearer Weise von der exakten Position der Temperaturanomalie relativ zur atmosphärischen Strömung abhängig ist.

Weitere Untersuchungen werden mit einem Modell durchgeführt, das durch die initialisierten Re-Analysefelder des Europäischen Zentrums für mittelfristige Wettervorher-

sage (EZMW) angetrieben und auf einem begrenzten, den Nordatlantik einschliessenden Gebiet integriert wird. Diese Konfiguration erlaubt realitätsnahe Simulationen des Wettergeschehens über dem Nordatlantik. Zwei Sorten von Experimenten werden durchgeführt: Einerseits solche, in denen der dominante Mode der Meeresoberflächentemperatur unterdrückt und andererseits solche, in denen derselbe Mode verstärkt wird; wobei sich letztere als erfolgversprechender erwiesen. Ähnlich wie in den idealisierten Simulationen wird eine Verstärkung der Sturmbahn sowie des stationären Troges im Geopotential im Zusammenhang mit einer verstärkten Dipol-Anomalie der Meeresoberflächentemperatur beobachtet. Das anomale atmosphärische Strömungsmuster entspricht einer Verstärkung des dominanten Modell-EOFs und lässt sich direkt mit dem ersten statistisch gekoppelten Muster von Meeresoberflächentemperatur und Geopotential vergleichen. Die durch die Meeresoberflächentemperatur-Anomalie hervorgerufene Änderung in der Sturmbahn steht in analoger Weise direkt mit den statistischen Resultaten in Beziehung. Die Strömungsanomalien sind wiederum stark von Vorzeichen, Struktur und exakter Position der Meeresoberflächentemperatur-Anomalie sowie vom atmosphärischen Strömungshintergrund abhängig.

Die Resultate sowohl der statistischen wie der dynamischen Studien stützen die folgende Hypothese: Die grossräumige Struktur des gekoppelten Systems von Ozean und Atmosphäre über dem Nordatlantik wird auf Zeitskalen von Tagen bis Monaten primär durch die atmosphärische Zirkulation bestimmt. Der Dipol-Charakter des dominanten Mode des Geopotentials kann mit einem eigentlichen Eigenmode des Nordatlantiks in Verbindung gebracht werden, während die Dipol-Struktur der Meeresoberflächentemperatur primär durch die atmosphärische Strömung bedingt zu sein scheint. Die anomale Meeresoberflächentemperatur beeinflusst ihrerseits einzelne Zyklonen durch latente und sensible Wärmeflüsse. Solch wiederholte Einflüsse auf einzelne Zyklonen schlagen sich in Struktur und Amplitude des Sturmzugs nieder, welcher seinerseits auf die grossskaligen Strömungsmuster rückwirkt.

Die vorliegende Studie zeigt, dass die Verwendung von statistischen Analysemethoden in Verbindung mit dynamischen Modellen zum Verständnis der gekoppelten Variabilität von Ozean und Atmosphäre in mittleren Breiten beitragen kann. Die statistische Analyse von beobachteten Daten dient zur Bestimmung der dominanten Muster gekoppelter Variabilität und erlaubt die Formulierung von Hypothesen ihrer Interaktion. Weiter bildet sie die Basis zur Konzeption und Validierung von dynamischen Modellen. Die Modelle selber erlauben die Überprüfung der vorgängig formulierten Hypothesen und ermöglichen die Untersuchung beteiligter physikalischer Prozesse.

Chapter 1

Introduction

The North Atlantic sector experiences considerable climate variations. For example since the mid-1960's, there has been a steady increase in the frequency and intensity of wintertime storms (WASA Group 1998) and an upward trend in winter rainfall and winter temperature (Hurrell 1995a) over Europe. Also the atmospheric circulation exhibits substantial variability, reflected in weather patterns and circulation systems that occur on many time scales, lasting from a few days (synoptic scale) to a few weeks ('Grosswetterlage') to a few months (characteristics of particularly cold winters or hot summers) and up to several years or even centuries. It is important to understand the mechanisms responsible for these variations and considerable effort has been undertaken recently to address these questions (CLIVAR Science Plan 1995).

The conditions of the world's oceans typically fluctuate on time scales that are much longer than those of the atmosphere, and the specific heat content of water far outreaches that of air. Hence the contrasting properties of ocean and atmosphere render the coupled system of significant importance for the understanding of midlatitude climate variability. It is generally recognised that the linkage between oceanic and atmospheric fluctuations is an important component of the climate system, and has far-reaching practical implications, particularly in the realm of extended-range prediction of weather and climate (Palmer and Anderson 1994; Rowell 1998).

Coupled and uncoupled variability of ocean and atmosphere in the North Atlantic region on time scales ranging from several days to months will form the centerpiece of this thesis. As a preliminary to the research issues addressed in this study, selected aspects of the North Atlantic climate system are discussed in this Chapter (see Peixoto and Oort 1992 for a review of North Atlantic climate). An introduction to the concept of teleconnections is followed by a discussion of the principal mode of North Atlantic (climate) variability, the midlatitude storm track, the processes of midlatitude air-sea interaction and the role of ocean surface conditions for the atmospheric flow evolution. This Chapter is concluded by a presentation of the aims of the present study.

Teleconnections

The term 'teleconnection pattern' refers to a pattern of synchronous signals over geographically disparate regions, reflecting recurrent large-scale patterns of circulation anomalies in –

generally – surface pressure or geopotential height fields that span vast geographical areas. Although these patterns typically last for months, they can sometimes be prominent for several consecutive years, thus reflecting an important part of both the interannual and inter-decadal variability of the atmospheric circulation. Many of the teleconnection patterns are also planetary-scale in nature, and span entire ocean basins and continents. Teleconnection patterns reflect large-scale changes in the atmospheric wave and jet stream patterns, and influence temperature, rainfall, storm tracks and jet stream location and intensity over large distances.

The atmosphere is a nonlinear system with an infinite number of degrees of freedom (cf. Palmer 1993). Nonuniform boundary conditions – continents, orography – place constraints on the possible modes of atmospheric variability. Hence the existence of recurrent and persistent large-scale flow patterns is a remarkable property of the atmosphere which merits further investigation.

Recent studies of teleconnection patterns are based on multivariate statistical analysis methods (cf. Lanzante 1984; Barnston and Livezey 1987). These methods are superior to grid-point-based analyses, typically determined from one-point correlation maps, in that the teleconnection pattern is identified based on the entire flow field, and not just from – arbitrarily chosen – height anomalies at a few select locations. Nevertheless, most of the well known teleconnection patterns have first been identified by inspection of correlation maps (Walker and Bliss 1932; Wallace and Gutzler 1981). The structures have been reproduced and objectively (re-) defined by application of modern methods.

The North Atlantic Oscillation

The dominant teleconnection of the North Atlantic sector is the North Atlantic Oscillation (NAO). It links the pressure distribution between the Greenland-Iceland region and the central North Atlantic (Fig. 1.1). It has a seasonal cycle with a maximum in wintertime and its interannual and decadal variations comprise an irregular reversal of the polarity of the North-South aligned dipole anomaly between the two forementioned regions. The *positive* phase of the NAO is characterised by a strong Icelandic low and Azores high and hence a strong North-South pressure gradient, as illustrated in Fig. 1.1. The pressure gradient is weak during the *negative* phase of the NAO, which exhibits a sign reversal of the pressure anomaly with respect to the positive phase.

The NAO is one of the major teleconnection patterns of the Northern Hemisphere (Barnston and Livezey 1987), first observed in the 18th century¹ as reported by van Loon and Rogers (1978). In contrast to many other teleconnection patterns, it does not exhibit large variations in its climatological mean structure from month-to-month throughout the year (Glowienka-Hense 1990).

The phenomenon is often measured in terms of a single index parameter. The original index of Walker and Bliss (1932) involved surface pressure measurements at various locations

¹The missionary Hans Egede Saabye made the following observation in a diary which he kept in Greenland during the years 1770-78: "In Greenland, all winters are severe, yet they are not alike. The Danes have noticed that when the winter in Denmark was severe, as we perceive it, the winter in Greenland in its manner was mild, and conversely".

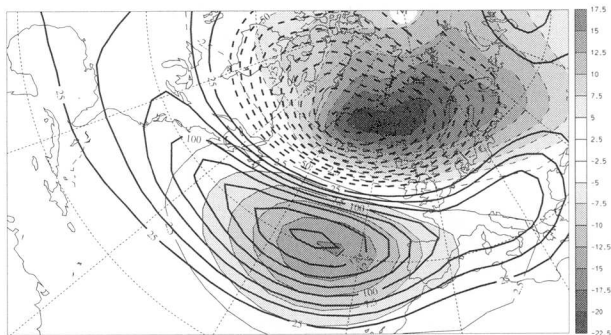


FIG. 1.1: Composite pattern of the North Atlantic Oscillation, based on NMC data 1962-1992 and Hurrell's index. Shown are the differences highest-lowest 10% of NAO index months for surface pressure (shaded, contour interval 2.5 mb, negative contours dashed and zero line omitted) and geopotential height at 500 mb (shaded, contour interval 25 mb, negative contours dashed and zero line omitted).

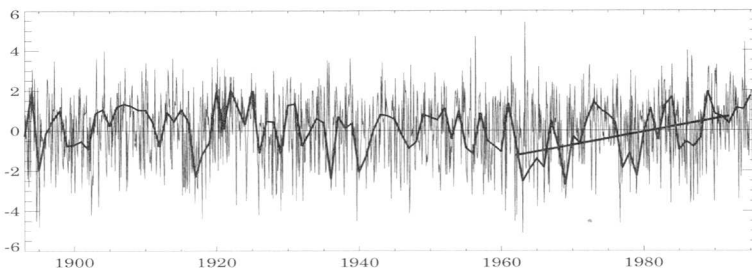


FIG. 1.2: NAO index 1895-1995 (Hurrell 1995a) and winter mean index (thick line) with the recent strengthening period 1962-92 (heavy thick line). See text about details.

with different weighting factors, whereas Rogers (1984) defined a NAO index based on sea level pressure anomalies from Ponta Delgada, Azores, and Akureyri, Iceland, and Hurrell (1995a) extended the index back in time to 1865 by using data from Lisbon, Portugal and Stykkisholmur, Iceland (Fig. 1.2). A proxy of the NAO index has recently been extended back to 1701 by tree-ring chronology (Cook et al. 1998) and back to 1645 by analysis of ice-core data (Appenzeller et al. 1998). Its (decadal) frequency spectrum is still controversial, but there is growing evidence of a cut-off for periods longer than about 15 years, except an amplifying 70-year oscillation after 1850 – or at least an increasing amplitude of the NAO's decadal component.

Both phases of the NAO are associated with basin-wide changes in the intensity and location of the North Atlantic jet stream and storm track (Lau 1988; Hurrell 1995b; Rogers 1997) and differences in mean mid-Atlantic wind speed (about 4 m s^{-1} , Bacon and Carter

1993). The NAO is reflected in large-scale modulations of the normal patterns of zonal and meridional heat and moisture transport (Hurrell 1995a), which in turn are linked to changes in temperature and precipitation patterns often extending from eastern North America to western and central Europe (Walker and Bliss 1932; Rogers and van Loon 1979; Rogers 1984; Wanner et al. 1997), even affecting North Africa (Lamb and Pepler 1987).

The North Atlantic ocean and its ecosystem is also affected by the NAO (Dickson et al. 1996), as reflected for example in changes in fish production and the abundance of zooplankton (Friedland et al. 1993; Fromentin and Planque 1996). Heat flux anomalies driven by the NAO account for between 10% and 40% of the variance in sea surface temperature anomaly-tendency over much of the North Atlantic during winter (Cayan 1992b). The NAO is also responsible for driving large-amplitude hydrographic changes to considerable depths in the ocean through its effect on deep ocean convection. As the Atlantic wind field evolves from the negative to the positive phase, observations give clear evidence of a progressive shutdown in the convective activity of the Greenland Sea and Sargasso, and of a steadily deepening exchange in the Labrador Sea (Dickson et al. 1996), also affecting the sea-ice distribution.

Recent statistical analyses of the strengthening of the NAO from 1962 to 1994 (heavy thick line in Fig. 1.2) indicate that it accounts for 31% of the hemispheric interannual variance (Hurrell 1996). On subtracting the amount of the land surface temperature trend associated with NAO, the residuum temperature does not reveal a linear trend, and this can be attributed to either the recent temperature trend being an internal climate variability or a global warming projected onto the NAO. GCM models provide ambiguous results in this context (cf. Liang et al. 1996, Houghton et al. 1996; Mitchell and Johns 1997).

From the early 1960's until the end 70's, the negative phase of the NAO was dominant but decreasing in strength (Fig. 1.2), when the so-called "great salinity anomaly" was decaying in the North Atlantic (Dickson et al. 1988). The transition towards the positive phase took place in winter 1979/80, with the atmosphere remaining predominantly in this mode through the 1994/95 winter season. During this 15-year interval, a substantial negative phase of the pattern appeared only twice (1984/85 and 1985/86). However, November 1995 - February 1996 was characterised by a return to the strong negative phase of the NAO (Halpert and Bell 1997) while the 1996/97 winter season has exhibited a more variable nature of the NAO, with negative phases occurring in December 1996 and January 1997, and positive phases occurring in February and March 1997. The latter was reflected in the more frequent and intensive storms observed during the second half of the FASTEX (Joly et al. 1997) field experiment (February 1997).

The NAO appears to play a role in seasonal forecast for the European - North Atlantic sector (Johansson et al. 1998) that is comparable to that of the ENSO phenomenon for tropical regions (e.g. Hastenrath 1991; Latif and Barnett 1994) and via the Pacific North American (PNA)-teleconnection (Wallace and Gutzler 1981) for North America. To understand and possibly predict the evolution of the NAO, two broad hypotheses for the observed variability provide a valuable framework: uncoupled and coupled modes of variability of ocean and atmosphere (cf. Palmer 1996 for a review).

NAO-like fluctuations observed in models with either an active ocean or forced with temporally non-varying ocean conditions (cf. Lau 1981; Delworth 1996; Saravanan and McWilliams 1998) and in atmosphere-only models (cf. Hendon and Hartmann 1985; James

and James 1989; Robinson 1991, Marshall and Molteni 1993) suggest that the NAO can be viewed as an internal atmospheric mode on monthly to seasonal time scales. Note in this context that the stochastic model results of Hasselmann (1976) suggest that the variability of the North Atlantic is merely the response of the ocean to chaotic, high-frequency forcing by the atmosphere. One possible player in internal atmospheric variability might be the stratospheric polar vortex, since a strong statistical connection between the former and the NAO has been observed (cf. Perlwitz and Graf 1995; Kodera and Koide 1997; Thompson and Wallace 1998). Uncoupled variability could also be viewed as passive response of the atmosphere to internally-generated oceanic variations. While being responsive to changes in the atmosphere, the oceans display an inherently long time scale due to their large heat capacity and inertia. Griffies and Bryan (1997) show for example that the most predictable variables (up to 20 years) in the ocean component of a coupled GCM were large scale averages of water mass properties in the upper thermocline.

In contrast, decadal variability over the North Atlantic sector might be related to the *coupled* ocean-atmosphere system, including processes which determine longer period fluctuations in the NAO: Low frequency responses of the ocean to atmospheric forcing could feed back on the atmosphere, resulting in oscillatory behaviour (Latif and Barnett 1996). Using a coupled model, Latif (1998) and Grötzner et al. (1998) identified a mode of coupled air-sea variability in which the memory of the system resides in the ocean, giving rise to oscillatory behaviour on decadal time scales of a NAO-like pattern.

The broad palette of possible forcing and feed back mechanisms related to the principal modes of atmospheric variability in both the North Pacific (PNA) and North Atlantic ocean (NAO) could also indicate that these oscillations might be interpreted in terms of basin-scale normal modes of the (coupled) climate system which can be excited by different (internal and external) factors². There is growing evidence for a complex interplay of different mechanism on different time scales being responsible for the excitation and maintenance of the dominant mode of the North Atlantic sector.

Storm Track

Besides the large-scale teleconnection patterns of the atmospheric variability as discussed in the previous Sections, the (statistics of) high-frequency transients are also an important aspect of midlatitude weather and climate.

The term “synoptic storm track” usually refers to the statistical distribution of the paths of cyclone centers as analysed from synoptic sea-level pressure charts, the first picture being published by Köppen (1881), reproduced in Fig.1.3, who notes that “the propagation of barometric minima not only follows certain directions, but certain regions, paths as well, which could be addressed as the tracks of the minima. The distribution of water and land as well as orography seem to determine these tracks, which follow to some extent the major coastlines”³. The importance of specific regions of the Northern Hemisphere that display a

²Webster (1982) notes that the regions of maximum interannual variability appear to be spatially coherent with the major teleconnection patterns, that is, the centers of action of both forced teleconnections and of “natural” variability appear to occupy the same geographical locations.

³“die Fortpflanzung der barometrischen Minima [geschieht] nicht nur überwiegend in gewissen Richtungen,

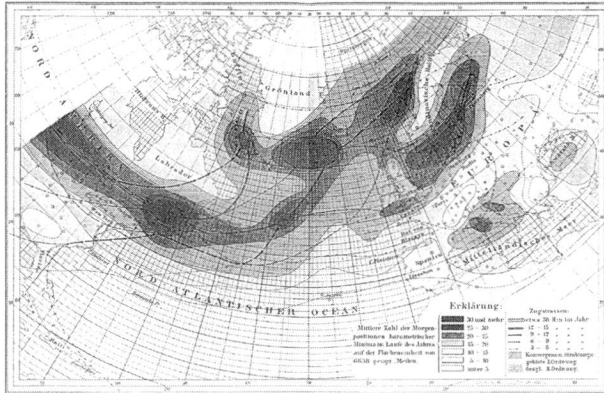


FIG. 1.3: Köppen's climatology (1881), based on synoptic charts of the years 1873-1879. Shading depicts the mean number of cyclones per year and area and the arrows indicate the tracks of depressions.

high rate of alternation between cyclones and anticyclones has been emphasised by Petterssen (1956). Cyclones and anticyclones have been observed to travel along separate paths, the former traveling northeastward and merging with the semipermanent subpolar lows and the latter traveling southeastward and merging with the subtropical anticyclones.

Diagnostic analysis by Blackmon (1976) demonstrated the existence of latitudinally confined regions of large 2-6 day geopotential height field variance in the Northern Hemisphere, extending from the east coast of North America and Asia across the Atlantic and Pacific oceans, respectively (see Fig. 1.4). These regions of large bandpass-filtered variance correspond quite closely to maxima in the variance of the 500 mb meridional wind component and in the poleward heat flux by the bandpass-filtered transient eddies at 850 mb (Blackmon et al. 1977). The high-frequency geopotential height fluctuations with periods shorter than 6 days assume the form of waves, elongated in the meridional direction, with a mean wavelength of 4000 km, a westward tilt with height, and a mean eastward phase propagation of 12-15 ms^{-1} . These characteristics support an interpretation in terms of finite-amplitude baroclinic waves whose structure and evolution varies with geographical location (Wallace et al. 1988). On the basis of these results, the elongated maxima in geopotential height variance, corresponding to regions of strongest baroclinic wave activity are referred to as the "dynamic storm tracks" (Fig. 1.4). Wallace et al. (1988) notes that the term "baroclinic waveguide" would have been more appropriate, because it accounts for the fact that both high and low pressure systems leave their imprint in the geopotential height variance. Nevertheless, the contribution of the cyclonic disturbances dominates due to their smaller scales

sondern es werden dabei auch mit Vorliebe gewisse Gegenden aufgesucht, gewisse Wege eingeschlagen, welche man wohl als die Zugstrassen der Minima bezeichnen kann; und zwar sind auch hier in erster Linie die Vertheilung von Wasser und Land, in zweiter die orographischen Verhältnisse die offenbar bestimmenden Faktoren und schmiegen sich ... diese Zugstrassen mehr oder weniger genau den wichtigsten Küstenlinien an.

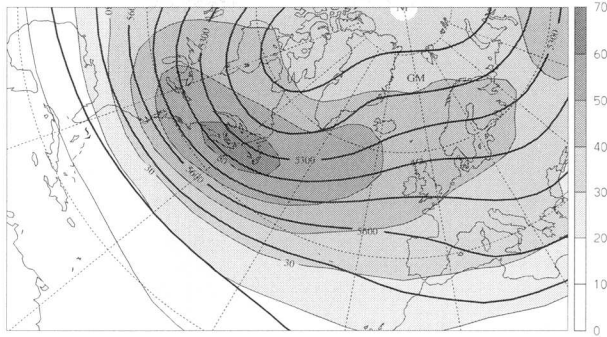


FIG. 1.4: Winter (DJF) mean 1962-1992 of geopotential height at 500 mb (thick lines, contour interval 100 gpm) and dynamic storm track (shaded, contour interval 10 gpm).

and higher travelling speed.

The relationship between the “synoptic” and “dynamic” storm track is not straightforward; and moreover the “synoptic” storm track is usually not represented as a mathematical field, so that quantitative investigation is difficult. The technical aspects and a comparison of the two approaches in determining the storm track will be further discussed in a separate Section below (Section 2.2). When not explicitly stated otherwise, the term storm track will refer to the dynamic storm track in this study.

The time mean storm tracks are linked to the climatological stationary waves. In the Northern Hemisphere the wintertime storm tracks are located in regions of intense baroclinicity (cf. Pierrehumbert 1984) downstream of the eastern Asian and North American climatological mean trough (Fig. 1.4, cf. Blackmon et al. 1977). The direct thermal effects of the single eddies act to weaken the baroclinic wave guide (Simmons and Hoskins 1979), the mean diabatic heating and the eddy vorticity fluxes are found to render the storm tracks “self-maintaining” (Hoskins and Valdes 1990, e.g. the GCM simulations of Stephenson and Held 1993).

In addition to the annual cycle in the extension, location and intensity of the storm tracks, they also undergo large variations on both interannual and intraseasonal time scales (cf. Nakamura 1992; Blender et al. 1997). The latter variations influence extratropical weather and climate, and hence a better understanding of processes governing such variations is basic to extended-range forecasts, and possibly extending the predictability limit beyond that attained by purely deterministic methods (Fraedrich et al. 1990). Although considerable observational evidence exists that storm track variations are systematically related to large-scale circulation anomalies (cf. Lau 1988; Nakamura and Wallace 1990; Rogers 1990; Rogers 1997), the mechanisms underlying these relations remain uncertain.

Several studies have been undertaken to examine mechanisms for producing, maintaining and modifying storm tracks in idealised models. Whitaker and Dole (1995) show that zonally localised regions of baroclinicity can lead to the localisation of transient eddy activity, although downstream radiation of energy through the ageostrophic geopotential fluxes can

also serve to maintain eddy activity over less baroclinic regions downstream (Chang and Orlanski 1993). The barotropic waveguide effects of the time-mean background flow can also be a factor influencing the storm track structure (Lee and Anderson 1996). Moreover low-frequency, large-scale circulation anomalies appear to organise the anomalous momentum fluxes attributable to bandpass eddies and hence affect the position of the storm track relative to the large-scale flow (Branstator 1995). Whitaker and Dole (1995) propose two competing processes for storm track organisation, one associated with a local maximum in surface baroclinicity and the other with a local minimum in horizontal deformation. In effect they argue that for a given surface baroclinicity distribution, the horizontal deformation defines the exact location of the storm track. However, the interaction between the large-scale flow and the eddies is not one way, since the eddy fluxes can also feed back strongly on the quasi-stationary waves. The results of the cited studies suggest that it is not a single mechanism, but rather the interplay of multiple factors that is responsible for the existence of the storm tracks.

There are still several problems regarding the correct representation of the intensity and location of the two major storm tracks in current GCMs⁴ (Robertson and Metz 1990; Boer et al. 1992; Stephenson and Held 1993; Hall et al. 1994; Kushnir and Held 1996; Latif 1998). The main reasons for this deficiency might be the relatively low resolution of the models and hence the inaccurate representation of individual synoptic scale systems and especially the eddy momentum fluxes (Held and Phillips 1993; Kushnir and Held 1996).

Aspects of midlatitude air-sea interaction

By virtue of their mechanical and thermal inertia, the oceans tend to integrate the atmospheric forcing over considerable time scales (Hasselmann 1976). Therefore, the role of the oceans in extratropical variability is a contentious issue, especially their possible impact on storm track position and amplitude and on large-scale atmospheric variability. A comprehensive review of the work in this field up to the early 1980's can be found in Frankignoul (1985). *The effects of extratropical SST anomalies on the atmospheric circulation are not well understood, in contrast to the tropics* (cf. Latif and Barnett 1994; Lau 1997).

Some considerations about ocean-atmosphere interaction on interannual to decadal time scales have already been given in relation to the NAO, but here the discussion concentrates on interaction on monthly to seasonal time scales in the North Atlantic sector.

An observational study by Ratcliffe and Murray (1970) provided evidence for a feed back relationship between Atlantic sea surface temperatures (SST) in the Newfoundland region and monthly atmospheric circulation anomalies over the North Atlantic and Europe. Blocking and generally unusual conditions over northern Europe have been found to be associated with abnormally cold water near the coast of Newfoundland (Namias 1964). However, many recent statistical studies of air-sea interaction on monthly time scales point to the dominance of the atmosphere in midlatitude coupling (cf. Wallace et al. 1990; Zorita et al. 1992; Deser and Timlin 1997). These findings are consistent with the notion of Bjerknes (1964), i.e. that

⁴Besides the time mean flow, the exact representation of transients is crucial for a reliable simulation of mid-latitude climate.

that a passive ocean paradigm is valid for intraseasonal to inter-annual time scales but that basin-wide coupled processes are necessary for longer interdecadal time scales.

The effects of extratropical SST anomalies on the atmospheric circulation have been assessed repeatedly with idealised (quasi-geostrophic) models (Hoskins and Karoly 1981; Webster 1981; Shutts 1987), in primitive equation studies (cf. Hendon and Hartmann 1982) and with GCM integrations (cf. Ting 1991, and reviews by Frankignoul 1985 and Lau 1997). *The results are less convincing than the analogous calculations with tropical SST anomalies.* The difficulties stem partly from the fact that the natural variability of the midlatitude atmosphere is very large, thus there is a small signal to noise ratio.

The inconsistency between observational and modelling studies warrants further investigation. A better understanding of the effect of midlatitude SST anomalies is also valuable since the potentially predictable part of the low-frequency variability of the atmosphere on time scales from weeks to months is possibly controlled by external (e.g. SST) forcing, while the atmospheric variability caused by internal processes generally becomes unpredictable within one or two weeks (Lorenz 1969). Furthermore, the slowly varying ocean surface conditions can influence the persistence and/or recurrence of large scale circulation anomalies lasting from a few days to weeks or months, which could allow an extension of predictability at least during certain weather regimes.

To present a hypothesis for midlatitude atmosphere-ocean interaction on monthly to seasonal time scales, it is convenient to select the key processes that have to be considered. In midlatitudes in winter the heat flux from ocean to atmosphere is a function of both air properties and wind speed. In the presence of a high amplitude of the latter, latent heat flux anomalies are largest for large sea-to-air humidity difference, while sensible heat flux anomalies are largest for large air-sea temperature difference (cf. Cayan 1992a). These temperature and humidity differences are mainly caused – on the short time scale – by the advection of air masses with different properties and not by local changes in water temperature (Kraus and Businger 1994), consistent with the persistence time of SST anomalies up to several months (Davis 1976). The sensible heating will occur predominantly in the flow of cold air off the continents over warm waters that occurs behind moving low pressure disturbances, and the latent heat release will be mostly in the warm moist air that is rising ahead of them. Hence the largest fluxes are to be observed over dynamically active regions, like the area of high baroclinicity off the North American east coast, owing much of its existence to the presence of the storm track (Sutcliffe 1951). This is illustrated by the mean fluxes of latent and sensible heat for the winter 1992 (Fig. 1.5), which closely resemble the climatological fields (cf. Esbensen and Kushnir 1981; Lambert and Boer 1989).

While the effect of the heat fluxes might not be large enough to trigger the initial growth of cyclones and hence to excite a (planetary) signal, single cyclones surpassing the anomalous SST might be considerably affected (Reed et al. 1993). The western North Atlantic off the North American seaboard has been identified by adjoint techniques (Bergot et al. 1996; Langland and Rohaly 1996) to be dynamically critical for prediction of cyclogenesis and hence the atmospheric flow evolution appears to be highly sensitive to even small changes of boundary conditions in this area.

Since specific features of the cyclones – like the position of the cold sector and the low-level jet ahead the cold front – appear to be relevant in determining the surface fluxes,

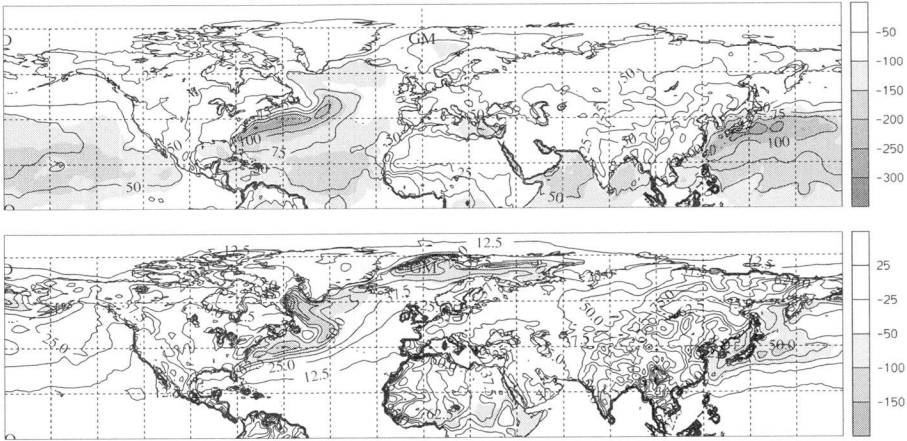


FIG. 1.5: ECMWF Reanalysis winter (DJF) mean 1992 of latent (upper panel, shaded, contour interval 50 W m^{-2}) and sensible (lower panel, shaded, contour interval 25 W m^{-2}) heat flux and respective standard deviation of 12 hourly data of the same period (thin lines, half contour intervals, zero line omitted).

sensitivity of the response to model resolution and complexity (cf. parametrisation schemes, Davis and Emanuel 1988) might be expected, which could explain to some extent the large differences between various model studies, as mentioned by many authors⁵ (Giorgi 1990; Boer et al. 1992; Kushnir and Held 1996). Assuming an average extent of a midlatitude cyclone of 4000 km but relevant frontal structures of the order of 300 km (cf. Davies 1997; Davies and Wernli 1997), *at least* a 3° resolution might be requested in midlatitudes (cf. Latif 1998) Namely simulations with low-resolution (lower than about T30 to T42) GCMs might not be capable to render the full palette of frontal structures (Davies et al. 1991) associated with midlatitude cyclones and the resulting structure and amplitude of surface fluxes (Lambert and Boer 1989) and might thus be inappropriate to investigate details of midlatitude SST forcing and storm track behaviour.

Besides the question about the significance of the effect of extratropical SST anomalies, the structure of the response is still controversially discussed. A higher resolution simulation (Palmer and Sun 1985; uniform spatial resolution of 330 km, 5 vertical levels) forced by a SST anomaly in the North Atlantic displays an equivalent barotropic response comprising a surface high to the east northeast of a surface warm anomaly, which resembles the observed atmospheric structure correlated with this SST pattern (cf. Peng and Fyfe 1996). These results have been reproduced by Ferranti et al. (1994) with a slightly different SST anomaly and they are in general agreement with the results of Peng et al. (1995). Note that a coarse resolution GCM (R15) appears not to be capable of producing an equivalent barotropic response (Kushnir and Held 1996), mainly due to deficient eddy (momentum) fluxes.

⁵Recall in this context the dependence of the storm track on model resolution noted in the previous Section.

Based on these results, two hypotheses for the processes determining the atmospheric response to extratropical SST anomalies emerge:

- The surface fluxes of latent and sensible heat (and momentum) of every single cyclone surpassing the anomalous SST are altered, leading to changes in the rate and location of growth and in the transport of moisture and momentum of single cyclones. Due to these modified single cyclones, changes in location and intensity of the storm track are to be expected. The upper-level vorticity fluxes associated with the changes of the storm track then contribute to an anomalous (equivalent barotropic) response in the mean flow, a process that has been observed to be important in studies of free atmospheric low-frequency variability (cf. Branstator 1992; Ting and Lau 1993) and in the study of the extratropical response to tropical SST anomalies by Held et al. (1989).
- The *statistics* of preexisting, nonlinear, equivalent barotropic variability are modified by the perturbed lower boundary condition, such that the anomalous SST affects the probability of select atmospheric flow regimes (cf. Palmer 1998). In this context, one should also consider the possibility that the anomalous SST configuration results from the dominance of a specific flow regime. It is crucial to determine whether this forced anomaly acts to stabilise or destabilise the atmospheric conditions which led to its existence (Palmer 1993).

In both cases, the geopotential height and storm track signals might be considered as inseparable parts of a “coherent structure”, which responds to the SST anomaly. Therefore, a distinction between the two processes remains a delicate issue. It should also be noted that various configurations of SST anomalies might lead to atmospheric responses different in structure and probably even in the mechanisms involved.

An identification of one of these mechanisms is further complicated by the fact that the atmospheric response to SST forcing might be highly sensitive to the state of the – midlatitude – atmosphere where the anomaly is introduced, as suggested by Webster (1981) (also Webster 1982) and illustrated by the results of Peng et al. (1995), who found a response qualitatively similar to Palmer and Sun (1985) only in their integrations with November initial conditions (T42, 21 sigma levels). January calculations result in just the opposite response, with a low downstream of a warm anomaly. Note that they found a marked nonlinearity, only the warm anomaly producing a significant response in November. The different early and midwinter response characteristics are found to be associated with the reduced Atlantic jet stream in November and enhanced jet in January, inducing anomalous storm track eddy vorticity fluxes, which in turn appear to maintain the different atmospheric responses under the early and middle winter conditions (Ting and Peng 1995). In addition, the response in the two main midlatitude ocean basins – the Atlantic and Pacific ocean – to a comparable SST anomaly appears to differ considerably due to the different configurations and mean flow structures (Kushnir and Held 1996).

The differing nature of the thermodynamic and dynamic balances in the atmosphere, the surface fluxes, and the roles of the transient motions in the two cases is evidently not fully understood. In addition, the response of the atmosphere to middle- and high-latitude SST anomalies is of high relevance for medium and long-range weather forecast as well as for a better understanding of the climate system and warrants further investigation.

Aims of this Study

In this thesis, a study is made of the structure and dynamics of the coupled modes of atmosphere and ocean in the North Atlantic sector on monthly to seasonal time scales. As noted earlier, the effect of the sea surface temperature on the atmospheric circulation is not yet fully understood. To assess this issue, a twofold approach has been followed (see Chapter 2) and it involves both statistical and modelling tools.

The statistically coupled large-scale patterns of air-sea interaction are objectively identified with multivariate analysis in Chapter 3. In particular the dominant coupled modes of sea surface temperature (SST), geopotential height at 500 mb and storm track are examined and lag correlation analysis is carried out. Also a brief account is given to the interrelations between the long-term trends in the aforementioned variables.

To learn more about the (nonlinear) interaction of ocean and atmosphere, as reflected in the statistically coupled patterns, consideration is given of the effect of the SST configuration on the atmospheric flow evolution in an idealised model setting (Chapter 4).

Finally the effect of SST anomalies is addressed in a realistic set up by undertaking sensitivity experiments for selected months and seasons with a limited area NWP model of the North Atlantic region (Chapter 5).

Chapter 2

Basic Notions and Tools

The objectives of this Chapter are to introduce the basic notion that will be needed, and the statistical tools and numerical models that will be used in the subsequent Chapters. After an introduction to the multivariate statistical analysis methods (Section 2.1), the objective identification of the storm track will be discussed (Section 2.2). A short description of the numerical models will conclude this Chapter (Section 2.3).

2.1 Theory of Singular Value Decomposition

While principal component analysis (PCA) provides an orthogonal basis for a given data set¹ that maximises the explained variance, singular value decomposition (SVD) analysis yields linearly coupled patterns which maximise the explained cross-covariance between two time-dependent data sets. The approach adopted here follows that of Bretherton et al. (1992) and Cherry (1997) (See also the review of PCA and SVD presented by Widmann 1996 and von Storch and Navarra 1995).

In climatological studies, SVD has been employed to investigate selected aspects of large scale flow on different time scales (e.g. Renwick and Wallace 1995; Hu 1997) and its regional impact (e.g. Widmann et al. 1995; Widmann and Schär 1997). The method has proved to be helpful in the investigation of air-sea interaction in the North Pacific (e.g. Wallace et al. 1992), North Atlantic (Peng and Fyfe 1996; Venegas et al. 1997) and South Atlantic (Venegas et al. 1997). Furthermore, both the variability of sea-ice (Fang and Wallace 1994) and surface heat fluxes (Iwasaka and Wallace 1995) have been related to large-scale flow anomalies by SVD analysis. In addition, the SST forced atmospheric variability in coupled and uncoupled GCM simulations has been assessed by application of SVD analysis (O'Brien and Chassignet 1995; Ward and Navarra 1997).

In the following Sections, we will consider the basic matrix decomposition and its application to the cross-covariance matrix of two time series of scalar fields, also elucidating the close relation to principal component analysis. Some derived quantities and a brief comparison to

¹Note that methods like cluster analysis (Mo and Ghil 1988), minimisation of average time derivatives (Marshall and Molteni 1993) and neuronal networks (Eckert et al. 1996) can also be used to identify recurrent large-scale patterns of variability, but these methods do not automatically provide mutually orthogonal patterns.

other methods will be presented at the end of this Chapter.

2.1.1 The Matrix Decomposition

Every real N_x by N_y matrix \mathbf{A} can be factorised by application of singular value decomposition:

$$\mathbf{A} = \mathbf{L}\hat{\mathbf{S}}\mathbf{R}^T \quad (2.1)$$

where $\mathbf{L} \in \mathbb{R}^{N_x \times N_x}$ and $\mathbf{R} \in \mathbb{R}^{N_y \times N_y}$ are orthogonal matrices. The matrix $\hat{\mathbf{S}} \in \mathbb{R}^{N_x \times N_y}$ is of the following format:

$$\hat{\mathbf{S}} = \begin{cases} \begin{pmatrix} \mathbf{S} \\ \mathbf{0} \end{pmatrix} & (N_x > N_y) \\ \mathbf{S} & (N_x = N_y) \\ \begin{pmatrix} \mathbf{S} & \mathbf{0} \end{pmatrix} & (N_x < N_y). \end{cases}$$

Where \mathbf{S} is a diagonal matrix $\in \mathbb{R}^{\min(N_x, N_y) \times \min(N_x, N_y)}$. The diagonal elements σ_i of \mathbf{S} are real nonnegative numbers, termed *singular values*. There are R nonzero singular values (R being the rank of \mathbf{A} , $R \leq \min(N_x, N_y)$), ordered by convention like:

$$\sigma_1 \geq \sigma_2 \geq \dots \geq \sigma_R \geq \sigma_{R+1} = \dots = \sigma_{\min(N_x, N_y)} = 0$$

The first R column vectors of the matrices \mathbf{L} and \mathbf{R} are unique, unless two singular values are identical, and are termed *left singular vectors* (\mathbf{l}_k) and *right singular vectors* (\mathbf{r}_k), respectively. Since \mathbf{L} and \mathbf{R} are orthogonal matrices, the \mathbf{l}_k and \mathbf{r}_k form two sets of orthonormal vectors with respect to the standard metrics in \mathbb{R}^{N_x} and \mathbb{R}^{N_y} , respectively.

2.1.2 SVD of a Cross-Covariance Matrix

Given two time series of scalar fields², so-called *left* $x(\mu_i, t_l)$ and *right* $y(\nu_j, t_l)$ fields at N_x (N_y) stations μ_i (ν_j) for T times t_l . Let \mathbf{X} and \mathbf{Y} be $T \times N_x$ and $T \times N_y$ matrices with $X_{li} = x(\mu_i, t_l)$ and $Y_{lj} = y(\nu_j, t_l)$. Assuming that the means of the columns (i.e the temporal means at each station) of \mathbf{X} and \mathbf{Y} are vanishing, the cross-covariance matrix \mathbf{C}_{xy} is defined as

$$\mathbf{C}_{xy} = \frac{1}{T-1} \mathbf{X}^T \mathbf{Y} \quad (2.2)$$

a N_x by N_y symmetric matrix with nonnegative elements representing the cross-covariances between the time series of the two fields. Note that the factor $\frac{1}{T-1}$ (which is the unbiased estimator of the expectation value of the covariance) is of no importance for the following discussion, and will therefore be omitted.

The goal is to find linear combinations of the data $\mathbf{X}\mathbf{p}_k$ and $\mathbf{Y}\mathbf{q}_k$ [$k = 1, \dots, R$, $R = \min(N_x, N_y)$] with the maximum covariance, subject to the $N_x \times 1$ vectors \mathbf{p}_k and $N_y \times 1$ vectors \mathbf{q}_k , satisfying the orthogonality constraints (δ_{ij} the Kronecker- δ)

$$\mathbf{p}_i^T \mathbf{p}_j = \mathbf{q}_i^T \mathbf{q}_j = \delta_{ij}$$

²Two-dimensional vector fields can be treated by using complex notation, i.e. (u, v) as $u + iv$

The solution is found by taking the singular value decomposition of \mathbf{C}_{xy} , denoted here by $\mathbf{C}_{xy} = \mathbf{L}\hat{\mathbf{S}}\mathbf{R}^T$ with properties as described in the previous Section and the singular values (σ_k) representing the cross-covariance of $\mathbf{X}\mathbf{l}_k$ and $\mathbf{Y}\mathbf{r}_k$. It can be shown (Bretherton et al. 1992; Widmann 1996) that the solutions \mathbf{l}_k and \mathbf{r}_k are the requested \mathbf{p}_k and \mathbf{q}_k , respectively. The real data fields can thus be approximated by the left and right singular vectors as³

$$\begin{aligned} \mathbf{X} \leftarrow \tilde{\mathbf{X}} &\equiv \mathbf{X}^*\mathbf{L}^T \quad \text{or} \quad \mathbf{x}(t) \leftarrow \tilde{\mathbf{x}}(t) \equiv \sum_{k=1}^N x_k^*(t)\mathbf{l}_k \\ \mathbf{Y} \leftarrow \tilde{\mathbf{Y}} &\equiv \mathbf{Y}^*\mathbf{R}^T \quad \text{or} \quad \mathbf{y}(t) \leftarrow \tilde{\mathbf{y}}(t) \equiv \sum_{k=1}^N y_k^*(t)\mathbf{r}_k \end{aligned} \quad (2.3)$$

where⁴

$$\begin{aligned} \mathbf{X}^* &= \mathbf{X}\mathbf{L} \quad \text{or} \quad x_k^*(t) \equiv \mathbf{x}(t)\mathbf{l}_k^T \\ \mathbf{Y}^* &= \mathbf{Y}\mathbf{R} \quad \text{or} \quad y_k^*(t) \equiv \mathbf{y}(t)\mathbf{r}_k^T \end{aligned} \quad (2.4)$$

are the expansion coefficients (always denoted by asterisk) or *left* and *right scores*, respectively (both together termed k^{th} pair of scores). The two time series of expansion coefficients will tend to be correlated, since (with $\mathbf{x}_k^* \in \mathbb{R}^{1 \times T}$)

$$\text{cov}(\mathbf{x}_k^*, \mathbf{y}_k^*) = \text{corr}(\mathbf{x}_k^*, \mathbf{y}_k^*) \sqrt{\text{var}(\mathbf{x}_k^*)\text{var}(\mathbf{y}_k^*)} \quad (2.5)$$

Therefore, the pairs of patterns obtained by SVD analysis are synchronous in time and represent the dominant coupled modes of co-variability. Note that there always exists a mathematical solution to the SVD problem. Thus the resulting coupled patterns might sometimes be a mathematical artefact (Cherry 1996), rather than representing a physical linkage, as discussed in Section 2.1.6.

2.1.3 The Linkage between PCA and SVD

As already noted by Bretherton et al. (1992), the SVD is equivalent to PCA if \mathbf{X} and \mathbf{Y} are the same, i.e. the left and right data fields are identical. But there is even more of a relationship between the two methods than that, as shown in the following.

Simultaneous Rotation to Congruence

Consider first the problem of identifying coupled patterns from a different point of view. Given two mean centered data matrices \mathbf{X} and \mathbf{Y} as defined in the previous Section, the problem of finding an orthogonal basis for each field maximising the cross-covariance can be thought of as searching for the directions in the left and right data space such that when the variables in the two sets of data are projected onto these axes, they are as close as possible. This step will be repeated in the remaining subspace (considering the orthogonality to the previous pair(s)) and continued up to R such pairs of directions. In other words, we seek (orthogonal) rotation matrices \mathbf{A} and \mathbf{B} such that the quantity

$$\|\mathbf{X}\mathbf{A} - \mathbf{Y}\mathbf{B}\|_F^2 \quad (2.6)$$

³the $\tilde{}$ denoting the approximation due to the restriction as imposed by $N \leq R = \min(N_x, N_y)$

⁴Note that $\mathbf{L} \in \mathbb{R}^{N_x \times R}$, while $\mathbf{l}_k \in \mathbb{R}^{1 \times N_x}$.

is minimised, where

$$\|\mathbf{G}\|_F^2 = \sum_{i=1}^{N_x} \sum_{j=1}^{N_y} G_{ij}^2 \quad (2.7)$$

refers to the Frobenius norm of a matrix. This way, the rotation matrices are attempting to match the l^{th} observation of \mathbf{X} with the l^{th} observation of \mathbf{Y} in such a way as that the sum of the squared differences between the rotated observations is minimised. The orthogonal rotations we are looking for are just provided by SVD analysis (Bretherton et al. 1992), the solution of the maximal covariance problem is thus the same as for the quest for simultaneous orthogonal rotations. See Cheng and Dunkerton (1995) about further use of orthogonal rotations applied to regionalise the coupled patterns.

SVD as Simultaneous Orthogonal Rotation of PCA Expansion Coefficients

The variances [$\text{var}(\mathbf{x}_k^*)\text{var}(\mathbf{y}_k^*)$] as maximised by PCA of each field alone appear on the right side of Eq. 2.5. Of course, the resulting correlation of scores from separate PCAs of the two fields might not be high, the two fields not being coupled at all. SVD can then be thought of as a simultaneous orthogonal rotation of PCA expansion coefficients to congruence ((Cherry 1997)). Let us denote SVD of \mathbf{X} and \mathbf{Y} alone as

$$\begin{aligned} \mathbf{X} &= \mathbf{L}_x \mathbf{S}_x \mathbf{R}_x^T \\ \mathbf{Y} &= \mathbf{L}_y \mathbf{S}_y \mathbf{R}_y^T \end{aligned}$$

with \mathbf{L}_x (\mathbf{S}_x) and \mathbf{L}_y (\mathbf{S}_y) the eigenvectors (eigenvalues) of the covariance matrices $\mathbf{C}_{xx} = \mathbf{X}^T \mathbf{X}$ and $\mathbf{C}_{yy} = \mathbf{Y}^T \mathbf{Y}$, respectively (the factor $\frac{1}{T-1}$ being suppressed). The matrix of principal components expansion coefficients for \mathbf{X} is (according to Eq. 2.4)

$$\mathbf{X}_x^* = \mathbf{X} \mathbf{R}_x = \mathbf{L}_x \mathbf{S}_x$$

and similarly for $\mathbf{Y}_y^* = \mathbf{L}_y \mathbf{S}_y$. Writing \mathbf{C}_{xy} in terms of the singular value decompositions of \mathbf{X} and \mathbf{Y} gives

$$\begin{aligned} \mathbf{C}_{xy} &= \mathbf{X}^T \mathbf{Y} \\ &= \mathbf{R}_x^T \mathbf{S}_x \mathbf{L}_x^T \mathbf{L}_y \mathbf{S}_y \mathbf{R}_y^T \\ &= \mathbf{R}_x^T \mathbf{X}^{*T} \mathbf{Y}^* \mathbf{R}_y^T \\ &= \mathbf{R}_x \mathbf{C}_{x^*y^*} \mathbf{R}_y^T \end{aligned}$$

where $\mathbf{C}_{x^*y^*}$ is the cross-covariance matrix of the principal components expansion coefficients from \mathbf{X} and \mathbf{Y} . Denoting the singular value decomposition of $\mathbf{C}_{x^*y^*}$ by

$$\mathbf{C}_{x^*y^*} = \mathbf{L}^* \mathbf{S}^* \mathbf{R}^{*T}$$

and substituting into the above system of equations yields

$$\begin{aligned} \mathbf{C}_{xy} &= \mathbf{R}_x \mathbf{L}^* \mathbf{S}^* \mathbf{R}^{*T} \mathbf{R}_y^T \\ &= \mathbf{L} \mathbf{S} \mathbf{R}^T \end{aligned} \quad (2.8)$$

with \mathbf{LSR}^T the singular value decomposition of \mathbf{C}_{xy} , thus $\mathbf{L} = \mathbf{R}_x \mathbf{L}^*$ and $\mathbf{R} = \mathbf{R}_y \mathbf{R}^*$, while \mathbf{S} and \mathbf{S}^* are identical.

Consider again Eq. 2.7, the formulation of the simultaneous orthogonal rotation problem. Find orthogonal matrices \mathbf{L} and \mathbf{R} to minimise

$$\|\mathbf{X}^* \mathbf{L} - \mathbf{Y}^* \mathbf{R}\|_F^2$$

\mathbf{L} and \mathbf{R} coming from the singular value decomposition of $\mathbf{C}_{x^*y^*}$ minimise this expression. Substituting from Eq. 2.8 yields

$$\begin{aligned} \|\mathbf{X}^* \mathbf{L} - \mathbf{Y}^* \mathbf{R}\|_F^2 &= \|\mathbf{X} \mathbf{R}_x \mathbf{L}^* - \mathbf{Y} \mathbf{R}_y \mathbf{R}^*\|_F^2 \\ &= \|\mathbf{X} \mathbf{L} - \mathbf{Y} \mathbf{R}\|_F^2 \end{aligned}$$

Thus the SVD expansion coefficients $\mathbf{X} \mathbf{L}$ and $\mathbf{Y} \mathbf{R}$ can be thought of as orthogonally rotated principal component expansion coefficients \mathbf{X}^* and \mathbf{Y}^* and the singular vectors in \mathbf{L} and \mathbf{R} are orthogonally rotated PCA eigenvectors.

This leads to one practical result considering the interpretation of coupled patterns derived by SVD analysis. Consider carrying out separate PCAs of the two fields. If the resulting expansion coefficients are strongly correlated (and the patterns are geophysically relevant), there results high indication of coupling. Alternatively, the patterns obtained by SVD analysis should be compared to the corresponding field's EOFs, since close match of the respective patterns is indicative of physically relevant modes, as suggested by Wallace et al. (1992), who contrasted the two approaches, not considering them as being closely linked by simultaneous orthogonal rotation.

2.1.4 Reconstruction

The coupled modes provided by SVD analysis can be used to reconstruct one field from the other. The SVD decomposition can be interpreted as a linear mapping from the 'left' space to the 'right' space, through the diagonal elements of the matrix \mathbf{S} (Eq. 2.1). The right field can be decomposed in two parts, one leading to the observed covariances (σ_k), while the other part does not contribute to these covariances. The first part is thus perfectly linearly related to its left-field counterpart and this relation can be used to obtain an approximative reconstruction of the right field using the left field as a predictor. An analogous relation holds for the case when the left field is reconstructed from the right one.

We will switch to index notation as already set out in Eq. 2.3 and 2.4. The cross-covariance of the expansion coefficients of the same mode are maximised by the SVD analysis and equal to the corresponding singular value σ_m :

$$\langle x_m^*(t) y_n^*(t) \rangle \equiv \sum_{l=1}^T x_m^*(t_l) y_n^*(t_l) = \sigma_m \delta_{mn}$$

The right expansion coefficient consists of one part linearly coupled with the left expansion coefficient (responsible for the detected covariance) and a residual term $\Delta_k(t)$ for which $\langle \Delta_k(t), x_k^*(t) \rangle = 0$:

$$y_k^*(t) = \frac{\sigma_k}{\langle y_k^{*2}(t) \rangle} x_k^*(t) + \Delta_k(t)$$

or symmetrically, with a redefined sigma and the hat $\hat{\cdot}$ indicating the approximation (the part not contributing to the covariance – $\Delta_k(t)$ – is not known):

$$\sigma'_k \equiv \frac{\sigma_k}{\sqrt{\langle x_k^{*2}(t) \rangle \langle y_k^{*2}(t) \rangle}} \quad (2.9)$$

$$\frac{\hat{y}_k^*(t)}{\sqrt{\langle y_k^{*2}(t) \rangle}} = \sigma'_k \frac{x_k^*(t)}{\sqrt{\langle x_k^{*2}(t) \rangle}} \quad (2.10)$$

Thus the part of the right field which can be reconstructed using the first N coupled modes is:

$$\hat{\mathbf{y}}(t) = \sum_{k=1}^N \hat{y}_k^*(t) \mathbf{r}_k \quad (2.11)$$

The quantity determining the quality of the reconstruction – σ'_k – is just the correlation of the left and right scores (compare with Eq. 2.5), hence a measure of the amount of the right field being reconstructable from the left one. Thus the coupled pattern provided by a SVD analysis allows one to reconstruct the linearly dependent part of one field from the other, and this technique could be useful in both statistical forecasting and downscaling (Widmann et al. 1995). We apply this method when considering the relations among the long-term trends of our data set in Section 3.4.

2.1.5 Explained (Cross-) Covariance and Selection Rules

The pair of left and right singular vectors ($\mathbf{l}_k, \mathbf{r}_k$) together with expansion coefficients ($x_k^*(t)$ and $y_k^*(t)$) are termed the k^{th} mode. By using the approximate expansions of the left and right field (Eq. 2.3) to build a synthetic cross-covariance matrix⁵ $\tilde{\mathbf{C}}_{xy}^N = \tilde{\mathbf{X}}^T \tilde{\mathbf{Y}}$, we can measure the goodness of this approximation of the original cross-covariance matrix \mathbf{C}_{xy} by the *cumulative squared covariance fraction (CSCF)*, defined as

$$CSCF^N := 1 - \frac{\|\mathbf{C}_{xy} - \tilde{\mathbf{C}}_{xy}^N\|_F^2}{\|\mathbf{C}_{xy}\|_F^2}$$

It can be shown (Bretherton et al., 1992) that

$$\|\mathbf{C}_{xy}\|_F^2 = \sum_{k=1}^R \sigma_k^2$$

and the above formulation is consistent with

$$CSCF^N = \sum_{k=1}^N SCF^k \quad (2.12)$$

where

$$SCF^k = \frac{\sigma_k^2}{\sum_{k=1}^R \sigma_k^2} \quad (2.13)$$

⁵ N denoting the modes used in the approximation indicated by $\tilde{\cdot}$

is the *squared covariance fraction* of the k^{th} mode. Note that since SCF involves squared variances rather than variances, it approaches unity faster with the inclusion of additional modes than the cumulative variance fraction. On the basis of Eq. 2.5 and the findings of the previous Section, a suitable measure for the strength of the coupling as well as the fraction of variance explained by one particular mode yields the *reconstructed right variance fraction* (r_k denoting the correlation of the left and right scores of the k^{th} mode)

$$RRVF^k = r_k^2 SCF^k = r_k^2 \frac{\sigma_k^2}{\sum_{k=1}^R \sigma_k^2} \quad (2.14)$$

as proposed by Bretherton and Widmann (1997, personal communication). Throughout this study, both SCF^k and $RRVF^k$ will be presented in percent, i.e. multiplied by a factor of 100.

In addition to the amount of cross-covariance explained by one particular or a series of modes (expressed by SCF^k and $CSCF^k$, respectively), it is also important to address the question how many modes describe a signal, i.e. a systematic property of the data. In this study, we use the tendency of higher modes to resemble basic functions of the domain (like spherical harmonics) together with the amount of explained $CSCF^k$ to choose this limit, since the focus is not on a detailed distinction between signal and noise.

Another issue is the question whether the derived modes of coupled patterns are independent. While non-unique patterns are obtained if two or more singular values are identical, in practical applications the singular values will not be identical, although possibly sometimes closely spaced. In this case, the modes can be regarded as linearly dependent, and any linear combination of the involved modes can be regarded as the ‘proper’ pattern of this mode. North et al. (1982) – considering both sampling errors as well as the limited length of the data set – give a useful rule of thumb for the uncertainty $\delta\sigma_k$ for the singular value σ_k

$$\delta\sigma_k \sim \sqrt{\frac{2}{T}} \sigma_k \quad (2.15)$$

Note that this ambiguity of the pattern order and independence can – in certain cases – also be thought of as a reflection of non-stationary features, like travelling waves and corresponding “waveguides” (Blackmon et al. 1984; Kushnir and Wallace 1989).

2.1.6 Comparison to Canonical Correlation Analysis and Caveats

Canonical correlation analysis (CCA) identifies coupled patterns with maximally correlated expansion coefficients in two time series of fields with optional PCA prefiltering⁶ (Zorita et al. 1992; Kharin 1995; Perlwitz and Graf 1995; Renwick and Wallace 1995; Cherry 1996; Kushnir et al. 1997). In contrast, singular value decomposition (SVD) maximises the cross-covariance between the pattern’s expansion coefficients. CCA may be affected by highly correlated, but unimportant (in the sense of low amplitude, i.e. low variation and/or covariation) variables within a set. In contrast, SVD identifies strong links between the patterns and simultaneously

⁶This step considerably decreases the number of degrees of freedom in the two time series of data fields and makes CCA more stable with respect to sampling variability (Barnett and Preisendorfer 1987).

large amplitudes of their expansion coefficients. There is no a priori superiority of one of the two methods. The appropriate choice depends on the precise question and the properties of the data set (Bretherton et al. 1992).

SVD analysis has been useful for a variety of meteorological applications regarding coupled patterns of physical relevance. Nevertheless, restrictions on interpretation of SVD results have been cautioned (Hu 1997). Newman and Sardeshmukh (1995) note that SVD can lead to unrealistic relations of two data series even though the calculated correlation between them might be high. They showed that if $\mathbf{x}(t)$ and $\mathbf{y}(t)$ are linearly related ($\mathbf{y} = \mathbf{Ax}$), this relation will be correctly identified by SVD analysis only if the linear relation \mathbf{A} is an orthogonal matrix (due to the orthogonality constraint to the SVD modes). Therefore, while the first mode will be generally meaningful, the higher order modes can deviate from physical couplings by orthogonality. Another problem arises from the sampling errors (North et al. 1982) and the fact that there might be “theoretically at least, an infinite number of processes with the same cross-covariance structure” (Cherry 1996). Therefore, Hu (1997) suggests that SVD results can be used only *after* their physical relation has been at least proposed by other means. Together with the considerations in Section 2.1.3, we suggest checking the robustness of the SVD patterns by carrying out separate PCAs for each field and comparing the resulting patterns with those obtained by SVD analysis, a close match being indicative of the dominant modes of each field being at least involved in the coupling. Note also that any non-linear relations between the two fields can hardly be detected by SVD analysis (see later).

Furthermore, the patterns obtained by SVD (or any similar method) are expected to be very strongly influenced by the geometrical shape of the region and – due to the high spatial autocorrelation of many atmospheric fields – to a large extent independent of where the region is located. As a consequence, the dependence of the patterns on variations of the domain shape should be carefully assessed (cf. Buell 1979).

2.2 Storm Track Identification

In this Section, the – somewhat technical – aspects of the two approaches in determining the storm track, i.e. the identification of “dynamic” and “synoptic” storm track are discussed.

2.2.1 Variance Filtering

The dynamic storm track is usually calculated from (daily) mid-atmospheric geopotential height data (500 mb is a standard level). A broad range of different filtering methods have been proposed in recent years from straightforward variance (cf. Hoskins and Valdes 1990) to digital high-pass (Blackmon 1976, Wallace et al. 1988) and recursive (Murakami 1979) filtering. The shapes and locations of the features usually referred to as the “storm tracks” (Section 1) do not appear to be sensitive to the exact form of the high- or band-pass filter applied (Wallace et al. 1988). The recursive Murakami-filter (Murakami 1979) has the advantage of reduced needs in data length – no additional data at begin and end of the sampling period – and computing time compared to the other methods. A comparison

(Christoph et al. 1995) of the conventional digital filter (Blackmon 1976) with the recursive Murakami-filter revealed only very small differences⁷. Throughout the present study, the storm track will be calculated by application of the recursive Murakami-filter to geopotential height at 500 mb. The lower and upper cutoff frequency (0.5 filter response) have been set to $\omega_1 = 2\pi/8.0 \text{ day}^{-1}$ and $\omega_2 = 2\pi/2.5 \text{ day}^{-1}$. This results in a maximum of the amplitude function close to a period of 4 days, where a relative maximum in the power spectrum of the 500 mb geopotential height field is observed (Fraedrich and Böttger 1978).

2.2.2 Objective Identification of Cyclones

In recent years, many cyclone-identification algorithms have been developed, based on (daily) surface pressure maps, differing in their methodology. There are – at least – two possible approaches, the identification of i) local minima (Blender et al. 1997) or ii) closed isolines (Knig et al. 1993) of surface pressure. The method based on local minima appears to be able to detect cyclones in an earlier stage of development. The implementation of Heini Wernli (personal communication) identifies closed isolines in the sea-level pressure field, and generates a field which is equal to the pressure difference relative to the value of the enclosing isoline at every point inside a closed isoline and zero outside. While a dynamic storm track is mainly employed in this study, the objectively identified cyclones will be used for quantitative comparison of growth and decay rates of synoptic disturbances as well as for providing further evidence for results based on the “dynamic” storm track. Based on NMC analysis data 1962-1992, the dynamic and synoptic storm tracks have been compared. For this purpose, monthly mean fields are derived for cyclones and anticyclones on the Northern Hemisphere (Wernli and Bresch 1997). The long term winter (DJF) mean fields of both the dynamic storm track and objectively identified cyclones do not differ considerably (Fig. 2.1, upper left panel) and the respective first mode of variability (upper right panel, identified by SVD analysis – see Section 2.1) is very similar, a behaviour observed for higher order modes as well. The first mode of variability of objectively identified anti-cyclones reflects the activity of the Azores high and is related to a northward deflection of the dynamic storm track (Fig. 2.1, lower left panel). These results confirm the close relationship between the dynamic and synoptic storm track.

2.3 The Models

2.3.1 The Limited Area NWP Model

The case studies presented in Chapter 5 are performed using the Europa Modell (EM) of the German weather service, developed by Majewski (1991). The EM is a meso- α -scale limited area NWP-model based on the hydrostatic set of primitive equations with hybrid vertical coordinates (Simmons and Burridge 1981). In this study it is operated with 20 vertical levels

⁷The Pacific storm track obtained by filtering the detrended geopotential height anomalies for two selected periods and 10 year mean data appears to be very similar for both methods, only the maximum amplitude is about 6% lower for Murakami filtering.

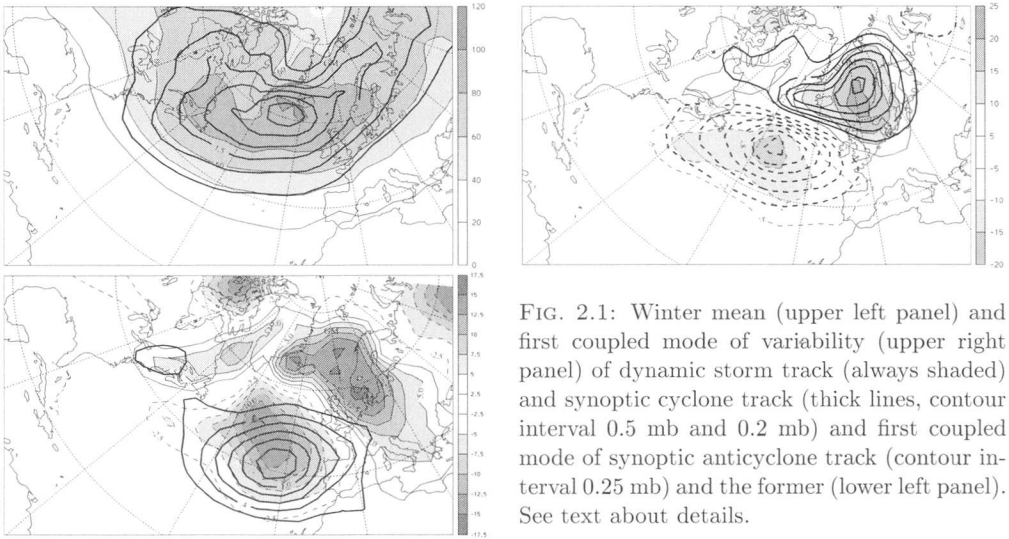


FIG. 2.1: Winter mean (upper left panel) and first coupled mode of variability (upper right panel) of dynamic storm track (always shaded) and synoptic cyclone track (thick lines, contour interval 0.5 mb and 0.2 mb) and first coupled mode of synoptic anticyclone track (contour interval 0.25 mb) and the former (lower left panel). See text about details.

(the operational configuration) on a special domain covering the eastern United States, the North Atlantic ocean and Europe with a horizontal resolution of 1° by 1° (Fig. 2.2), which allows the simulation of details in frontal structure etc., as requested by the arguments in Section 1.

The parametrised physical processes include a surface layer formulation, a boundary layer and turbulence scheme, a soil model with three soil layers for the heat and water budgets as well as a snow representation scheme, grid-scale cloud microphysics of Kessler-type, a mass-flux scheme for moist convection (Tiedtke), a radiative transfer package, and a fourth-order horizontal diffusion scheme.

The simulations undertaken in this study are initialised by the European Center for Medium-Range Weather Forecasts (ECMWF) Reanalysis (ERA) fields (Gibson et al. 1996) interpolated to the EM model grid and relaxed to the analyses at the lateral boundaries (Davies 1976) every 6 hours. Simulations of European climate with the present model have proved to closely reproduce the observed monthly mean circulation including mean time variability driven by both analysis and GCM (ECHAM) boundary fields (Cress et al. 1995; Podzun et al. 1995). Furthermore, its aptitude for regional climate change studies has been broadly tested (Schär et al. 1996).

2.3.2 The Idealised Model

In the idealised model studies (Chapter 4), a derivative of the EM model (see above) has been used. An idealised setting with only one ocean and land mass has been chosen. Thus the model is operated on a *half*-hemispheric domain (8°N to 82°N by 180°W to 180°E) with a horizontal resolution of 2° by 2° . The land mass is flat with a roughness-length that corresponds to small trees and the area North of 70°N is represented by an ice shield

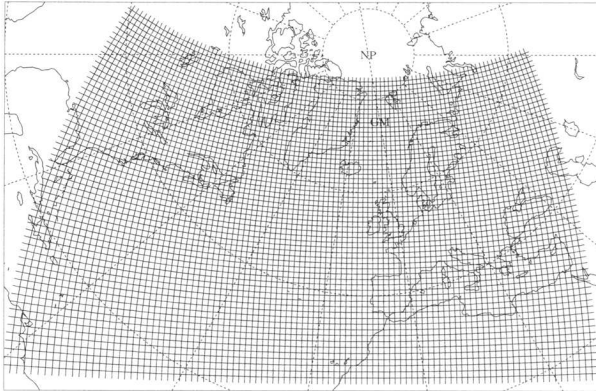


FIG. 2.2: Model grid used in Chapter 5. The rotated pole is centered at $170^{\circ}\text{E } 35^{\circ}\text{N}$.

(Fig. 2.4). It is run with the physics package as described above (Section 2.3.1), but with fixed soil parameters (no soil model). Periodicity around the longitudinal boundaries has been implemented⁸ and the southern and northern boundaries are relaxed⁹ to the initial state (unperturbed, see below).

This simplified model is operated at a time step of 400 seconds with 27 vertical levels¹⁰, with high resolution at low levels and reaching up to the upper stratosphere to avoid model drift due to radiation. External parameters have been specified (after a series of sensitivity experiments) as follows: i) the Ozone distribution has been set to a zonally homogeneous mean NH winter profile with a slight southward shift over the land mass and ii) the soil parameters have been set according to smoothed zonal mean NH vales while iii) the solar irradiation angle has been kept varying with time.

To initialise the idealised model, we started from a zonally homogeneous basic state close to the 10 year ECMWF winter mean climatology (Hoskins et al. 1989) over the North Atlantic sector, as shown in Fig. 2.3 and a surface temperature distribution (Fig. 2.4) corresponding to climatology (Reynolds and Smith 1995), with the characteristic position and eastward widening of the main baroclinic zone in the ocean basin and land surface temperature 8.5 K colder than the ocean.

To instigate the growth of observed mid-latitude synoptic scale systems, an upper-level potential vorticity (PV) anomaly¹¹ (Fig. 2.5, left panel) has been imposed in the center of the

⁸The periodicity has been implemented by extending the model grid at the eastern and western boundary by as many points as needed by the discretisation scheme in order to ‘see’ around the boundary (EM model: 4) and mutually copying these points previous to each time-step.

⁹Due to the fact that the radiation scheme acts on all grid points while the discretised differential operators treat the boundaries in a special way (leading – for example – to a permanent cooling of the northern boundary), free slip boundary conditions were not appropriate.

¹⁰The model levels are at 990, 960, 930, 900, 860, 820, 780, 710, 640, 570, 510, 450, 390, 340, 300, 260, 210, 180, 160, 130, 110, 80, 60, 45, 35, 25 and 20 hPa.

¹¹See Hoskins et al. (1985) about the PV perspective – PV-conservation, PV-inversion and the principle of

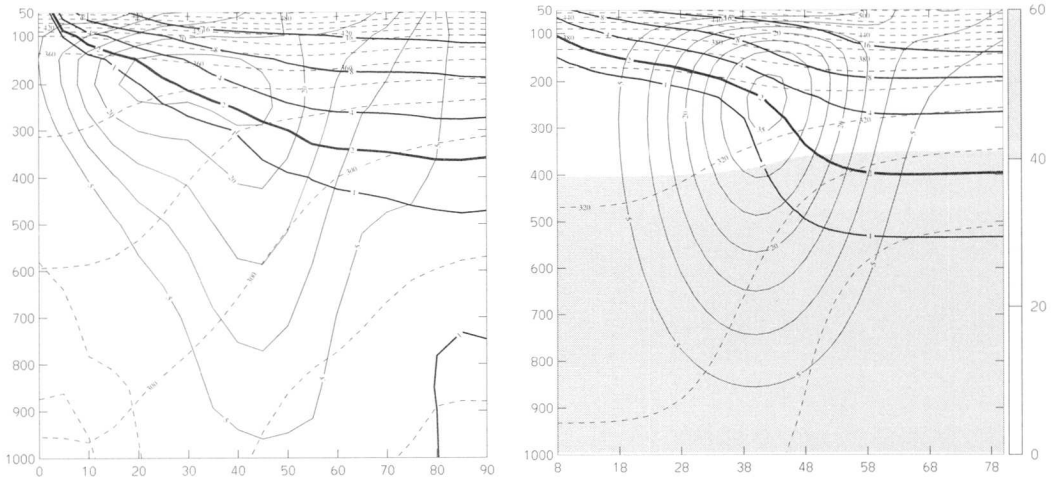


FIG. 2.3: Zonal mean latitudinal cross-section of the 10 year ECMWF winter climatology over the North Atlantic sector (left panel) and corresponding model (perturbed) initial state (right panel). Mean zonal wind (thin lines, contour interval 5 m s^{-1}), Θ (thin dashed lines, contour interval 20 K) and PV (thick lines, contours at 1, 2, 4, 8 and 16 pvu ($1 \text{ pvu} = 10^{-6} \text{ K m}^2 \text{ kg}^{-1} \text{ s}^{-1}$)).

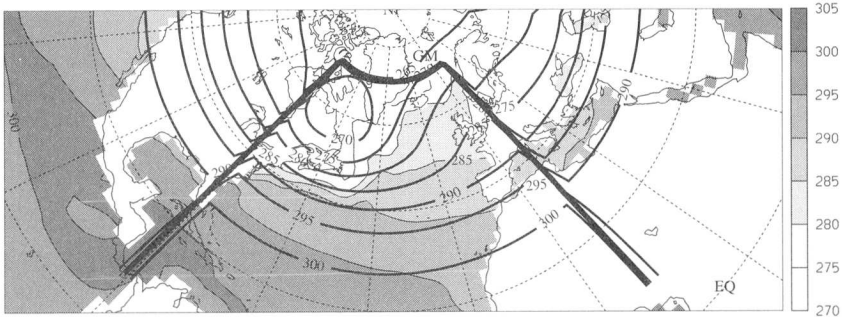


FIG. 2.4: Surface temperature distribution of the idealised model (thick lines, contour interval 5 K , negative contours dashed and zero line omitted), compared to climatology (shaded, contour interval 5 K). The very thick black line indicates the boundary of the ocean basin (central part of the model).

ocean basin as initial disturbance to the unperturbed zonally homogeneous basic state. The corresponding wind- and mass-fields of the modified initial state (Fig. 2.5, right panel) are obtained by the inversion of the potential vorticity in the quasi-geostrophic limit (Fehlmann 1997). The initial PV anomaly triggers the development of a first cyclone, thus inducing enough instability for further cyclone growth. After less than a month, a realistic flow

PV-partition of the flow in terms of coherent and distinct elements

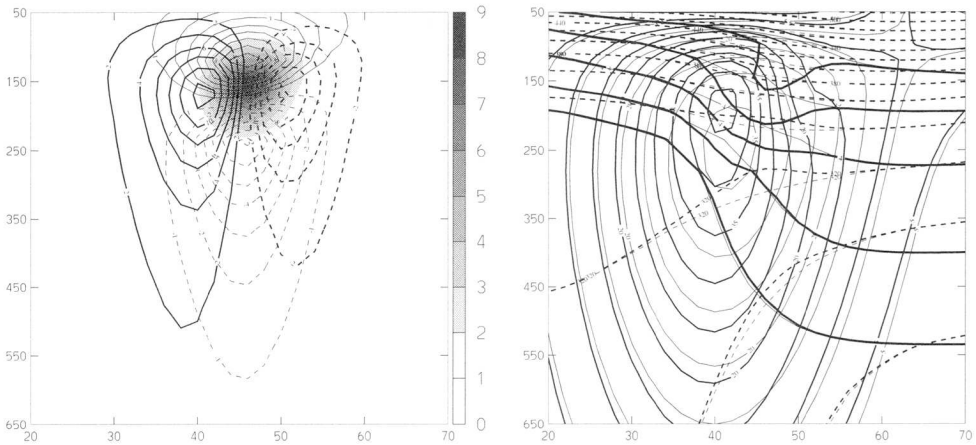


FIG. 2.5: Latitudinal cross-section in the center of the ocean basin through the PV anomaly imposed to the basic state (left panel, shaded PV in pvu, thin lines theta perturbation, interval 2 K and thick lines zonal wind anomaly, interval 2 m s^{-1}) and cross-section of the resulting perturbed initial state (right panel, conventions as in Fig. 2.3).

evolution with the main activity concentrated over the ocean basin has been established, as will be demonstrated in Chapter 4.

2.3.3 Model Comparison in Terms of EOFs

In addition to the common comparison of different runs of the models presented above in terms of (rms) difference fields, the model response to boundary forcing will be assessed based on EOF patterns. There are mainly two possible candidates of relevant patterns, the model's own EOFs and the climatological patterns derived from observational data, both approaches being followed in the present study.

The model EOFs are calculated by application of PCA to the six-hourly model output (geopotential height at 500 hPa, for example) of the control (CTRL) and experiment (EXP) simulations. First, a comparison with the EOFs calculated from the observational (here ERA) analysis data used to initialise the model can be undertaken to check for the models ability to correctly simulate weather and climate, any considerable difference between the first model and analysis EOFs indicating possible model deficiencies, like systematic errors. Secondly, the leading model EOFs represent a kind of optimal slice – in terms of, for example, the geopotential height field – through the model's phase space, since they explain the maximal amount of model variance. If now the leading EOFs of the CTRL and EXP runs closely resemble each other, the differences between the EXP and CTRL simulations can be expressed in terms of the leading model (CTRL) EOFs and the amplification of a given recurrent pattern in the EXP run with respect to the control simulation can be quantified. If, in contrast, the first EOFs of EXP and CTRL simulations differ considerably, this could lead to the interpretation that the EXP simulation comprises a mode not present in the

CTRL simulation. Similar considerations would be applicable to SVD analysis of model output, which allows the comparison of co-varying patterns¹²

A comparison of the model results in terms of the climatological EOFs instead of the model EOFs allows a direct assessment of the ability of the imposed forcing to influence a recurrent mode of the climate system. Note that this approach can also be followed to address the storm track response of the model when the simulation is not long enough to calculate storm track EOFs from the model data. Furthermore, the direct comparison to climatological EOFs does not suffer from model details and might present a suited method for model intercomparison.

A more detailed investigation of the model EOFs or (SVD patterns) and their differences compared with EOFs from other model runs and/or climatological patterns might also be suited to obtain information about the model's forced variability, guidance on systematic errors in the model's response to various (SST) forcing, clues to physical mechanisms and a basis for model output statistics. An application of SVD analysis to model and observed fields for an ensemble of GCM simulations has been undertaken by Ward and Navarra (1997), who addressed (potential) seasonal forecast skill and reproducibility.

In the present study, the comparison of different simulations by means of model EOF patterns will be undertaken for the case studies (Chapter 5). The model results will also be compared in terms of the climatological patterns of Chapter 3.

¹²This approach can be particularly helpful when time-dependent forcing has been imposed in the EXP simulation, since it allows the identification of coupled modes of the forcing with a selected model variable.

Chapter 3

Statistical Analysis

The representation of the complexity of the spatial and temporal structure of meteorological data can be reduced by application of multivariate statistical analysis techniques. For example these techniques can provide information about the (coupled) spatial structure of one (or more) observed fields by identifying the dominant (coupled) patterns of spatial variability, and thereby filtering out small-scale noise. Here singular value decomposition (SVD) is applied to sea surface temperature (SST), geopotential height at 500 hPa and the associated storm track fields over the North Atlantic sector.

An introduction to the statistical analysis techniques has been presented in Chapter 2 (Section 2.1). After a short description of the data sets, the coupled modes of large-scale variability of the aforementioned fields will be presented for winter season on a monthly basis and compared to the results of a whole year analysis and with other studies. Their temporal relationship will be investigated by lag correlation and in addition consideration given to the interrelations of the linear trends.

3.1 Data

The data-base for the analysis spans the three decades from 1962 to 1992. It comprises i) the monthly SST data set of Reynolds and Smith (1995) on a grid of 2° by 2° from 45°S to 69°N , and ii) the twice-daily 500 hPa geopotential analysis fields of NCEP interpolated to a 5° by 3° grid from 18°N to 87°N . From the latter fields the monthly mean patterns are derived for the three winter months of December, January and February, and the corresponding dynamic storm track fields are obtained using the band pass Murakami digital filter applied to 500 hPa geopotential height to obtain a storm track pattern for every calendar month (see Christoph et al. (1995) and the discussion in Section 2.2).

Prior to analysis, the data is modified sequentially by : (i) applying a $\cos(\textit{latitude})$ areal-weighting to take into account the uneven spatial density of the grid, (ii) subtracting out the contribution associated with both the long-term linear trend and the seasonal cycle to allow the patterns to characterise more clearly the intraseasonal month-to-month variability¹.

¹If neither the long-term linear trend nor the seasonal cycle are removed prior to SVD analysis, the first mode describes mainly the summer/winter and the second mode the autumn/spring difference, the modes presented in this study therefore appearing as number 3 and higher, somewhat distorted by the orthogo-

These two steps are the prelude to performing a singular value decomposition (SVD) of the detrended data for the various pairs of the three fields. The robustness of the coupled patterns was assessed by Monte Carlo tests involving perturbed time series.

3.2 Coupled Patterns

An SVD analysis is performed as outlined in Section 3.1 to yield the set of coupled modes of SST, geopotential height and storm track in the North Atlantic sector.

We will restrict our discussion principally to (i) the winter season since the couplings are strongest during this period and to (ii) the first few coupled modes, since they explain a major amount of the fields' variances and covariance and appear to be physically interpretable. The higher order modes are not as clearly separated in terms of the explained (co-)variance and hence probably not linearly independent (see Section 2.1.5). Furthermore, the leading EOFs of the respective fields closely match the patterns of the first coupled modes, providing evidence that the identified patterns represent recurrent coupled physical modes (as suggested in Section 2.1.3).

In addition to the coupled patterns, we will show composite plots based on the months with highest (lowest) 10% of the scores that will be termed upper (lower) quantile. In contrast to the figures showing the SVD patterns directly, these latter plots provide an estimation of the extent 'real' situations are characterised by one coupled mode alone². Lag composite plots are investigated as well, where the composite of the months with the highest (lowest) 10% of the left scores is shown together with the composite of the *subsequent* right fields (one month later). Throughout this study, the scores are normalised by their standard deviation, and the figures of the left and right singular vectors depict an amplitude related to one standard deviation of their respective scores.

The justification for restricting our analysis to the North Atlantic domain³ is illustrated by Fig. 3.1. It shows the first two coupled modes of the complete (in space and time, see Section 3.1) SST and geopotential height data sets. The first northern hemisphere geopotential height mode is dominated by the Pacific North American pattern (PNA), the principal mode of the Pacific sector (Wallace and Gutzler 1981; Mo and Livezey 1986; Wallace et al. 1990, 1992; Lin and Derome 1997; Sheng et al. 1998), closely linked to ENSO (Philander 1990). The SST counterpart shows high loadings in the equatorial Pacific, and an extended cold anomaly in the central North Pacific, both related to ENSO and North Pacific wintertime blocking (Renwick and Wallace 1996). The second mode is dominated by the Atlantic sector, a tripole SST anomaly linked to a similar structure in the height field with the southernmost center outside the data domain. The resemblance to the NAO pattern is striking. Note also the equatorial Pacific warm tongue already present in the first mode, evidence for a possible direct link ENSO - NAO (Fraedrich and Müller 1992). The dominance of either the

nality constraint.

²If the upper and lower quantile plot show clearly distinct features and their difference closely matches the corresponding SVD left and right pattern, there is high evidence that the observed mode is not an artefact of the applied method.

³A sector ranging from 100°W to 80°E and from 18°N to 88°N.

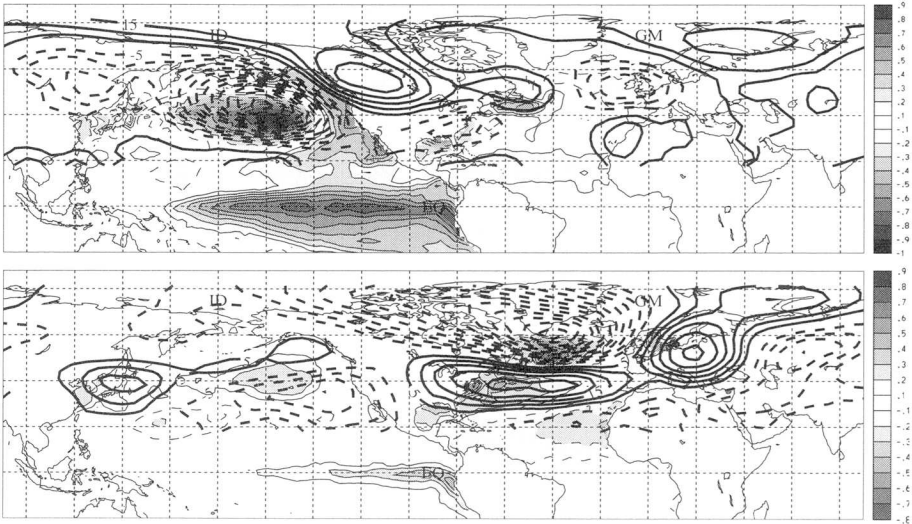


FIG. 3.1: First (upper panel) and second (lower panel) pair of coupled patterns of SST (shaded and thin lines, contour interval 0.1 K, negative contours dashed and zero line omitted) and geopotential height (thick lines, contour interval 5 gpm, negative contours dashed and zero line omitted) based on the whole data sets as described in Section 3.1. The patterns depict one standard deviation of the expansion coefficients.

Pacific or Atlantic sector in a specific mode is also observed for higher modes, and hence these two sectors can to a first approximation be regarded as separate entities. Planetary-scale phenomena (Rossby waves, large scale atmosphere-ocean interaction like ENSO) are not addressed correctly when restricting the analysis to one ocean basin, but the focus on one sector can help to elucidate the basin-wide mechanisms on a monthly up to seasonal time scale⁴.

3.2.1 SST – Geopotential Height

For the first coupled ‘SST- height’ pair (Fig. 3.2, upper panel), the height signature takes the form of a compact synoptic-scale low centred over southern Greenland and a longitudinally-elongated high located further south with separate maxima over the western ocean and central Europe; cf. the first EOF of other studies (e.g. Craddock and Flood 1969) and the leading surface pressure EOF (Kutzbach 1970; Trenberth and Paolino 1981). The SST pattern has a dipolar structure with centres south of Greenland and off the central US, and with a further signal in the Baltic⁵. These patterns account respectively for 26% and 25%

⁴To check the domain shape dependence of the observed patterns, SVD analyses on a series of different domains have been performed, confirming that the presented patterns are very robust.

⁵Note that the SST dipole pattern has been identified to be part of a larger structure covering the entire Atlantic ocean, with centers of action from 40°S to 70°N (cf. Venegas et al. 1997; Xie and Tanimoto 1998).

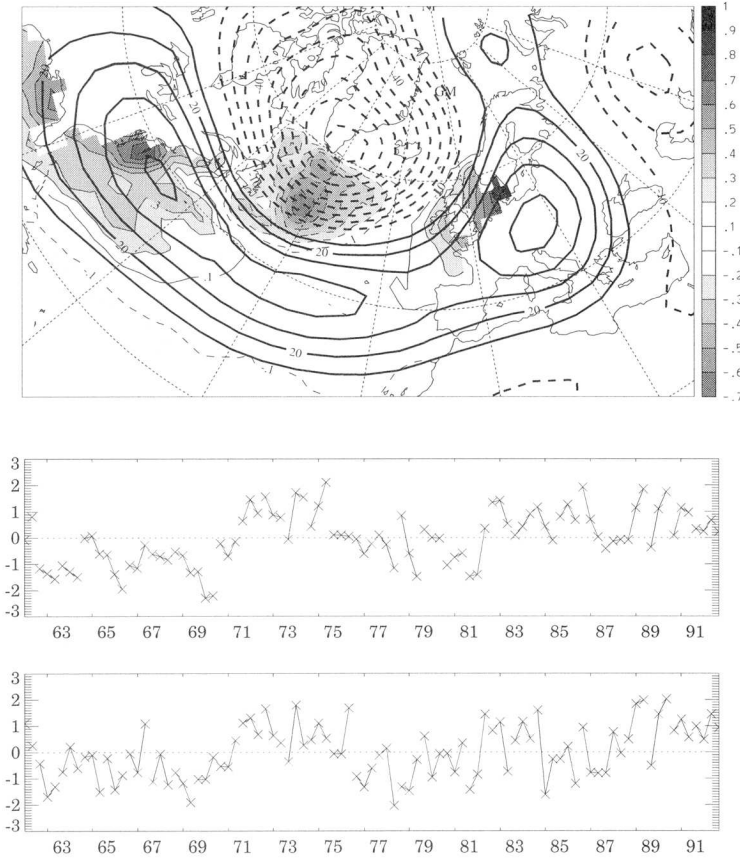


FIG. 3.2: Top panel: First pair of coupled patterns of SST (shaded and thin lines, contour interval 0.1 K, negative contours dashed and zero line omitted) and geopotential height (thick lines, contour interval 10 gpm, negative contours dashed and zero line omitted) based on monthly winter data over the North Atlantic sector. The patterns depict one standard deviation of the expansion coefficients. Expansion coefficients (scores) for the left (middle panel) and right (lower panel) patterns of the first coupled mode of SST and geopotential height. Lines connect the three winter months (DJF) and scores are measured in units of their respective standard deviation.

of the variability of the fields, and 31% (64%) of the (squared) cross-covariance with an RRVF value (see Section 2.1.5) of 43%. The coupled mode based on all months of the year closely matches the presented one (explaining about the same variance of each field, but only 22% of the cross covariance), with scores especially high in winter. The latter is indicative of the strong flow anomalies to be found during the winter season. Similar patterns have been derived in earlier studies (Wallace et al. 1990; Cayan 1992b; Peng and Fyfe 1996; Deser and Timlin 1997). The scores of the first mode (Fig. 3.2, lower panels) show large

month-to-month and year-to-year variations.

The structure of the first height field mode has an NAO-like signature with some Western Atlantic (WA) and Eastern Atlantic (EA) pattern characteristics⁶ as well (Wallace and Gutzler 1981). The link with the NAO is brought out in Fig. 3.3 : the upper panel shows the monthly and the winter-mean time series of the surface NAO index for the last 100 years (from Hurrell 1995a), and the lower panel depicts the corresponding time series for this first SVD-derived geopotential height pattern. For the period 1962-1992 the correlation between the winter mean NAO index and the score of the SVD mode amounts to 0.89. Therefore, it is reasonable to associate the first geopotential height pattern with the NAO-mode.

The composite maps for the first SST-height mode based on SST scores (upper/lowermost 10%) are presented in Fig. 3.4. The two extremes depict quite different flow regimes and a clear sign reversal of the SST anomalies, the upper quantile (positive sign of the patterns shown in Fig. 3.2) reflects a strong zonal flow over a region of enhanced SST gradient, while the lower quantile depicts a weaker trough coupled with a decreased SST gradient. The quantile plots based on the geopotential height scores (Fig. 3.5) resemble those based on the SST scores in the atmospheric flow field, while the SST signal is weaker, probably indicating that the northern part of the SST dipole (as well as the SST in the Baltic sea) is more directly affected by the atmospheric flow, as already observed by Bjercknes (1964).

The second ‘SST-height’ mode (Fig. 3.6) explains 14% and 18% of each field’s variance and 18% (22%) of the (squared) covariance (RRVF=14%). The patterns are dominated respectively by a warm pool SST anomaly and a northeastward shifted positive height anomaly. The composite plots of this mode (Fig. 3.7) resemble to some extent those of the first mode, they will be discussed together with the quantile plots of the coupled modes of SST and storm track below. It has to be noted that the second mode based on all months of the year shows similar features, explaining again somewhat smaller amounts of (co-) variance.

The first two winter modes thus explain 39% and 43% of SST and geopotential height variance, respectively, and account for 49% of the total covariance. Together with the third mode (not shown⁷), over 50% of both field’s variance and about 60% of the total covariance are explained.

3.2.2 SST – Storm Track

For the leading ‘SST-storm track’ coupled pair (Fig. 3.8), the SST pattern bears a close resemblance to that of Fig. 3.2, and the storm track pattern connotes a northward shift, eastward extension and a strengthening of the baroclinic activity (a similar structure is observed throughout the year). These signatures explain 26% of SST and 12% of the storm track variance, and 20% (45%) of the (squared) cross-covariance (the values for the whole year analysis are about 10% lower).

⁶The first coupled mode of total surface heat flux and geopotential height obtained by Iwasaka and Wallace (1995) is deflected towards the Western Atlantic pattern, while their corresponding surface pressure pattern is quite similar to the NAO pattern.

⁷similar features as observed in the first two modes are observed, the orthogonality constraint probably already severely affecting this mode, since the upper/lower quantile plots do not show as clear features as present in the first two modes (Figs. 3.4 and 3.7).

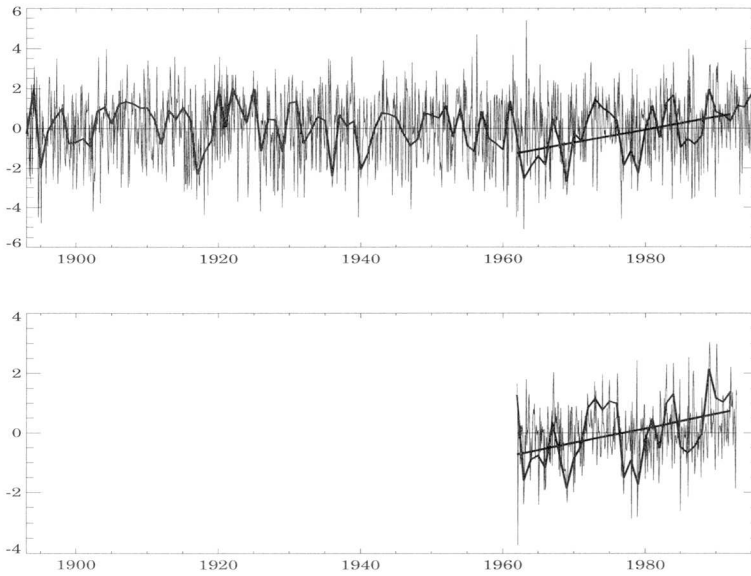


FIG. 3.3: NAO index 1895-1995 (upper panel, (Hurrell 1995a)) and winter mean index (thick line) with the recent strengthening period 1962-92 (very thick line) and scores of the first geopotential height mode for the period 1962-1992 (lower panel, winter mean scores as thick line). See text about details.

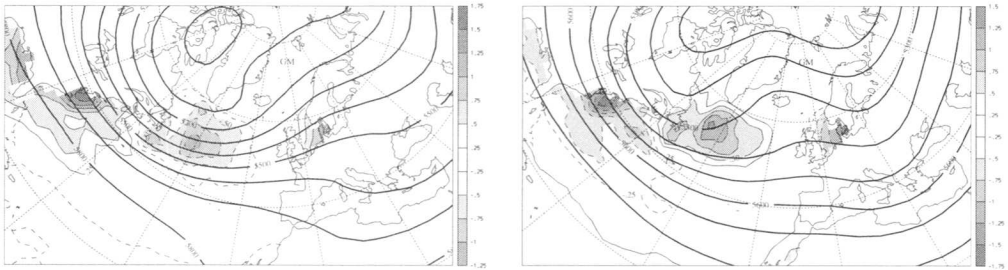


FIG. 3.4: Composite maps (left panel: upper quantile, right panel: lower quantile) of the first coupled mode of SST (shown the SST *anomaly*, shaded and thin lines, contour interval 0.25 K, negative contours dashed and zero line omitted) and geopotential height (thick lines, contour interval 100 gpm) based on SST scores. See text about details.

The corresponding composite plots based on SST scores are presented in Fig. 3.9, those based on storm track scores (not shown) look very similar, except for somewhat less pronounced SST anomalies. The zonal elongation of the storm track for high positive scores

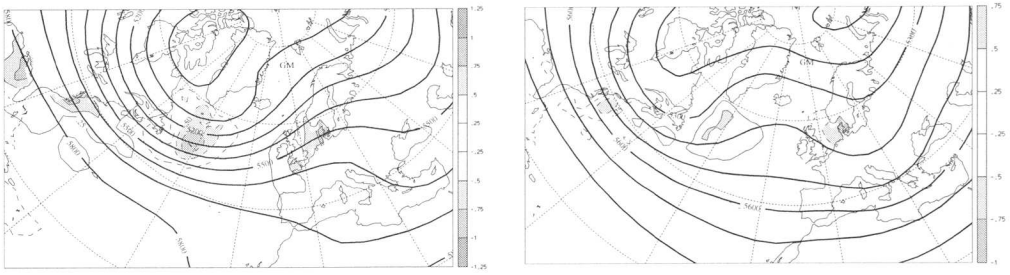


FIG. 3.5: As Fig. 3.4, but based on right scores.

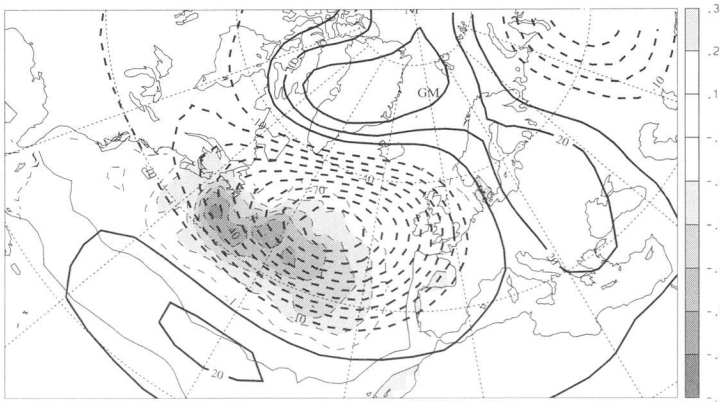


FIG. 3.6: As Fig. 3.2, but for the second coupled mode.

contrasts with the picture for negative scores, as was already observed for the first ‘SST-height’ mode.

The second ‘SST-storm track’ mode (Fig. 3.10) bears close resemblance to the second ‘SST-height’ mode and is probably related to blocking. This is illustrated by the composite plots (Fig. 3.11), where the storm track is zonally confined and strengthened for high scores (left panel), and northeastward deflected and weakened for low scores (right panel).

3.2.3 Geopotential Height – Storm Track

The patterns for the leading ‘height-storm track’ pair (Fig. 3.12) account for 22% (46%) of the (squared) cross-covariance (cf. Bresch 1995). The amplification of the storm track to the South of Greenland compares well with the difference field of cyclone events associated with the NAO as observed by Serreze et al. (1997) and the eddy heat transport considerations and concomitant variations in the occurrence of baroclinic systems by Carleton (1988). The patterns of geopotential height and storm track strongly resemble those shown in Figs. 3.2 and 3.8. Each pair of SST, height and storm track fields exhibits such a resemblance.

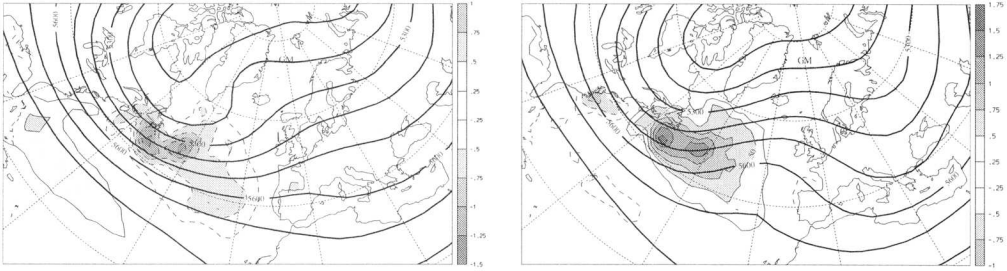


FIG. 3.7: As Fig. 3.4, but for the second coupled mode.

Therefore, no composite maps are shown for the ‘height- storm track’ pairs. Nevertheless, Fig. 3.4 and 3.9 together provide illustrations of the first North Atlantic mode (NAO-mode) and Fig. 3.7 and 3.11 the second mode.

The different storm track regimes identified so far are in agreement with Lau (1988), who identified geopotential height variability EOFs and related geopotential height regression maps and the findings of Blender et al. (1997), who presented a categorisation by cluster analysis into three types of cyclone tracks: stationary, north-eastward and zonally travelling storms. Similar patterns of variability have been obtained by Rogers (1990) through inspection of isopleths of the frequency of wave cyclones when rotated principal component scores of surface pressure were extremely high or low. More recently, Rogers (1997) investigated the primary mode of North Atlantic storm track variability identified by application of rotated principal component analysis (RPCA) to monthly fields of rms high-pass filtered (2-8 days) sea level pressure for winters 1900-1992. The mean sea level pressure difference occurring between the months with extreme positive and negative scores of the principal storm track component resembles a northeastward shifted NAO-like dipole and Rogers (1997) notes that this pattern does not suggest a strong storm track link to the NAO. Nevertheless, his first coupled mode of surface pressure and variability appears to be structurally comparable to our results, and the differences can be primarily explained by the different time periods and data sets used.

The flow patterns related to blocking were better represented in the coupled modes of height and storm track than SST. A tentative inference would be that the maintenance of blocking is primarily determined by the internal dynamics of the atmosphere (Mullen 1989) rather than boundary forcing.

It should also be noted in passing that SVD decompositions undertaken with fields comprising full year and winter seasonal mean data (see Kushnir and Wallace 1989) yield results comparable to those presented here. It is also evident that : the leading geopotential mode(s) are always closely linked to the NAO; the leading patterns for the seasonal analysis explain even higher cross-covariance fractions; and the year-to-year variability appears to be dominated by fewer modes than the month-to-month one.

Furthermore, both the coupled patterns of SST tendency and either geopotential height or storm track (not shown, since they are similar to the results obtained by Iwasaka and Wallace 1995) are comparable to those coupled with SST, probably due to the long persistence time

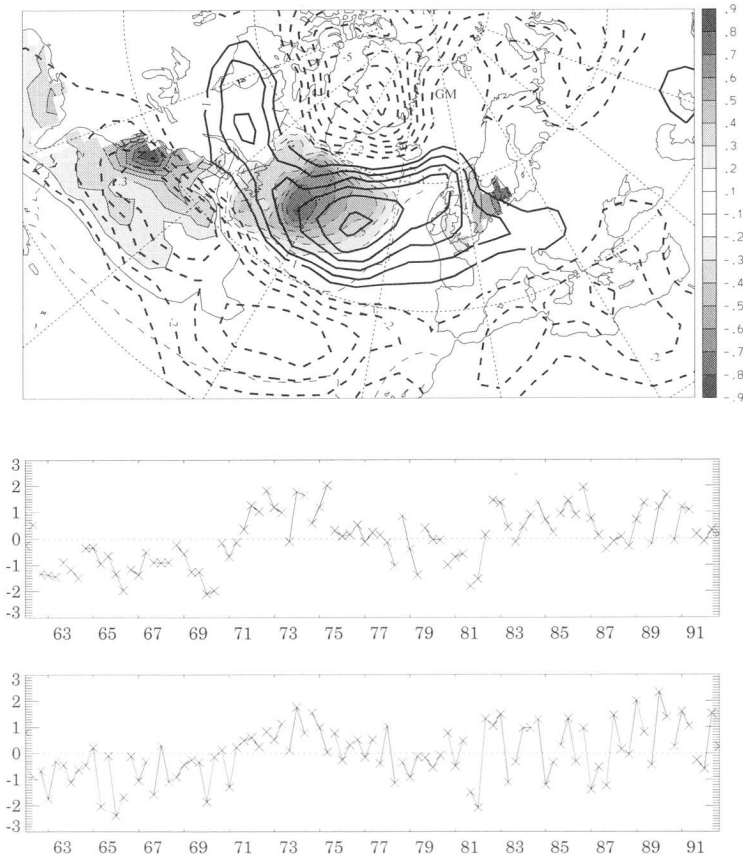


FIG. 3.8: As Fig. 3.2, but for the first pair of coupled patterns of SST and storm track (thick lines, contour interval 1 gpm, negative contours dashed and zero line omitted) and left (middle panel) and right (lower panel) expansion coefficients.

of the SST fields (up to several months, Davis 1976, Namias et al. 1988).

In summary the foregoing results suggest that the SVD analysis identifies recurrent coupled patterns that are representative of the primary modes of monthly variability of the examined fields. Moreover the dominant patterns (first two modes) are related to the NAO and explain on average over 30% of the month-to-month co-variability of the observed fields.

3.3 Temporal Interaction

As a first approach towards an understanding of the coupling mechanisms reflected in the modes discussed in the previous Section, lag correlation analysis has been carried out of

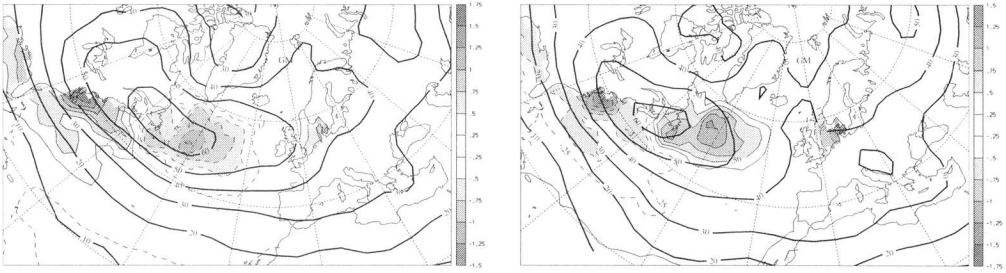


FIG. 3.9: Composite maps (left panel: upper quantile, right panel: lower quantile) of the first coupled mode of SST (shown the SST anomaly, shaded and thin lines, contour interval 0.25 K, negative contours dashed and zero line omitted) and storm track (thick lines, contour interval 10 gpm) based on SST scores. See text about details.

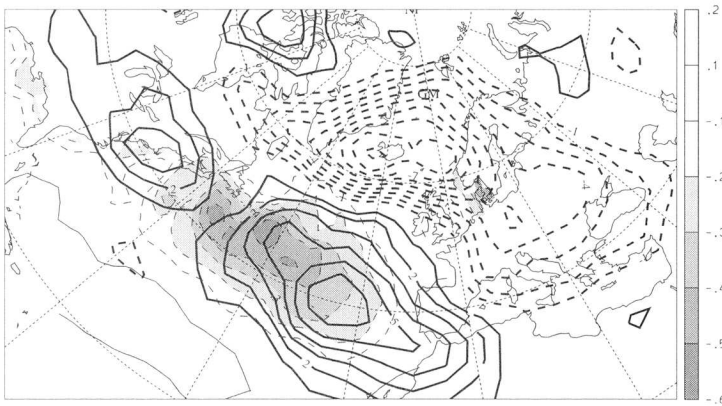


FIG. 3.10: As Fig. 3.8, but for the second coupled mode of SST and storm track.

the scores of the principal coupled modes (Bresch and Davies 1996). It will mainly serve to identify the direction of coupling between atmosphere and ocean, i.e. whether the atmosphere drives the ocean or vice versa. As in the previous Sections, we will mainly consider the winter season⁸ and therefore a lag of minus one month means that the correlations of the scores of the left field leading by one month (November, December, January) will be correlated with the winter season of the right field (December, January, February), while a lag of plus one represents November, December and January scores of the right field correlated with December, January and February scores of the left field. The significance levels of the presented correlations have been estimated following Sciremammano (1979), taking into account the respective field's autocorrelations. Fig. 3.13 (left panel) shows the result for the coupled modes of SST and geopotential height with significant correlations at zero lag and

⁸The scores throughout the year have been calculated using the winter patterns as presented in Section 3.2.

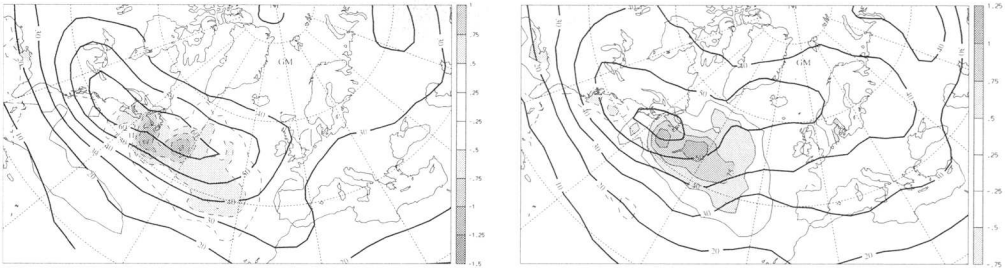


FIG. 3.11: As Fig. 3.9, but for the second coupled mode of SST and storm track.

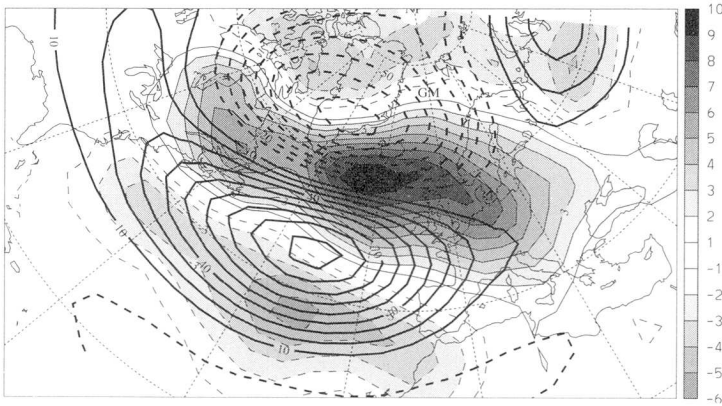


FIG. 3.12: First pair of coupled patterns of storm track (shaded and thin lines, contour interval 1 gpm, negative contours dashed and zero line omitted) and geopotential height (thick lines, contour interval 10 gpm, negative contours dashed and zero line omitted) based on monthly winter data over the North Atlantic sector. The patterns depict one standard deviation of the expansion coefficients.

with geopotential height leading SST by up to three months (similar amplitude for zero and one month lag⁹). The clear asymmetry of the lag correlation (especially for the principal modes) is thus indicative of the geopotential height field influencing the SST configuration (cf. Wallace and Jiang 1987; Wallace and Gutzler 1981). The analogous Figure (3.13, right panel) for the lag correlation of the scores of SST and storm track shows a similar asymmetry (cf. Fig. 3.13, left panel), but there is a more rapid decrease of the correlation for increasing lag. In contrast, the scores of the coupled modes of geopotential height and storm track do only correlate significantly at zero lag (correlation for first mode 0.78). A repetition of the lag correlation analysis with only the largest 25% of the respective scores reveals that the coupling mainly takes effect when the flow is in a state described by one of the dominant modes i.e. when the atmospheric flow is highly organised and hence capable to act coherently

⁹Repetition of the analysis for the coupled modes of SST and surface pressure leads basically to the same results.

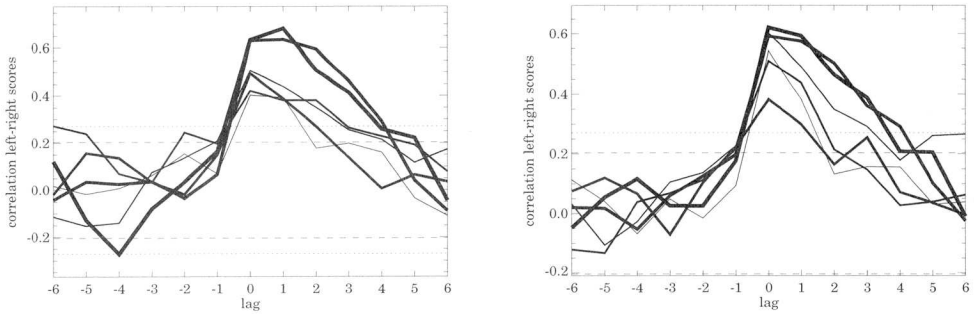


FIG. 3.13: Correlation of left and right scores for the first coupled modes of SST and geopotential height (left panel) and SST and storm track (right panel) as a function of lag (in months, negative lag values indicating SST leading geopotential height). Significance level dashed and (involving autocorrelations) dotted. Thickest line for first coupled pair, thinnest for 6th pair. See text about details.

upon the SST configuration. Motivated by the clear asymmetry revealed in Fig. 3.13, we performed lagged SVD analyses¹⁰, basically reproducing the results of Deser and Timlin (1997), i.e. the dominance of the atmosphere forcing the ocean.

Nevertheless, the analysis performed so far was entirely based on the linearly coupled modes. Lag composite plots based on high/low SST scores (Fig. 3.14) show atmospheric (response) patterns considerably different from Fig. 3.4, while the corresponding plots based on geopotential height scores are closely matching Fig. 3.5, and are therefore not shown. Note that the lag composite storm track plots based on SST scores reveal an even more pronounced difference (not shown). The asymmetry between the upper and lower quantile in Fig. 3.14 – together with the possibility that only strong SST anomalies influence the atmospheric flow – is indicative of the fact that a non-linear feedback of the SST configuration on the atmosphere cannot be captured by (even lagged) SVD analysis.

The picture is further complicated by the results of Ratcliffe and Murray (1970) – that contrast to some extent more recent studies – stating that the occurrence of warm (cold) SST anomalies in the so called RM-area¹¹ leads one month later to “progressive synoptic types” (blocking) in surface pressure, thus suggesting a clear feedback onto the atmosphere. Their results have been obtained by a study of composites of a few (~ 10) selected cases, which might pick out an effect obscured to methods covering a large domain and long times. Nevertheless, an attempt to reproduce their results using recent data and selecting events of high amplitude of the second mode resulted in situations as depicted in Fig. 3.15, where positive SST anomalies tend to precede more blocked-type flow and negative SST anomalies leading to more zonal flow – in contrast to the findings of Ratcliffe and Murray (1970) but in agreement with the results of Palmer (1995). While there seems to be an effect, it appears difficult to capture it by simple analysis, probably due to its non-linear mechanism, as will

¹⁰For example with left input fields leading the right ones by one month.

¹¹“A wide area south of Newfoundland”, more precisely a region comparable to our second SST pattern.

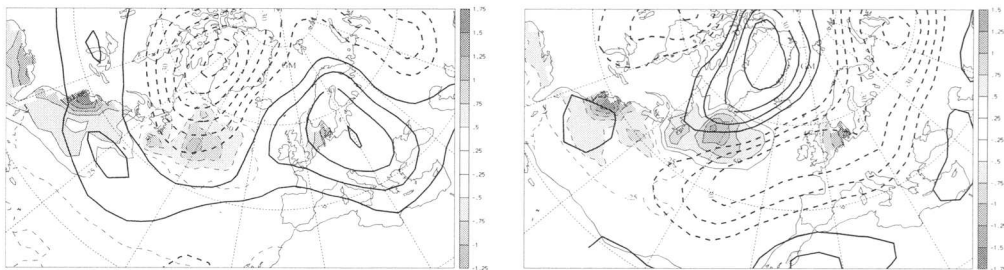


FIG. 3.14: Lag composite plots based on SST scores with subsequent (1 month later) geopotential height anomaly. Contour intervals 0.25 K (SST, shaded and thin lines) and 10 gpm (geopotential height, thick lines), negative contours dashed and zero line omitted. Note the differences between the structure of the upper (left panel) and lower (right panel) quantile. See text for details.

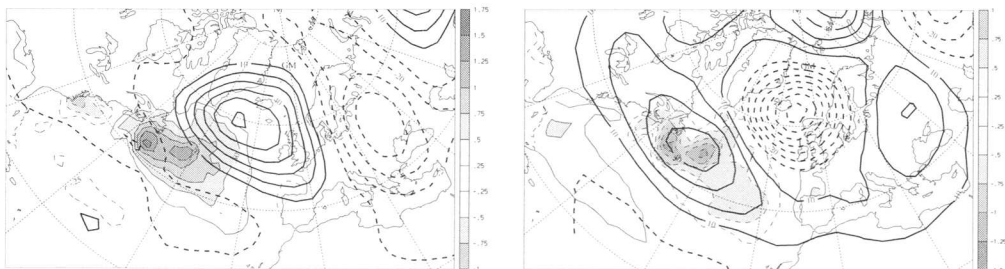


FIG. 3.15: Lag composite plots for the second coupled mode of SST and geopotential height. Shown are the mean over the 10 months with highest scores of the SST pattern (shaded and thin lines, contour interval 0.25 K, negative contours dashed and zero line omitted) and the mean over the geopotential height field of the respective subsequent month (thick lines, contour interval 10 gpm).

be further discussed below.

Furthermore, the use of ∇ SST instead of SST leads to patterns approximately similar to what would have been expected by taking ∇ of the SST patterns, the lag correlation with storm track – for example – being only a peak at zero lag¹², indicative of the importance of surface baroclinicity. The issue of the direction and strength of the forcing will be pursued further in Section 3.5.

3.4 Trends

During the period from 1962 to 1994 the NAO index (Fig. 3.3) exhibited an overall positive trend corresponding to a decrease (increase) in SLP over Greenland-Iceland (Central Atlantic), and furthermore the associated change in the thermal component of the tele-

¹²The lag correlation for geopotential height leading ∇ SST is considerably weaker as for zero lag as well.

connection pattern accounts for $\sim 31\%$ of the concomitant hemispheric surface temperature change (Hurrell 1996). Thus this phase of the NAO warrants further study, and it is the accompanying variation in the structure of the free atmosphere over the extratropical North Atlantic and the linkage with the underlying SST that forms the theme of this Section.

The strategy followed is to examine the ‘basic’ fields (i.e. SST, geopotential height at 500 hPa and storm track) in a three-stage process (Bresch and Davies 1998a). First a conventional trend analysis is made of each field for the entire period. The linear trend is evaluated at each grid point, assessed with the Mann-Kendall significance test (Kendall 1970) and accepted if significant at the 95% confidence level. The resulting fields are referred to hereafter as the ‘observed’ trend.

In the second stage the data is first modified as described in Section 3.1 and subject to a SVD analysis. Recall that the first geopotential height pattern, appearing in both the first coupled mode with SST and storm track, is closely related to the NAO, and is referred to as the NAO mode.

The third stage is designed to explore the significance and interdependence of the modes in relation to the ‘observed’ long-term trends. First the original raw (i.e. non-detrended) data is decomposed into the previously computed SVD modes (i.e. the seasonally-independent detrended modes), and the resulting time series of ‘raw’ scores subjected to a linear regression to yield the ‘raw’ long-term linear trends. This ‘construction’ procedure determines the amount of the observed long-term linear trend captured by the recurring monthly SVD modes. Further insight on the interdependence of the modes is sought by noting that, using the diagonal elements of the cross-covariance matrix of the coupled SVD modes, the right scores can be reconstituted from the left ones and vice versa (see Section 2.1.4). Thus this ‘reconstruction’ procedure builds upon the coupled nature of the modes and provides an estimate of the fraction of the trend in one field that can be linearly inferred from the trend in the other. It provides a measure of the effectiveness of estimating the trend of one coupled component from the other.

3.4.1 Observed Decadal Trends

In Fig. 3.16 the decadal trends for the 1962-1992 period of the SST and the 500 hPa geopotential height (Panel a) and storm track (Panel b) are shown. The SST trend is dominated by a dipole pattern in the western North Atlantic that has maximae of ~ 0.5 K per decade. Thus there is a significant enhancement of the baroclinicity in the Western Atlantic, and a more modest increase is also evident in the Eastern Atlantic. The signature does in fact spread through a major depth of the mixed layer. Levitus et al. (1994) found a similar linear trend at a depth of 125 m for the same period. The geopotential height trend assumes an NAO-like dipolar form, and the height change between Iceland and the Azores (~ 50 gpm) equates to an increase of ~ 2.5 ms^{-1} per decade in the zonal wind (cf. Kodera and Koide 1997), consistent with the recent increase in North Atlantic wave height (Kushnir et al. 1997). In comparison with the other two fields the trend in the dynamic storm track has a much richer spatial structure. There is an overall narrowing of the storm track’s width, and there is a decrease in amplitude over the Western Atlantic and strengthening over both mid-Atlantic and Europe. The dipolar trend in the geopotential signal is in harmony with

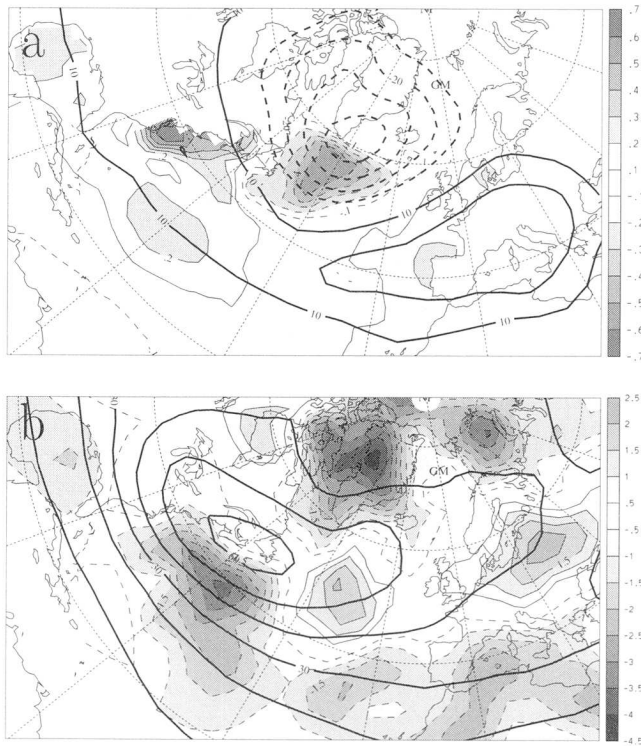


FIG. 3.16: Decadal winter trend based on 1962-1992 data over the North Atlantic sector for SST (Panel a, shaded, contour interval 0.1 K, negative contours dashed) and geopotential height at 500 mb (Panel a, thick lines, contour interval 10 gpm, zero line omitted, negative contours dashed). Panel b shows the decadal dynamic storm track winter trend (shaded, contour interval 0.5 gpm, negative contours dashed) and the mean winter storm track (thick lines, contour interval 10 gpm).

the concomitant strengthening of the SLP index of the NAO. Moreover there are physically inter-related features of the three trend patterns. Enhanced gradients of SST and geopotential height over the Western Atlantic are conducive to a more rapid eastward propagation of baroclinic disturbances originating off the eastern US seaboard, and this effect can contribute to an eastward translation of the oceanic maximum in the storm track's intensity. Likewise the occurrence of similar SST and geopotential trends off the European coastline favour more vigorous cyclones propagating further onto the mainland (cf. storm track signature over Europe).

3.4.2 (Re-) construction of the Trend Patterns

In the SVD analyses of the previous Section the first six modes of each set of coupled fields always explained more than 90% of their total squared cross-covariance, and it is only these modes that are retained for the computations in this Section. The modes are used to evaluate the ‘constructed’ and ‘reconstructed’ decadal trend patterns. Recall that the former is derived by projecting the raw (non-detrended) field upon the corresponding significant SVD modes of the detrended data of that same field, and the latter estimates the trend of one component of a mode-couplet from the temporal evolution of the significant modes of the other component (e.g. the SST scores are estimated from the original geopotential height scores). Constructed and reconstructed decadal-trend of a selection of fields are displayed in Fig. 3.17. The upper panel is for the SST. It shows that the structure of the ‘constructed’ (shaded) pattern (based upon the SVD modes of the ‘SST-height’) bears comparison with the ‘observed’ linear trend shown in Fig. 3.16a but its amplitude is less by $\sim 40\%$. The ‘reconstructed’ pattern, based upon the height field, fails to reproduce even the gross features of the observed trend. Deser and Blackmon (1993) attributed the gradual surface warming in the Gulf Stream region to altered ocean currents rather than atmospheric forcing. The pattern does however exhibit a modest and realistic positive trend in the North Sea that is not captured by the constructed field. The direct inference is that this feature might be related to atmospheric forcing, as suggested by Taylor (1996), on the basis of zooplankton fluctuations.

The corresponding results for the height field trends are shown in Fig. 3.17b. The constructed trend (shaded) captures more than 50% of the observed trend (cf. Fig. 3.16a), and in particular it reproduces the dipolar ‘Greenland-central Europe’ signal. In sharp contrast to the previous result, the reconstructed trend (based on the SST scores) is significant. It recovers the signal over Greenland and explains nearly 50% of its central amplitude, but it does not incorporate the signal over Europe. In this case the inferences are that the signal over Europe might be linked to internal atmospheric variability, whereas the large-scale dipole over the North Atlantic could be subject to significant SST influence.

Examination of the patterns for the storm track trends (Fig. 3.17c) indicates that the ‘constructed’ field captures rather less of the admittedly weak observed trend (cf. Fig. 3.16b) than does the ‘reconstructed’ field (derived from the SST scores). In particular the ‘reconstructed’ trend captures the decrease of the storm track amplitude off the east coast of North America and a signal over central Europe. Thus this result lends support to the hypothesis that the SST can exert a significant influence upon the storm pattern and its intensity. (Note that the reconstruction of the SST trend from the storm track scores was not successful).

The derived wintertime decadal trends of SST, geopotential height and storm track in the extratropical North Atlantic during the period 1962-1992 are related to and reflect the contemporaneous strengthening of the NAO. In particular the dipolar pattern of the SST and geopotential height trends in the Western Atlantic connote enhanced mean values of low-level baroclinicity and mid-tropospheric zonal flow, and together these characteristics are conducive to the observed eastward translation of the maximum in the storm track’s intensity. Likewise the similar, albeit weaker, SST and height signatures off the European

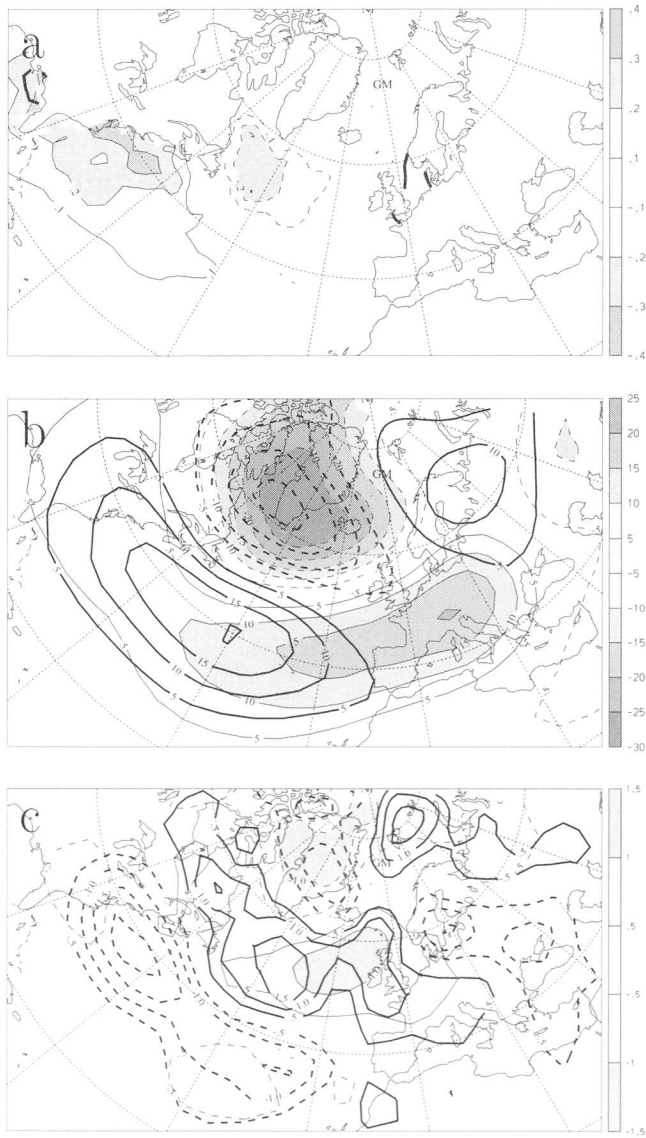


FIG. 3.17: Constructed (shaded) and reconstructed (thick lines) decadal trends for SST (Panel a, contour interval 0.1 K), geopotential height (Panel b, contour interval 5 gpm) and storm track (Panel c, contour interval 0.5 gpm). In all panels, the zero line is omitted and negative contours are dashed.

coastline favour the propagation of frontal-wave cyclones onto the mainland and this is in line with the observed modest increase in the storm track signature over Europe.

Linear trends constructed from the dominant SVD modes of individual fields possess patterns that, for each of the three fields, resemble the observed form but show only $\sim 50\%$ of the amplitude. In contrast the strength of the linear trend for one field ‘reconstructed’ from the evolution of the dominant SVD modes of a coupled field depends strongly upon the choice of fields. For example computation of the decadal height trend from the SST scores recovers the general pattern and $\sim 50\%$ of the amplitude, whereas the inverse reconstruction is unsuccessful over almost all the domain.

The comparatively short length (i.e. three decades) of the time-series used herein does not suffice to draw firm conclusions. However the results suggest that the dominant SVD modes do represent a significant part of both the intraseasonal variability and the decadal trends. The concomitant inference is that the strengthening phase of the NAO was characterised by changes in amplitude (and/or frequency) of recurrent weather modes rather than involving a transition towards a new regime. It has been emphasised by Palmer (1993) (and Palmer 1998) that nonlinear dynamics may well change the frequency distribution of weather regimes in the atmosphere, rather than changing the regimes. It will therefore be of interest to examine the more irregular behaviour of the NAO in recent years in terms of the same SVD modes.

Again our reconstruction procedure enables a significant portion of the height and storm track trends to be (statistically) inferred from the changes in the SST configuration, and thereby leaves open the dynamical issue of SST-forcing of the overlying atmosphere on both intraseasonal and longer time-scales.

3.5 Discussion

To identify the leading coupled modes of SST, geopotential height at 500 hPa and storm track of the wintertime circulation over the North Atlantic sector, SVD analyses of the seasonally detrended data have been performed. Distinctive recurrent coupled patterns have been identified, the first two modes explaining over 30% of the intraseasonal variability of the observed fields and their interrelations. The stability of the identified structures has been tested by several means: variation of the domain, Monte-Carlo time scrambling, comparison to the leading EOFs of the involved fields and inspection of composite maps.

The dipole of the first geopotential height pattern and the concomitant structure of the North Atlantic storm track is coupled to a dipole pattern in the SST field. This mode reflects strong and weak zonal flow regimes in its two extremes, as further illustrated by composite maps. There is some evidence that the atmospheric configuration might dominate this mode, since the SST pattern – at least its northern anomaly – can be regarded as the result of anomalous surface fluxes. The observed bimodality of the flow is further reflected in anomalies of surface pressure, temperature and precipitation over Northern Europe, espe-

cially related to a shift of the sensitive tail end of the cross-Atlantic storm track (Fraedrich et al. 1993).

The second coupled mode is dominated by a monopole in the central North Atlantic in geopotential height and SST and a deflection of the storm track. Inspection of the composite maps clearly reveals a blocked type of flow over the central North Atlantic, together with a northeastward deflected storm track for the lower quantile, contrasting to a zonal flow regime (with zonally elongated and confined storm track) in the upper quantile. Hence this mode can be interpreted in terms of zonal flow versus blocking (Namias 1964; Hoskins et al. 1983; Malberg and Frattesi 1995).

The results of a lag analysis of the scores correlations reveals that there appears to be stronger forcing of the ocean surface by the atmosphere than vice versa. This result is in line with some previous studies (Lanzante 1984; Zorita et al. 1992; Deser and Timlin 1997), where it is stated that the peak amplitude occurs for the atmosphere leading the ocean by 2-3 weeks with doubled amplitude compared to zero lag. Recall that any non-linear relations between the two fields observed might not be detected with SVD analysis. Hence these results only state that the forcing of the ocean by the atmosphere dominates the *linear* coupling, but they do not rule out feedback of the ocean to the atmosphere. Under conditions of high wind speed, the fluxes of latent and sensible heat will be considerably larger in the presence of warm compared to cold SST. While the ocean surface will be cooling in both cases, the different amplitude of the fluxes might lead to different atmospheric responses. Hence a linear analysis will probably just reveal the relation of high wind speed with ocean cooling, while the feedback of the ocean conditions on the atmosphere might not be captured due to their non-linear nature especially in mid-latitudes¹³. The fact that the storm track modes do not show such a clear time lag-structure (and correlating with geopotential height only at zero lag) indicates that the large-scale atmospheric forcing might primarily affect the SST advection (*compare* Deser and Timlin 1997) while the dynamics of the transient eddies can be (strongly) affected by the lower boundary conditions. The characteristic time scale of synoptic scale systems on the order of a few days also suggests that SST feedback might be contained within the contemporaneous correlations of the dominant modes of covariability even on weekly time scales. Furthermore, SST influence on the atmospheric flow evolution might also be manifest as increased persistence or variability of certain flow signatures. Again, as this effect might be specific to certain circulation regimes (and their sign and amplitude), it might not be identified by SVD analysis.

The investigation of the last 30 years' trends of the aforementioned fields suggests that the dominant SVD modes do represent a significant part of both the intraseasonal variability and the decadal trends. The concomitant inference is that the strengthening phase of the NAO was characterised by changes in amplitude (and/or frequency) of recurrent weather modes rather than involving a transition towards a new regime.

¹³In this context, Deser and Timlin (1997) suggested examining the weekly lag associations in the Tropics, where genuine two-way interactions take place: does the methodology (lagged SVD) separate the two directions of interaction?

Leer - Vide - Empty

Chapter 4

Idealised Study

In the previous Chapter a statistical study was made of the coupled modes of ocean and atmosphere on a monthly time scale. It was shown that the atmosphere dominates the linear coupling, but a feedback of the ocean to the atmosphere can not be ruled out.

In this Section, consideration is given to the effect of the SST configuration on the atmospheric flow evolution in an idealised model setting. The motivation is that this strategy might yield insight on the (nonlinear) interaction of ocean and atmosphere. While it would be necessary to study the coupled ocean-atmosphere system in order to establish a realistic relationship between the two components on intraseasonal and longer time scales, an atmospheric model with prescribed SST (and land surface) configuration is useful for understanding whether the atmosphere is able to respond to a persistent midlatitude SST anomaly, regardless of how the anomaly has been generated and maintained. In light of the persistence time scale of SST anomalies (Davis 1976), this restriction is not unrealistic on monthly to seasonal time scales.

The idealised model is run with full dynamics and physics of a NWP model but with no orography and with comparatively high horizontal and vertical resolution (see Section 2.3.2). The model geometry has been chosen to be simply a rectangular (in lat/lon) ocean basin of approximately the dimensions of the North Atlantic, so that the model is operated on a half-hemispheric domain with periodic boundary conditions in the zonal and relaxed boundaries in the meridional direction.

The model is initialised with a zonally homogeneous baroclinic basic state close to the 10 year ECMWF winter mean climatology. To instigate the growth of observed mid-latitude synoptic scale systems, an upper-level potential vorticity (PV) anomaly has been imposed above the center of the ocean basin. Recall that, except for the solar irradiation angle, all external model parameters (ozone distribution, soil parameters) are kept fixed to winter mean values. Each model simulation is run for 4 months, from 1st of November through end of February and the analyses (and figures) of this Chapter are based on the last 3 months of simulation time (DJF), so that the term ‘mean’ pertains to the December - January period.

In addition to a control simulation with a specified mean SST distribution, a series of experiments with imposed SST anomalies have been undertaken. The shape, amplitude and location of the imposed SST anomalies have been chosen to represent – in an idealised manner – the patterns revealed by the statistical analysis of Chapter 3. The atmospheric response is

investigated in terms of changes in the storm track position and amplitude and changes in the mean geopotential height and surface pressure fields relative to the control simulation, and the effect of the imposition of SST anomalies will also be assessed by comparison with the statistically derived coupled modes of atmospheric variability of the previous Chapter. The comparison with the statistically derived coupled modes of variability has to remain qualitative, the idealised configuration making a quantitative approach impossible. Thus the primary focus of the experiments is to examine the structure and amplitude of the atmospheric response to midlatitude SST forcing on monthly to seasonal time scales. (Note that a detailed investigation of the involved physical processes will not be undertaken.)

The control simulation and a detailed discussion of the model climate is presented in Section 4.1, followed by a documentation and a investigation of the effect of various SST configurations (Section 4.2) and a comparison of the simulations in terms of surface fluxes (Section 4.3). To facilitate comparison of the figures presented in this Section, fixed contour intervals have been used for similar figures.

4.1 Control Simulation

The control simulation (hereafter referred to as CTRL) has been run with the idealised model configuration described in Section 2.3.2. The sequence of the geopotential height and surface pressure fields during the first 5 days of January¹ (Fig. 4.1, upper panels) portray a realistic flow evolution with the main activity concentrated over the ocean basin. The PV distribution on the 310 K isentropic surface (Fig. 4.1, lower panels) includes some common features such as PV streamers and seclusion, (re-) merging and decay of PV elements (Appenzeller and Davies 1992; Fehlmann and Davies 1997).

Further indication of the relationship of the CTRL simulation to real climate can be derived from a comparison of the time-mean zonally averaged cross-section (Fig. 4.2, right panel) with the ECMWF 10 year climatology (Fig. 2.3, left panel). The model modifies the initial vertical structure (Fig. 4.2, left panel) toward the observed climatology but it does not reproduce the correct strength of the meandering of the mean flow (stationary planetary wave pattern), thus the southward extension (second maximum) of the jet is not as pronounced as in the ECMWF climatology.

The storm track of the CTRL simulation (Fig. 4.3), based upon the Murakami-filtering of the geopotential height field at 500 hPa, is comparable in amplitude to the observed North Atlantic storm track and is slightly intensified over the ocean basin downstream of the point of maximum surface baroclinicity (cf. Whitaker and Dole 1995). However it extends too far eastward and the unrealistic extension can be attributed to the maintenance of eddy activity far downstream of the region of maximum baroclinicity through the ageostrophic geopotential fluxes (Chang and Orlanski 1993) and the lack of gravity wave drag as a result of the flat land-mass (Palmer et al. 1986). This problem was also observed in the winter climate of the ECHAM3 model (Kaurola 1997) and when increasing the resolution of the ECMWF GCM, prior to parametrisation of the gravity wave drag (Palmer et al. 1986).

¹Similar figures could have been drawn for any time of the simulation, the selected period shows some notable features within the stipulated time period.

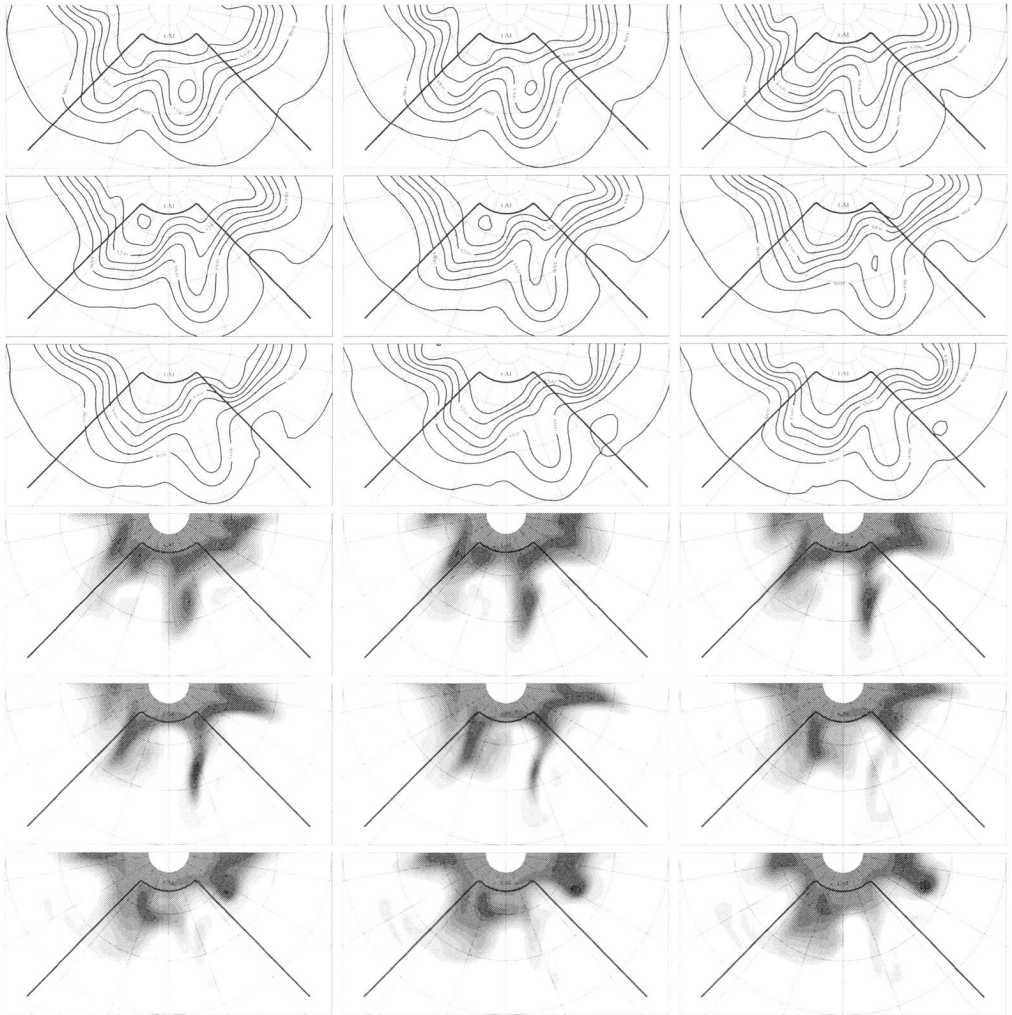


FIG. 4.1: Upper panels: Geopotential height at 500 hPa (thick lines, contour interval 100 gpm) of the first 96 hours of January every 12 h. Lower panels: PV distribution on the 310 K isentropic surface for the same period. Contour intervals at 0.4, 0.5, 0.6, 1, 1.5, 2, 2.5, 3, 3.5, 4, 5 pvu ($1 \text{ pvu} = 10^{-6} \text{K m}^2 \text{kg}^{-1} \text{s}^{-1}$). The very thick black line indicates the boundary of the ocean basin.

Furthermore, there is no clearly established stationary trough over the eastern part of the land area / western ocean and this might be linked to the absence of phase-locking of the planetary waves with respect to the land masses by orography and other asymmetries.

The time-mean surface pressure field (Fig. 4.4) shows a large low-pressure system in the northeastern part of the Ocean basin (cf. Icelandic low) and an extended area of high-

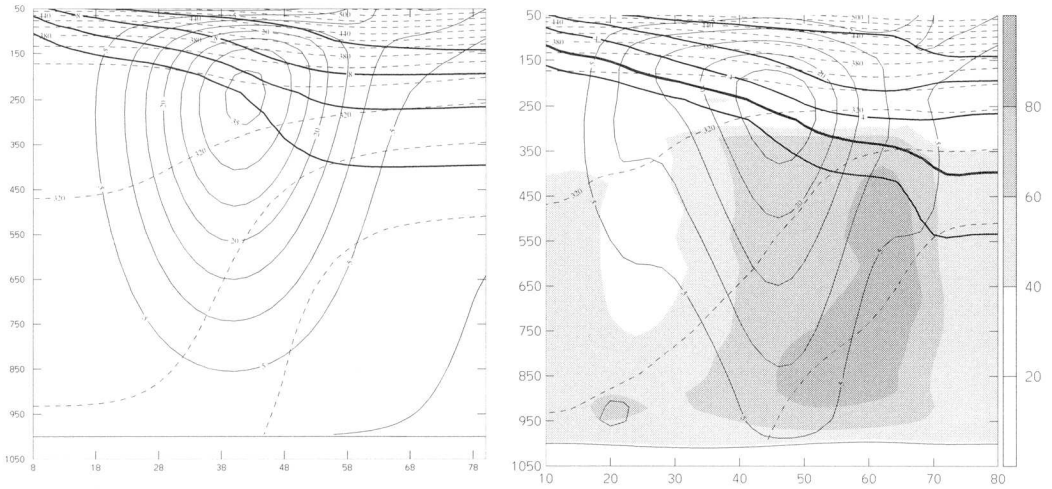


FIG. 4.2: CTRL simulation: Zonal mean cross section. Initial state (left panel) and simulation mean (DJF, right panel). Mean zonal wind (thin lines, contour interval 5 m s^{-1}), Θ (thin dashed lines, contour interval 20 K), PV (thick lines, contours at 1, 2, 4, 8 and 16 pvu) and relative humidity (shaded, in percent).

pressure with center over the eastern continent (cf. Asian high). The Murakami filtered surface pressure (reflecting the surface track of cyclones) is enhanced over the ocean basin and considerably weakened over land (probably due to surface friction). The distribution of the Murakami filtered PV at 310 K (Fig. 4.5, a measure of the PV storm track) corresponds to the observed PV variance (Fehlmann 1997), but penetrates also too far into the continent.

In summary, the CTRL simulation appears to reasonably well reproduce the mid-latitude synoptic scale systems (cf. Fig. 4.1), their climatology (cf. Fig. 4.3) and the mean vertical structure (cf. Fig. 4.2). Hence it is appropriate to use the idealised model to study the effect of localised SST anomalies on the atmospheric flow evolution.

4.2 Experiments

As noted earlier the sensitivity of the idealised model climate to the SST configuration is assessed by imposing a series of SST anomalies. The shape, amplitude and location of the imposed SST anomalies were chosen to represent – in an idealised manner – the patterns revealed by the statistical analysis of Section 3.2. To assess the relative importance of single constituents of a given SST pattern with respect to the atmospheric response, additional experiments with only selected *parts* of a given SST pattern have been undertaken.

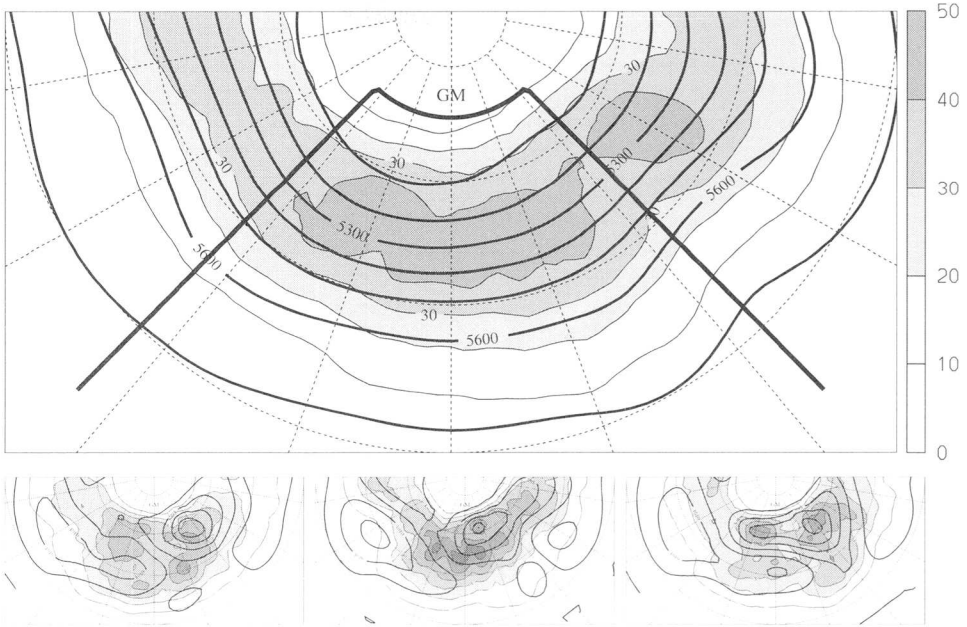


FIG. 4.3: CTRL simulation: Murakami filtered geopotential height at 500 hPa (shaded and thin lines, contour interval 10 gpm) and geopotential height (thick lines, contour interval 100 gpm). Upper panel simulation mean (3 months, DJF), lower panel monthly means of the three winter months (D,J,F). Negative are always dashed and the zero contour is omitted. The very thick black line indicates the boundary of the ocean basin.

4.2.1 SST Dipole Anomaly

A dipole anomaly derived from the first SST EOF (Fig. 4.6) is imposed in the first experiment (hereafter referred to as EXP 1). It is assigned a peak amplitude of 3.5 K and it strengthens the SST gradient in the western part of the ocean basin. The first statistically derived coupled mode of SST and storm track (Fig. 3.8) reveals that a SST dipole in the western North Atlantic is coupled to an amplification and zonal confinement of the storm track. A similar effect on the idealised control storm track might be expected as a response to the imposition of the idealised SST dipole. Likewise, an enhancement of the stationary geopotential height trough would be expected based on the first statistically derived coupled mode of SST and geopotential height (Fig. 3.2).

The results of the first experiment (Fig. 4.7) show that the imposed SST anomaly affects both the storm track and mean geopotential height field. The storm track is moderately intensified and the geopotential height trough is enhanced over the central ocean. The structure of the response is more clearly brought out by a comparison with the CTRL climate (Fig. 4.8). Whereas the winter mean storm track shows a moderate intensification, there is considerable variation among the individual months. The geopotential height response

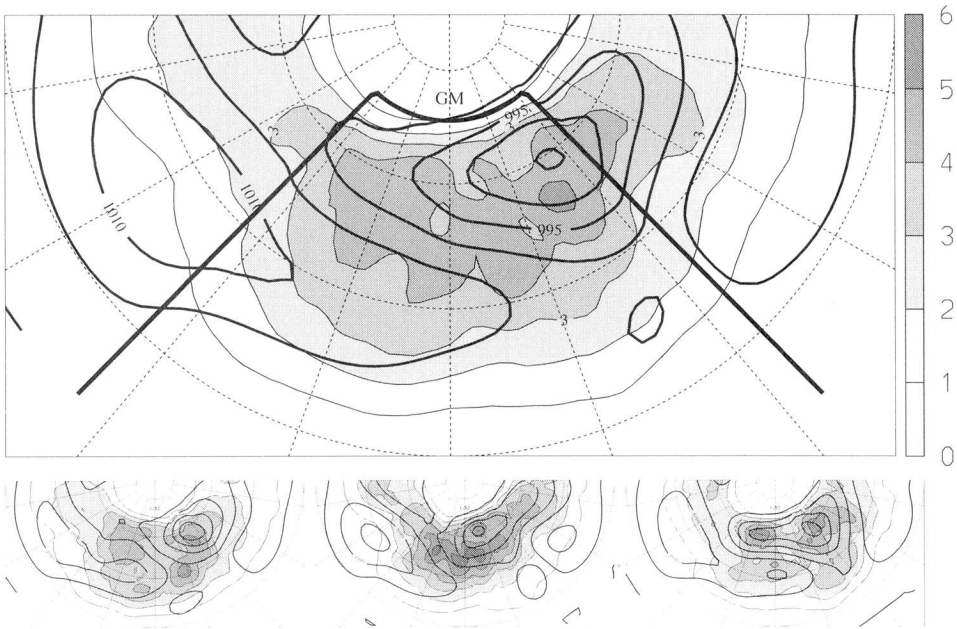


FIG. 4.4: As Fig. 4.3, but for Murakami filtered surface pressure (shaded and thin lines, contour interval 1 mb) and mean surface pressure (thick lines, contour interval 5 mb).

displays more consistency throughout the winter and differences larger than ± 25 gpm are significant at the 95%-level². Recall however that the stationary trough of the CTRL-simulation was itself unrealistically weak. Note further that the imposed SST anomaly can not only intensify, but also shift and distort the atmospheric flow patterns, which further complicates the assessment of the response in terms of difference fields with respect to the CTRL simulation.

The surface pressure response (Fig. 4.9, left panels) is in harmony with the geopotential height response, but it also has an additional region of negative surface pressure anomaly over the warm part of the imposed SST dipole. The Murakami filtered surface pressure – a measure for the surface storm track – is intensified, as is the Murakami filtered PV at 310 K (Fig. 4.9, upper right panel).

The time-mean zonally averaged cross-section of the EXP 1 simulation resembles the CTRL simulation (not shown), but the jet axis is shifted slight southward (cf. the enhanced meandering of the flow as apparent – for example – in Fig. 4.7 or 4.9).

While the imposition of the SST dipole does not result in atmospheric anomalies that project on the statistically derived coupled patterns, some particular features of the idealised

²Prior to a two-tailed Student's *t*-test, the six hourly model data has been filtered by application of a 3-day running mean to account for the characteristic time scale of synoptic-scale processes. It has to be noted that the test values based on unfiltered data were even higher.

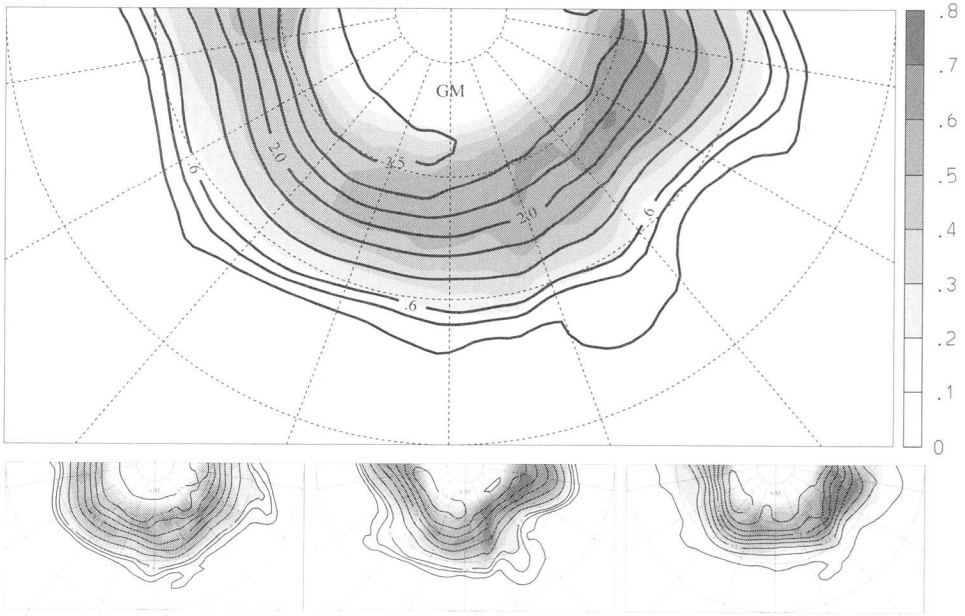


FIG. 4.5: As Fig. 4.3, but for PV at 310 K. Murakami filtered PV (shaded and thin lines, contour interval 0.1 pvu) and mean PV (thick lines, contours at 0.4, 0.5, 0.6, 1, 1.5, 2, 2.5, 3, 3.5, 4 and 5 pvu).

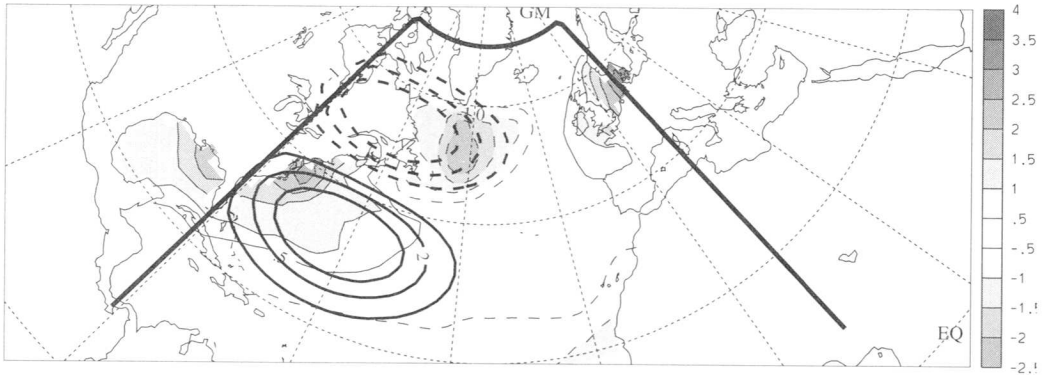


FIG. 4.6: First statistically derived SST pattern (shaded, contour interval 0.5 K, as in Fig. 3.2) and the dipole anomaly used in the EXP 1 simulation (thick lines, contour interval 1 K). See Fig. 2.4 about the idealised mean SST distribution.

model results (intensification of the storm track and geopotential height trough) can be

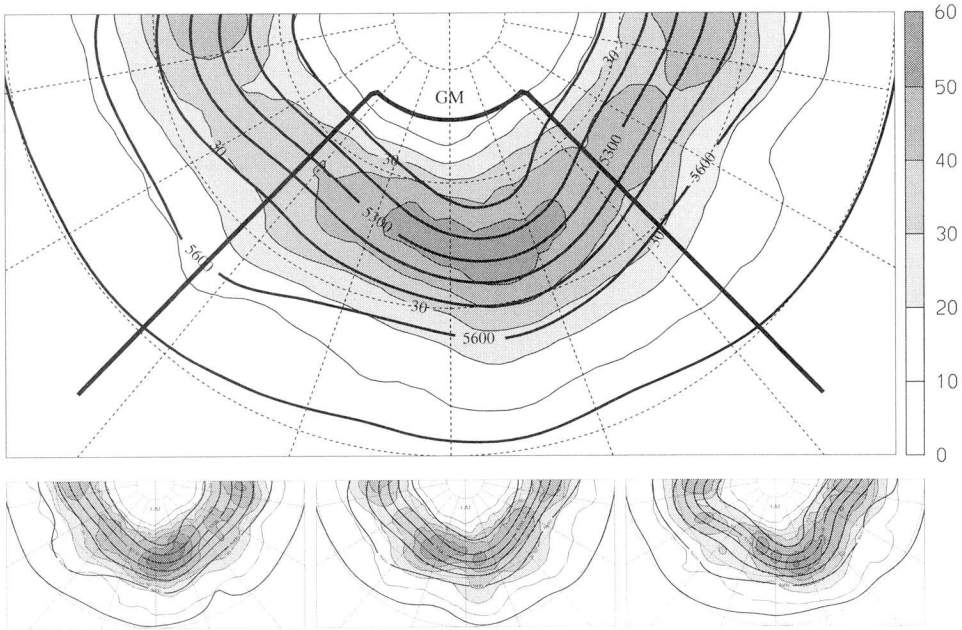


FIG. 4.7: As Fig. 4.3, but for the EXP 1 simulation.

related to the general structure of the first coupled mode. To help assess and calibrate the statistical significance of the response patterns (see above), two further modified sensitivity experiments were undertaken. Repetition of EXP 1 with only 75% of the amplitude of the SST dipole produced a slightly weaker response, structurally similar to EXP 1. The imposition of a SST anomaly with twice the amplitude as in EXP 1 (admittedly not a very realistic setting) produces a very strong response (Fig. 4.10), enhancing all the features observed in EXP 1 except for the 500 hPa storm track which shows no further increase of its amplitude. Note the strong increase of the surface cyclone track which appears to emanate from the positive SST anomaly. These additional experiments suggest that there is a significant atmospheric response to a modification of the SST configuration.

4.2.2 Decomposition, Shift and Reversal of Anomaly Pattern

To assess the question whether it is the dipole in its entirety (EXP 1) or the warm or cold anomaly alone that contribute most to the observed response, experiments were performed with separate parts of the dipole. The experiments with the warm anomaly alone and the cold anomaly alone will be referred to respectively as EXP 2 and EXP 3. Furthermore, an experiment with a northeastward shifted warm anomaly and one with inverse sign of the dipole will be presented. The discussion will follow after the description of all model experiments.

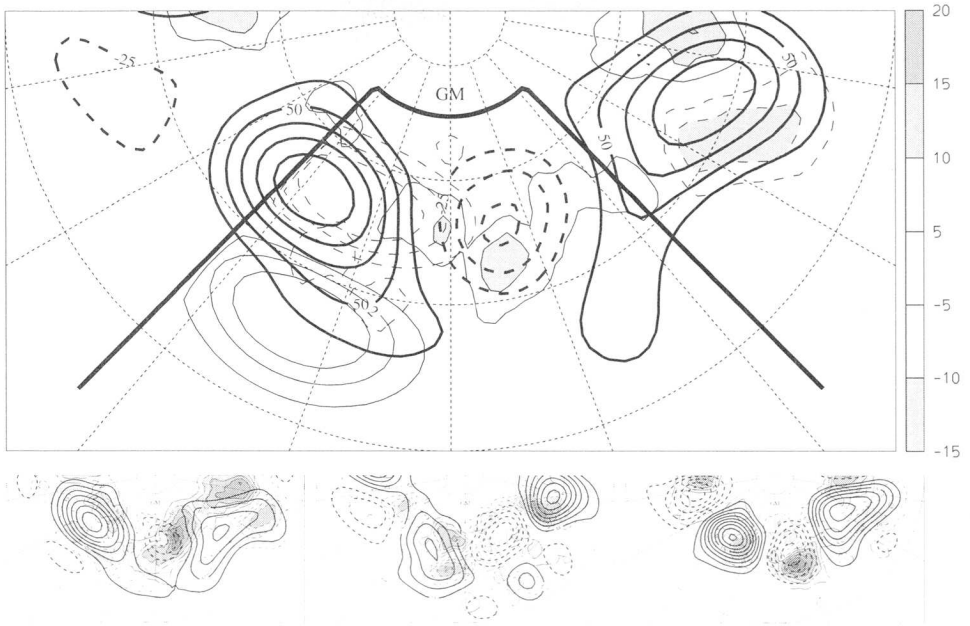


FIG. 4.8: As Fig. 4.3, but for the *difference* EXP 1 - CTRL, contour interval 5 gpm for the storm track (shaded) and 25 gpm for the geopotential height (thick lines) difference. Thin lines the imposed SST anomaly, contour interval 1 K.

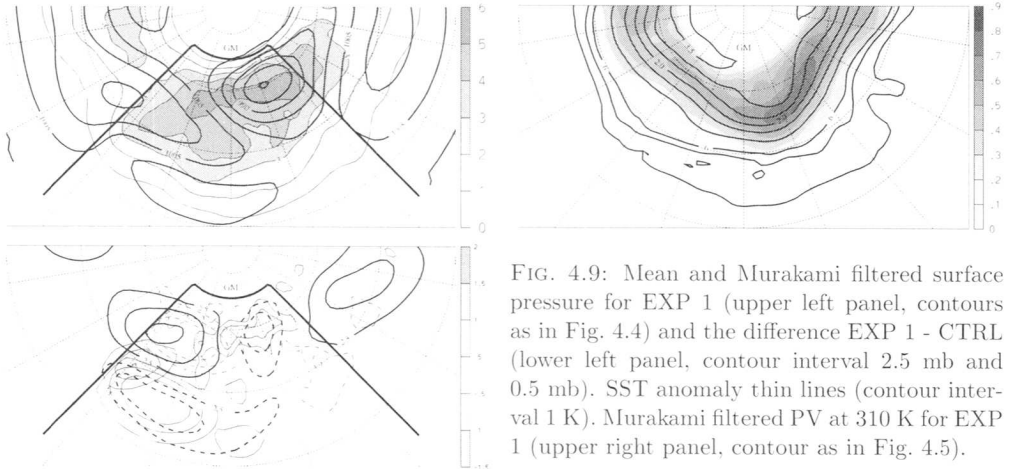


FIG. 4.9: Mean and Murakami filtered surface pressure for EXP 1 (upper left panel, contours as in Fig. 4.4) and the difference EXP 1 - CTRL (lower left panel, contour interval 2.5 mb and 0.5 mb). SST anomaly thin lines (contour interval 1 K). Murakami filtered PV at 310 K for EXP 1 (upper right panel, contour as in Fig. 4.5).

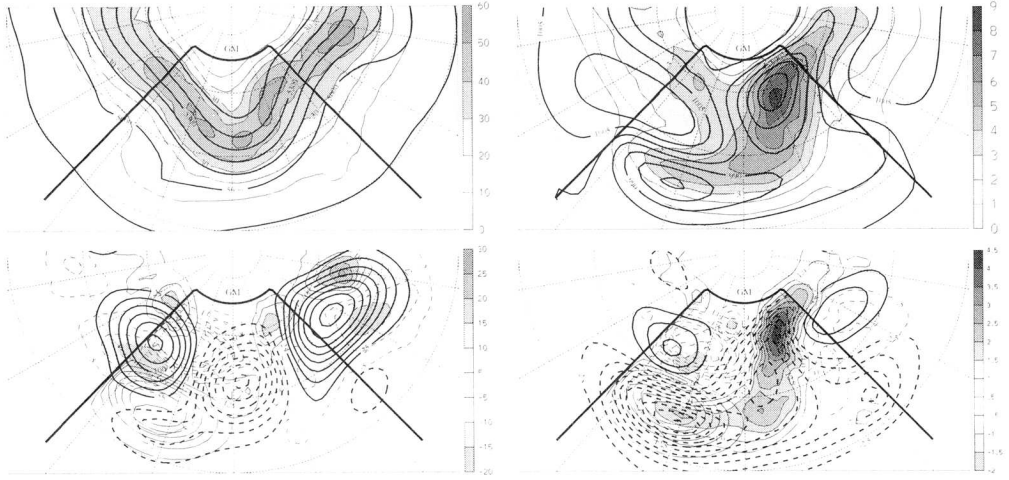


FIG. 4.10: As EXP 1, but with doubled amplitude of the imposed the SST anomaly: Mean and Murakami filtered geopotential height (upper left panel, contours 100 gpm and 10 gpm, respectively) and difference to the CTRL simulation (lower left panel, contours 25 gpm and 5 gpm, respectively). Mean and Murakami filtered surface pressure (upper right panel, contours 5 mb and 1 mb, respectively) and difference to the CTRL simulation (lower right panel, contours 2.5 mb and 0.5 mb, respectively). The thin lines depict the imposed SST anomaly, spaced by 1 K.

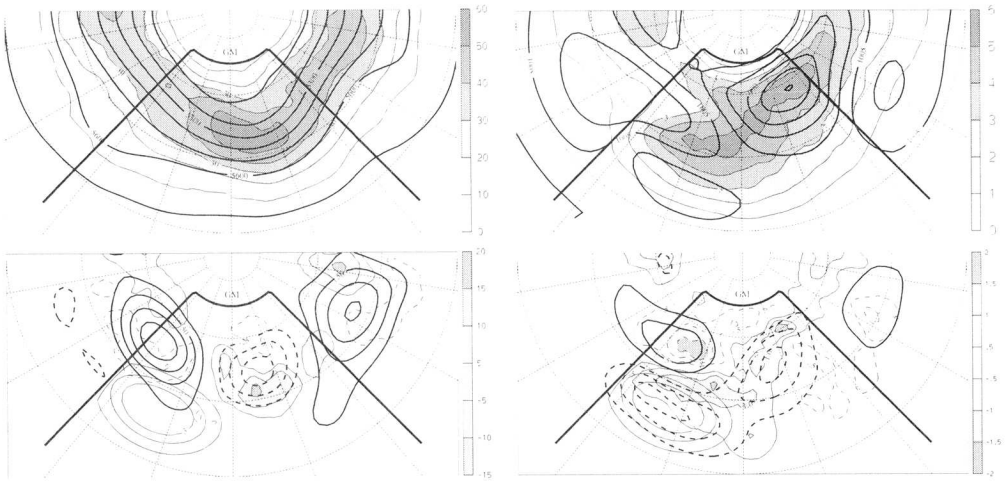


FIG. 4.11: As Fig. 4.10, but for EXP 2 (warm anomaly only).

The response to the warm anomaly alone (EXP 2) is presented in Fig. 4.11. The geopotential

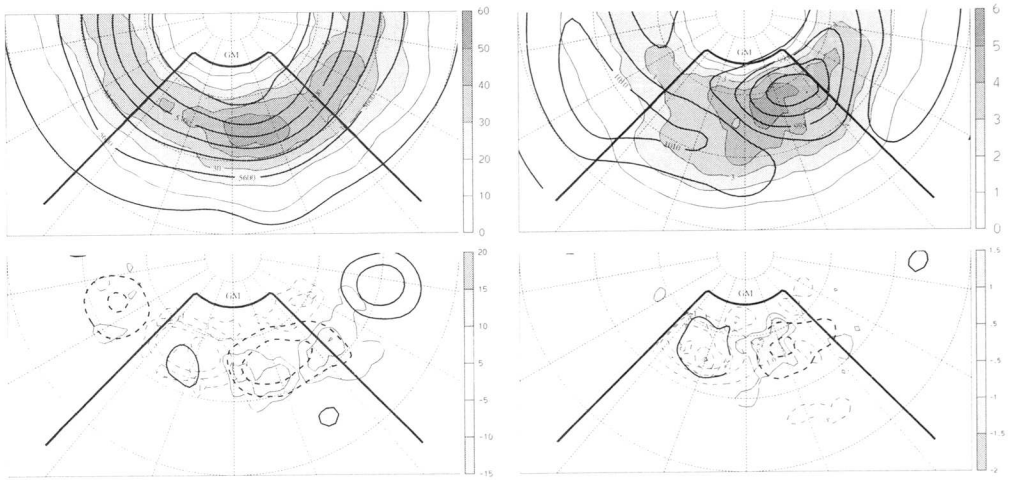


FIG. 4.12: As Fig. 4.10, but for EXP 3 (cold anomaly only).

height and storm track response is comparable to the signal of the entire dipole anomaly (Fig. 4.7) and the surface pressure and surface storm track response is somewhat stronger. While the geopotential height response in the simulation with the cold anomaly only (EXP 3, Fig. 4.12) is considerably reduced, the storm track is still stronger compared to the CTRL run and the surface pressure response is considerably weaker in comparison with the warm anomaly case. The month-to-month variation of the storm track difference EXP 3 - CTRL is much larger than for EXP 2 - CTRL (not shown). It suggests that the significance of the storm track signal of the cold anomaly only experiment is smaller than for the warm anomaly only run.

Recall that the composite plots in Chapter 3 (Fig. 3.5) reveal that it is essentially the northern part of the SST anomaly which is linearly coupled to the first geopotential height mode. Therefore, the cold anomaly is the part of the SST dipole more directly affected by the atmosphere.

To check whether the effect of the positive anomaly is related to the increased SST gradient and hence to enhanced surface baroclinicity or just to the presence of the warmer surface water, EXP 2 has been repeated with a positive SST anomaly shifted northeastward (EXP 2b, thin lines in Fig. 4.13). Note that this particular SST anomaly is roughly comparable to the second SST EOF (Chapter 3, Fig. 3.6). The geopotential height and surface pressure response is still apparent (Fig. 4.13) and comparable to EXP 2 in its structure relative to the SST anomaly, but there is a slight decrease of the storm track. Hence at least the storm track response appears to be sensitive to the exact location of the (warm) SST anomaly with respect to the mean SST gradient. The position relative to the mean atmospheric flow can also be of great importance (cf. Ting and Peng 1995).

To examine further the linearity of the atmospheric response, an experiment is undertaken with inverse sign of the original SST dipole anomaly. This leads to a reversed sign of the storm

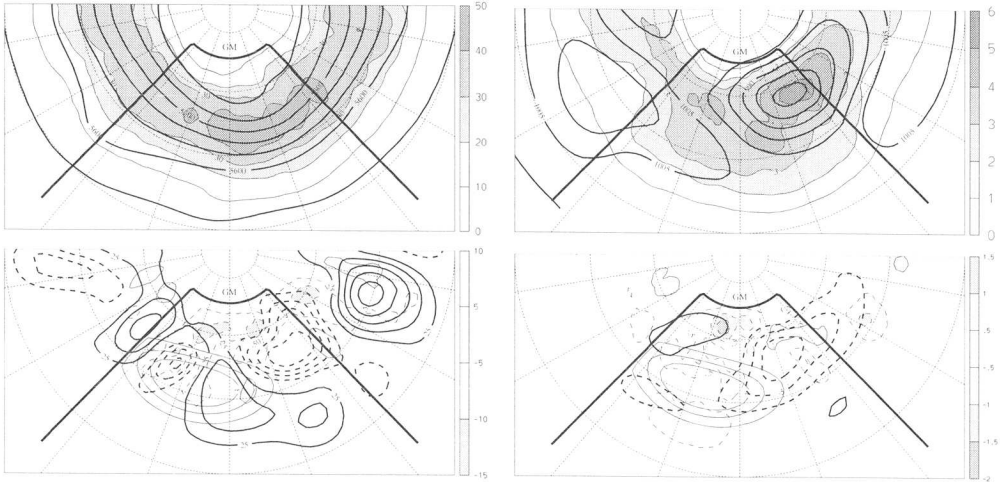


FIG. 4.13: As Fig. 4.10, but for EXP 2b (northeastward shifted warm anomaly only).

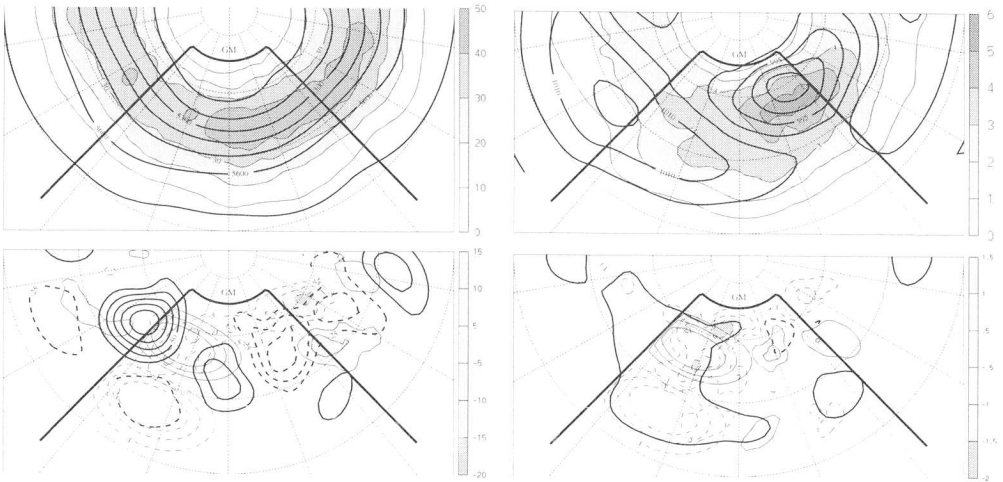


FIG. 4.14: As Fig. 4.10, but with reversed sign of the SST dipole anomaly.

track's amplitude (Fig. 4.14), i.e. a slight weakening. In contrast, the weak geopotential height response does not match the inverse pattern of Fig. 4.7, i.e. the sign of the height response is not reversed. In effect, the idealised model response to a SST dipole in the western ocean is non-linear.

With the exception of the reversed dipole experiment, there is a comparable structure of the geopotential height response, and it is stronger for experiments involving positive SST

anomalies. Thus the warm part of the SST dipole accounts for a larger amount of the total response. The experiments indicate that most of the increase of the geopotential height trough can be attributed to the imposed SST anomalies, while at least a part of the positive height response upstream and farther downstream of the forcing might be unrealistic. Hence these parts of the response might have been considerably weaker if the CTRL simulation would already have shown a stationary trough.

The decrease of storm track activity in the experiment with a northward shifted positive SST anomaly compared to the enhancement observed in all other runs indicates that a strengthened SST gradient³ which increases the surface baroclinicity can influence the storm track position and amplitude.

4.3 Comparison of Surface Fluxes

Further insight to the relative importance of the different SST anomalies can be sought from a comparison of the surface fluxes. The average flux of latent heat for the CTRL simulation is shown in Fig. 4.15 (uppermost left panel), together with the heat flux anomalies of the various experiments with respect to the CTRL simulation (i.e. EXP - CTRL). The location of the CTRL-simulation mean flux relative to the ocean boundaries and its amplitude are reasonable compared to observed climatology (Fig. 1.5). The CTRL mean and the anomalous (EXP - CTRL) sensible heat fluxes show very similar structures as the latent heat fluxes, but considerably smaller amplitudes (not shown). Comparison of the standard deviation of the CTRL simulation latent heat fluxes (thick solid contour in uppermost left panel of Fig. 1.5) with the signals of the different experiments indicates that the heat flux differences are quite large, and this consolidates their statistical significance.

The fluxes of EXP 1 (dipole anomaly) can principally be viewed as a superposition of EXP 2 (warm only) and EXP 3 (cold only). The largest flux differences are observed over the warm SST anomaly. In accordance with the results of the previous Section, the warm anomaly appears to be more important.

The dipole structure of the flux difference of EXP 2b (northeastward shifted warm anomaly) reflects a northward shift of the climatological mean surface flux pattern with no amplification. Recall that this experiment showed a weakening of the storm track, which indicates that the atmospheric response is sensitive to the position of the SST (and hence flux) anomalies with respect to the atmospheric flow.

Surprisingly, there is no considerable latent heat flux over the positive anomaly of the experiment with reversed sign of the dipole. This indicates again that the atmospheric response to a given SST anomaly is sensitive to the relative position of the anomaly with respect to the mean flow. In contrast, the heat loss of the atmosphere over the southern negative anomaly is large. This agrees with the weaker storm track observed in this experiment (Fig. 4.14).

In addition to the spatial structure of the mean latent heat flux distributions of the various experiments, a study was made of the temporal evolution of the flux anomalies. The

³by either a warm anomaly in the south or a cold anomaly to the north of the zone of large mean SST gradient or both

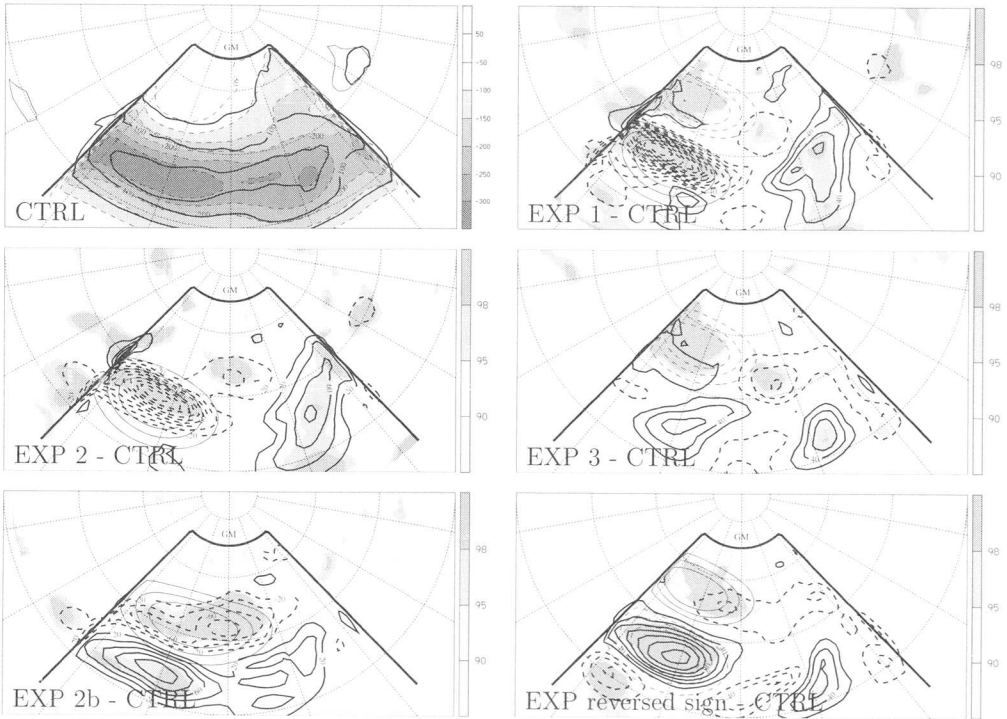


FIG. 4.15: Simulation average (DJF) surface fluxes of latent heat of the various experiments (as labeled, contour interval 20 W m^{-2}) with respect to the CTRL simulation (upper left panel, shaded, contour interval 50 W m^{-2}). Thick black line the standard deviation). T-test significance levels of the differences indicated by shading.

time evolution of the difference EXP 1 - CTRL of latent and sensible heat flux averaged over the area of the positive SST anomaly of EXP 1 (Fig. 4.16, upper panel) is mainly directed upward into the atmosphere and shows large variability in the 2-7 day band, which can be associated with the passage of midlatitude synoptic storms. The same variability is observed for the fluxes averaged over the area of the negative SST anomaly, but they do not show a clear preference for one sign, as reflected in the almost vanishing mean values (lower panel). Therefore, the anomalous heat flux averaged over the whole dipole anomaly is dominated by the upward flux occurring over the positive SST anomaly. This is confirmed by the time series of the experiment with the warm anomaly only (EXP 2, not shown), which closely resemble the upper panel of Fig. 4.16. Hence the time evolution of the anomalous fluxes reflects the passage of single synoptic systems, as confirmed by inspection of the time series of the fluxes of the other experiments (not shown).

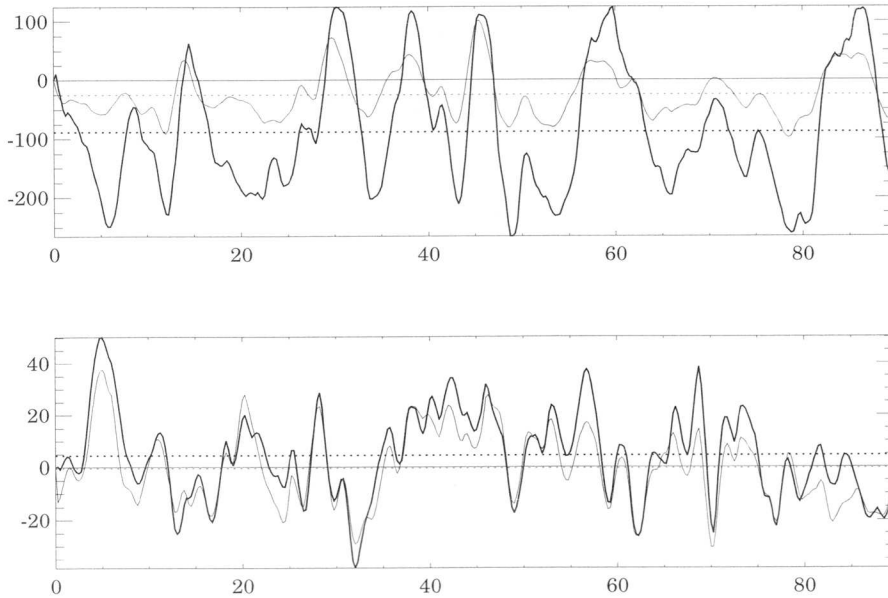


FIG. 4.16: Time evolution of the difference EXP 1 - CTRL of latent (bold) and sensible (thin) heat flux averaged over the area where $\Delta\text{SST} > +1$ K (upper panel) and $\Delta\text{SST} < -1$ K (lower panel). Vertical axis in W m^{-2} , horizontal axis days since 1st of December. Dashed lines the respective time mean fluxes. Note that negative fluxes are directed from the ocean into the atmosphere.

4.4 Summary and Discussion

The effect of the distinctive SST patterns identified in Chapter 3 has formed the basis for a sequence of simulations with an idealised primitive equation model. The model's control climate contains the salient features of midlatitude weather systems and its mean state reasonably resembles the observed climatology. The storm track can be regarded as an idealisation of the observed North Atlantic storm track. Compared to observations, the region of maximum amplitude over the ocean and its decrease over land are fairly well represented, but the storm track extends too far eastward. Also the stationary geopotential height trough over the western landmass / eastern ocean basin is weak in comparison with observations.

The atmospheric response to the imposition of a SST dipole anomaly in the western ocean consists of a moderately enhanced storm track downstream of the anomaly and an amplification of the stationary geopotential height trough. Experiments with either the warm or cold constituent of the SST dipole anomaly alone reveal that the warm component is responsible for a larger amount of the total response and this is confirmed by inspection of the

surface fluxes of latent and sensible heat. A decrease of storm track activity was observed in the experiment with a northward shifted positive monopole SST anomaly and in a simulation with inversed sign of the SST dipole. In all the simulations involving SST anomalies that strengthen the SST gradient, the storm track is enhanced. The imposed SST dipole anomaly increases the surface baroclinicity and leads to anomalous fluxes of latent and sensible heat, with increased fluxes from the ocean upward into the atmosphere over warm anomalies. Hence it is hypothesised that the growth of single synoptic scale systems can be enhanced and the recurrence of such effects influences the storm track position and amplitude. This is confirmed by investigation of the time series of the anomalous surface fluxes which reflect the passage of single synoptic systems. These results point to a contribution of baroclinic instability to the enhanced eddy kinetic energy downstream of the jet and to the elongation (and amplification) of the storm track (cf. Frisius et al. 1998). Inspection of the surface fluxes of latent and sensible heat also points to the sensitivity of the atmospheric response to the precise location of the SST anomaly relative to both the mean SST distribution and the atmospheric (mean) flow (cf. Ting and Peng 1995). The mutual correspondence of the storm track and geopotential height signals indicates that the atmospheric flow response is achieved through both the contribution of the transient disturbances on the quasi-stationary waves (cf. Hoskins and Valdes 1990; Sheng and Derome 1993) as well as the steering effect of the large scale flow on the eddy evolution (cf. Branstator 1995; Whitaker and Dole 1995).

While the imposition of the SST dipole does not result in atmospheric anomalies that project on the statistically derived coupled patterns (Section 3.2), some particular features of the idealised model results can be related to the general structure of the first coupled mode. The intensification of the storm track and the concomitant strengthening of the geopotential height trough indicate that the SST dipole forces only selected features comprised in the whole coupled atmospheric patterns. Furthermore, the modelled atmospheric response has been shown to be both nonlinear and highly sensitive on the precise location of the SST anomaly. While the atmosphere has been identified to dominate the linear coupling, the ocean configuration has been shown to feed back onto the atmosphere in a way difficult to be isolated by means of a linear statistical analysis.

Chapter 5

Case Studies

The idealised experiments of the previous Chapter pointed to an effect of the SST configuration on the atmospheric flow evolution on monthly to seasonal time scales. However, the detailed structure of the response is certainly influenced by the idealised configuration of the ocean-land distribution and the lack of orography. To address the effect of SST anomalies in a realistic set up, sensitivity experiments were conducted for selected months and seasons with the limited area NWP model of the North Atlantic region described in Section 2.3.1. Such a model has the advantage that it has been subjected to testing in the demanding task of daily weather forecasting. In addition, this experimental set up permits a direct comparison of the model results with the statistically derived (coupled) patterns of Chapter 3.

The simulations are initialised with the European Center for Medium-Range Weather Forecasts (ECMWF) Reanalysis (ERA) fields interpolated to the model grid, and the model is relaxed to the analyses at the lateral boundaries every 6 hours. Thus the incident flow is the same for all simulations of a given case with the only difference being the SST configuration. Thus the local effect of the imposed SST anomaly in the North Atlantic region can be examined, while suppressing planetary feedback.

Two contrasting types of experiments have been performed to study the effect of the SST anomaly patterns evaluated with the statistical analysis (Chapter 3). The first consists of month long simulations with the first SST mode suppressed (filtered out), i.e. modification of the SST pattern back towards the long-term mean state. The statistical analysis indicated that the first geopotential height and storm track modes are reduced in amplitude in the absence of the first coupled SST mode. In this way, the sensitivity of the atmospheric patterns to the statistically coupled SST configuration can be investigated for any particular month. A series of month-long simulations of this kind have been performed for selected cases (see next Section).

In the second kind of experiment, one winter has been simulated with a variety of imposed SST anomalies, defined in terms of the leading SST EOFs (Section 5.2). These enable an assessment to be made of the influence of the prescribed SST anomalies.

For both kinds of experiments and all cases, control simulations with the unperturbed ECMWF Reanalysis SST fields were performed. Moreover since a strong asymmetry in the atmospheric response with respect to the sign of the SST anomaly has been observed in earlier studies (cf. Pitcher et al. 1988; Kushnir and Lau 1992), each experiment is examined

relative to the respective control run. To examine the influence of the initial conditions, the control and experiment simulations have been repeated both starting one day earlier and one day later to form a three member ensemble. The first two weeks of all simulations are used for spin-up and not included in neither the analyses nor figures. In all experiments presented below, the statistical significance has been assessed by a two-tailed Student's t-test over all three ensemble members¹.

5.0.1 Case Selection

The cases have been selected from the time period 1979 to 1992 (cf. ECMWF Reanalysis period). For the first kind of experiments, the key factor is the amount to which the SST configuration contributes to the high amplitude of the first atmospheric coupled mode. Months with clear dominance of the first coupled mode and especially high amplitude of the first SST pattern are selected. First winter months with highest scores of the first SST pattern² are identified and in a second step those with high scores of the first geopotential height and storm track mode³ (see Fig. 3.2 and 3.8). The selected case of December 1981 represents a low-NAO whereas December 1986 is a high-NAO phase. Note that due to the large month-to-month variation of the amplitude of the first coupled mode, month-long simulations (plus spin-up) are performed.

For the second kind of experiments winter seasons are sought that are i) close to the climatological mean and ii) do not vary excessively from month to month. This allows a comparison of the model results with the statistical analysis in a straightforward manner, since these analyses were based on anomalies from the climatological mean. Furthermore, it reduces the model sensitivity to anomalous background flow (cf. Peng et al. 1995). Therefore, a specific winter with small NAO index of the same sign for all three months (DJF) would be suited. The conventional NAO index was chosen since it is i) an a priori measure of the 'organisation level' of the flow and ii) highly correlated with the first geopotential height mode⁴. While there are only a few winters with small month-to-month fluctuations and small amplitude of the NAO index (Fig. 3.3), the winter season 1990/91 (also 1980/81) appears to fulfill the above requests and will be studied in Section 5.2.

¹Let $e_{ij}^k(t_l)$ and $c_{ij}^k(t_l)$ represent the model variable value of the EXP and CTRL simulation for one ensemble member k at grid point ij at time t_l (l =first time after spin-up...end of simulation). The series ($e_{ij}^1(t_1), e_{ij}^1(t_2), \dots, e_{ij}^1(t_T), e_{ij}^2(t_1), \dots, e_{ij}^2(t_T), e_{ij}^3(t_1), \dots, e_{ij}^3(t_T)$) and similar for $c_{ij}^k(t_l)$ have been tested for being significantly different by a two-tailed Student's t-test.

²We checked also for other modes being weak and repeated the selection using the first SST EOF and its scores, leading to the same results.

³Generally, episodes of a specific coupled mode (as identified by SVD) bearing strong momentaneous cross-covariance can – for example – easily be identified by searching for local maxima of the function

$$prod_k(t) = x_k^*(t) \times y_k^*(t) \quad (5.1)$$

where $x_k^*(t)$ and $y_k^*(t)$ are the expansion coefficients (scores) of the k^{th} mode of coupled patterns of the respective fields, as defined in Eq. 2.4.

⁴Thus it is also justified to address the question whether the imposition of the first SST mode affects the NAO index.

5.1 Filtered-out SST

In this Section, consideration is given to the cases where the first SST mode has been filtered out (cf. Bresch and Davies 1998b). The control simulation (hereafter referred to as CTRL) involves running the model with the ECMWF Reanalysis data for 45 days, starting at the first day of the selected month. The experimental runs (EXP 1,2, etc.) with changed SST configuration were run three times for every case (i.e. ensemble EXP), starting at the 1st, 2nd and 3rd day of the selected month and a reduced spin-up time to 14 and 13 days for the second and third ensemble member. Analyses and figures of this Chapter are presented for the last 30 days of simulation.

Filtering of the SST fields in the experimental simulations was performed as follows: First, the long-term SST mean as well as the first statistically-derived SST pattern have been interpolated onto the rotated model grid, with the first pattern being re-normalised to unit length. Second, the scores (hereafter referred to as *model scores*) of the SST pattern were calculated (Eq. 2.4) by projecting it on the the time series of ECMWF Reanalysis SST fields (after the long-term mean has been subtracted) for every time step. Third, the SST pattern multiplied by the *model scores* were subtracted for every time step from the original ECMWF Reanalysis SST time series to obtain the modified SST configuration used in the Experiment simulations. Symbolically, the procedure can be written as:

$$\mathbf{SST}_{Exp} = \mathbf{SST}_{ECMWF} - \underbrace{(\mathbf{SST}_{ECMWF} - \mathbf{SST}_{mean})\mathbf{p}'_k^T}_{\text{model score}} \cdot \mathbf{p}'_k \quad (5.2)$$

with the ' indicating interpolation on the model grid and \mathbf{p}'_k the first SST pattern for $k = 1$.

In the following two Sections, the December 1981 and 1986 ensemble cases are examined and a comparison is made with the control (CTRL) run.

5.1.1 December 1981

The 30 day mean for the CTRL simulation shows a strong trough over the eastern US seaboard and a ridge over central Europe that extends northwestward to Iceland (Fig. 5.1). The weak (blocked-type) flow is reflected in a NAO-index of -1.7. The CTRL storm track is slightly stronger in comparison with expectation based on the statistical linear relation with the geopotential height (Chapter 3, Fig. 3.12). The CTRL simulation closely follows the ECMWF Analyses, except for the more pronounced ridge in the eastern part of the domain in the CTRL simulation.

The filtering out of the first SST mode results in a difference of (ensemble) EXP mean SST and the CTRL SST as shown in Fig. 5.2. The amplitude represents about 2 times the scores standard deviation of the statistically derived pattern. Based on the statistical relations of Chapter 3, a strengthening of the flow over the eastern North Atlantic and Europe and an intensified storm track would be expected in response to the changed SST configuration.

The ensemble mean response (Fig. 5.3) does in fact show a reduction of the ridge over Europe, and a slight southward displacement and latitudinal confinement of the storm track

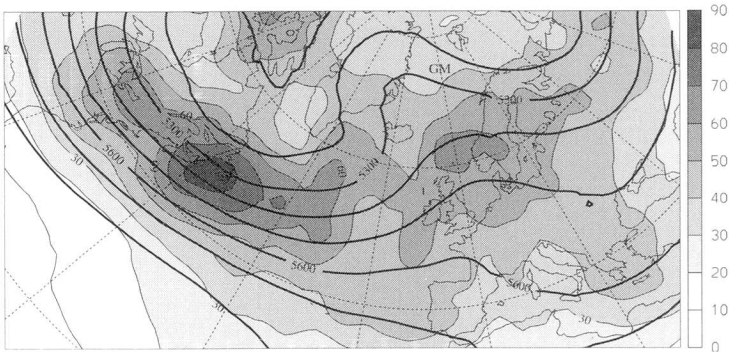


FIG. 5.1: CTRL simulation of December 1981 case, mean over last 30 days of simulation of geopotential height at 500 hPa (thick lines, contour interval 100 gpm) and storm track (shaded, contour interval 10 gpm).

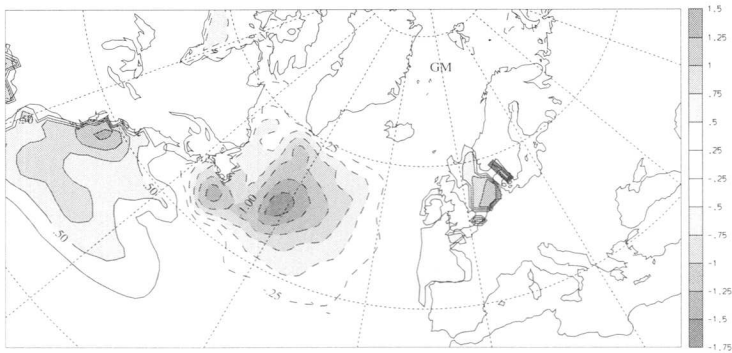


FIG. 5.2: December 1981 case: Difference of ensemble mean and CTRL SST (shaded and thin lines, contour interval 0.25 K, negative contours dashed and zero line omitted).

(features than can be seen in the surface pressure storm track as well, not shown). There is a notable enhancement of the cyclone activity over southeastern Europe, probably related to lee cyclogenesis at the southwestern edge of the Alps⁵. The geopotential height difference ensemble EXP - CTRL (Fig. 5.4) is significant in its centers and does not vary considerably among the ensemble members. It reflects a strengthening of the Icelandic low and enhanced trough off the North American seaboard, but the response does not really match the pattern of the statistical analysis (Fig. 3.2). In particular the strengthening of the storm track is weaker than would have been expected, probably due to the fact that the storm track in the CTRL simulation was – as mentioned above – already quite strong.

The surface latent and sensible heat fluxes (Fig. 5.5) are enhanced over the positive

⁵Nevertheless, the position of this particular feature of the response close to the eastern (relaxed) boundary of the model domain indicates that it should be addressed with caution.

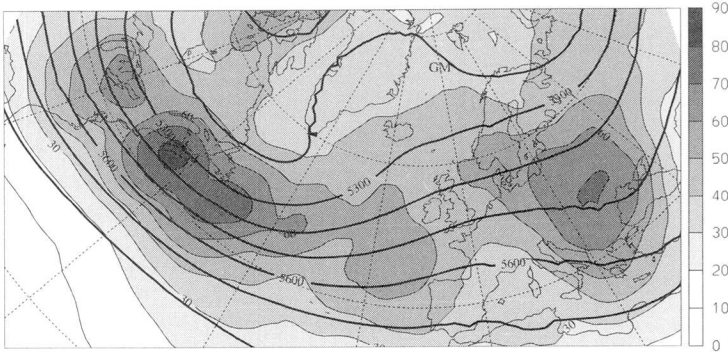


FIG. 5.3: As Fig. 5.1, but for ensemble mean of EXP simulation of December 1981 case.

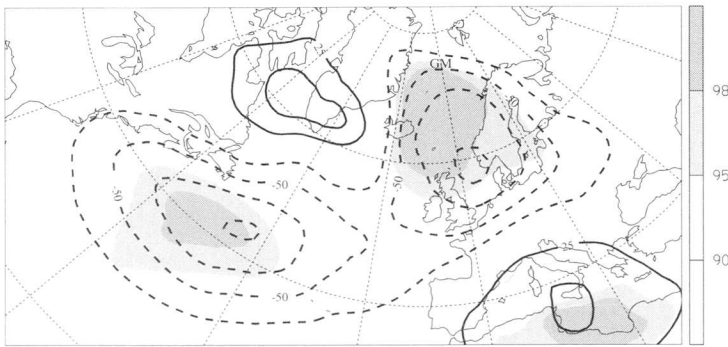


FIG. 5.4: Geopotential height difference ensemble EXP - CTRL for December 1981 case, contour interval 25 gpm, negative lines dashed and zero line omitted. The t-test significance levels are indicated by shading.

(southern) and damped over the negative (northern) anomaly, in line with both statistical and model results (Cayan 1992a; Power et al. 1995), and also the sensible heat fluxes are considerably smaller than those of latent heat (Cayan 1992c). Increased fluxes can arise from single events (cf. Oerlemans 1980; Davis and Emanuel 1988), when frontal systems with strong low level winds (advecting relatively cold and dry airmasses) overpass the anomaly.

The geographical distribution of the difference of the growth rate of cyclones between the ensemble of EXP simulations and the CTRL run (Fig. 5.6, right panel) indicates that the effect of the altered surface fluxes is not locally confined to the region of SST changes: For this particular case the area of maximal growth over Newfoundland of the CTRL simulation (Fig. 5.6, left panel) is shifted northward and there is a significant (95% level) increase over the central North Atlantic. In contrast, the decay rate does not differ significantly (therefore not shown).

For this case of December 1981, the filtering out of the leading climatological SST pattern

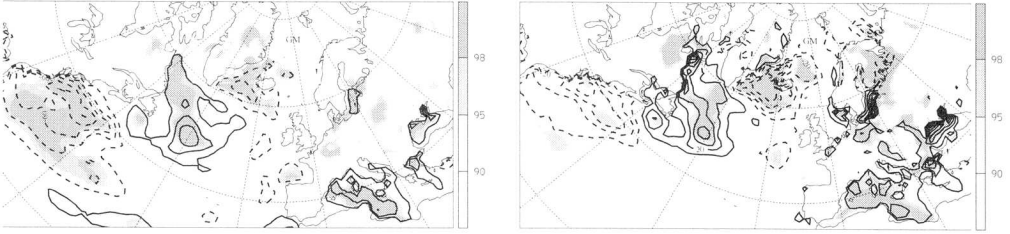


FIG. 5.5: December 1981 case: Difference EXP - CTRL of latent (left panel, contour interval 20 Wm^{-2}) and sensible (right panel, contour interval 10 Wm^{-2}) heat fluxes. The t-test significance level of the difference is shaded. Note that negative fluxes are directed from the ocean into the atmosphere.

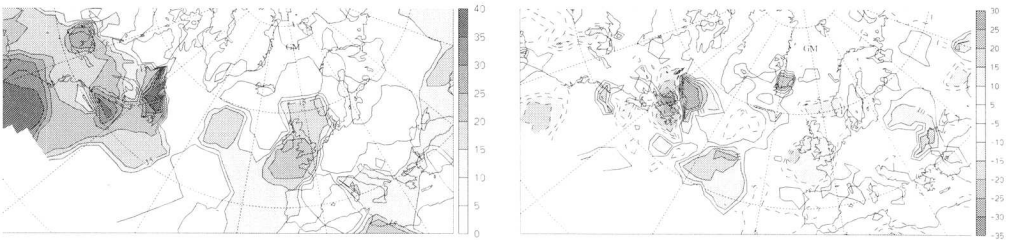


FIG. 5.6: December 1981 case: CTRL cyclone growth rate (left panel) based on local changes in surface pressure of synoptic scale systems identified as described in Section 2.2.2 and difference ensemble EXP - CTRL of cyclone growth rate (right panel). Contour interval 5 mb d^{-1} .

resulted in changes of geopotential height and storm track amplitude which can be attributed to the effect of the modified SST configuration on single cyclones, but the difference between EXP and CTRL simulation do not really project on the difference patterns expected from statistical analysis.

5.1.2 December 1986

Fig. 5.7 shows the mean geopotential height and storm track field for the CTRL simulation of the December 1986 case. It depicts a high index situation (NAO-index 1.8) with strong zonal flow and an associated latitudinally confined storm track. It has to be noted that the CTRL simulation deviates considerably from the ECMWF Reanalysis⁶.

Comparison of the SST difference EXP-CTRL (Fig. 5.8) and the statistically coupled patterns (i.e. inverse of Fig. 3.2), would suggest a weaker flow and storm track in the EXP simulations compared to the CTRL run.

While the storm track over the central North Atlantic is effectively weaker in the EXP

⁶The difference projects on the first geopotential height mode with a score representing about one standard deviation, thus close to Fig. 3.2.

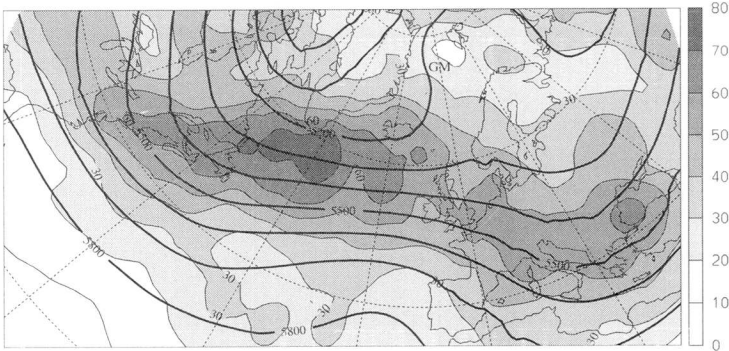


FIG. 5.7: CTRL simulation of December 1986 case. Contour intervals etc. as in Fig. 5.1.

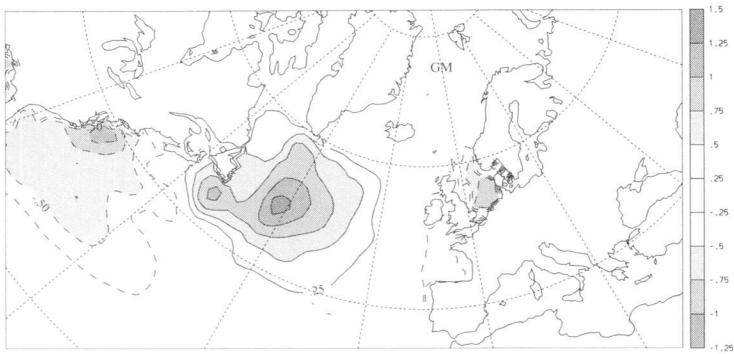


FIG. 5.8: December 1986 case: Difference of ensemble mean SST and the CTRL SST (shaded and thin lines, contour interval 0.25 K, negative contours dashed and zero line omitted).

ensemble (Fig. 5.9), the zonality of the flow has not been strongly affected by the changed SST configuration. The t-test statistics indicate only moderate (90%) significance of the geopotential height response (of the order of 25 gpm) over a very restricted area at the southern tip of Greenland (Fig. 5.10). The ensemble spread is large, the third ensemble member shows even a sign reversal of the response. It appears as if in this high-index situation, the reduction of the mean SST gradient does not automatically lead to a weaker flow regime, while the storm track is – in this particular case – modified as expected by the results of the statistical analysis. Due to the low significance of the response, this case is not further examined.

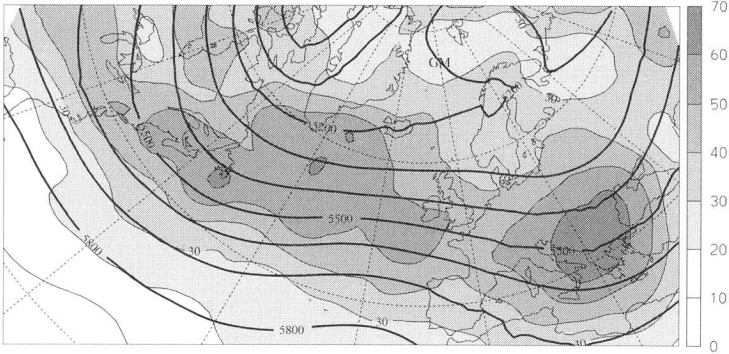


FIG. 5.9: As Fig. 5.7, but for ensemble mean of EXP simulation.

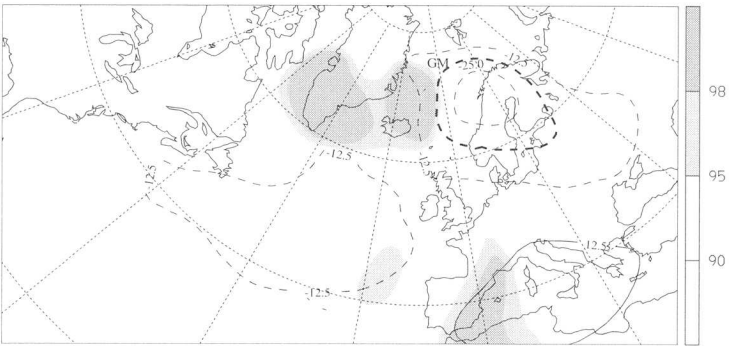


FIG. 5.10: Geopotential height difference ensemble EXP - CTRL for the December 1986 case, contour interval 12.5 gpm (25 gpm contour thick), negative lines dashed and zero line omitted. The t-test significance levels are indicated by shading.

5.2 Imposition of SST Anomalies

To clarify the influence of selected SST anomalies, as presented in the last Section, a series of whole winter simulations with imposed constant SST anomalies was undertaken. The focus is again on the first SST dipole pattern, while the impact of its single constituents will also be addressed. The second SST mode (see Fig. 3.6) will be considered as well, especially since this allows a direct comparison with results from literature.

As mentioned in Section 5.0.1, a winter with clearly defined and stable background flow was chosen for this study, reflected in NAO-indices of 1.0, 0.6 and 0.5 for December 1990, January 1991 and February 1991, respectively (mean NAO-index 0.7). Furthermore, the mean flow (as well as the SST) is close to climatology, which favours the comparison with statistical results.

The model (described in Section 2.3.1) has been run first with unchanged ECMWF

Reanalysis data (CTRL run) and then with various changed SST configurations (EXP simulations). The model runs were started 15th of November, the first 15 days used for spin-up and neither included in the figures nor the analyses (the mean fields presented are therefore 3-month means DJF). These runs are referred to as CTRL and EXP *simulations*. In order to assess – besides the atmospheric response to the imposed SST anomalies – the model sensitivity to initial conditions and the effect of the imposed SST on internal atmospheric variability, both the CTRL and EXP simulations were repeated starting one day earlier (14.11.1990, hereafter referred to as the D-simulations) and one day later (16.11.1990, F-simulations). Together with the run started 15th of November, this forms a three member ensemble of both the CTRL and EXP simulations. The term *CTRL ensemble* and *EXP ensemble* designate the whole three member control and experiment ensembles (in contrast to the CTRL and EXP *simulations*). Note that some analyses have been performed for the CTRL and EXP simulation only (i.e. only the simulations started 15th of November), since they are representative for the respective whole ensembles.

In the next Sections, the CTRL and EXP runs will be presented (Sections 5.2.1 and 5.2.2) and compared by means of selected aspects (surface fluxes, growth and decay rates of single cyclones, moisture distribution, vertical structure). Also a detailed analysis in terms of statistical patterns will be given in Section 5.2.7 where the the statistical significance of the results will be discussed as well.

5.2.1 Control Simulation

The CTRL simulation (Fig. 5.11) reproduces the ECMWF Reanalysis fields relatively well, but there are small differences at the southern tip of Greenland. Except for this region, where the CTRL simulation storm track is somewhat weaker than its Reanalysis counterpart, there are only small differences between the CTRL simulation and Reanalysis storm track. The three member ensemble mean of the CTRL simulations is presented in Fig. 5.12.

By comparison with Fig. 5.11, it turns out that there are no major differences between the CTRL simulation (i.e. the middle ensemble member) and the CTRL ensemble mean, the only the storm track is amplified over Newfoundland. A detailed comparison of all three ensemble members indicates that the CTRL spread is rather small, therefore the CTRL simulation does well represent the whole ensemble.

5.2.2 Experiments

SST dipole

The SST pattern imposed for EXP 1 (Fig. 5.13) is a smoothed version of the SST pattern derived by statistical analysis (Fig. 3.2). The peak amplitudes amount to +3.7 K and -4.0 K, and the average absolute amplitude is 2.3 K. Comparable amplitudes of SST anomalies have been observed throughout a whole winter a few times in the last 30 years (for example 1966, 1970, 1978 and 1983).

The results (cf. Fig. 5.14 and Fig. 5.15) show that the mean trough and the storm track are strengthened in response to the imposition of the SST anomaly of Fig. 5.13. The

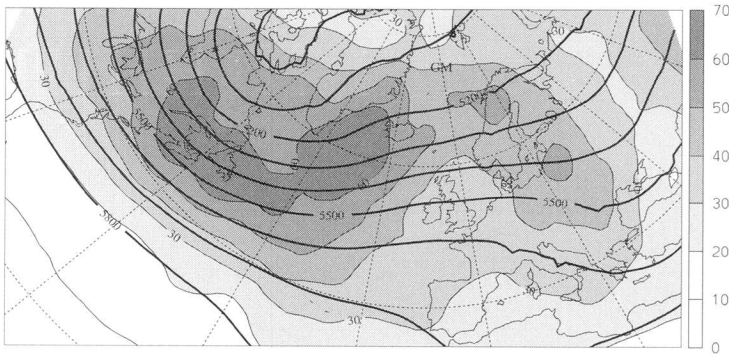


FIG. 5.11: CTRL simulation of winter 90/91, 3 month mean (DJF) of geopotential height at 500 hPa (thick lines, contour interval 100 gpm) and storm track (shaded, contour interval 10 gpm).

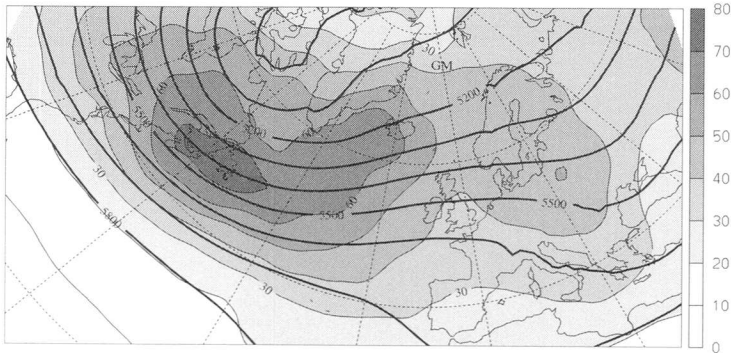


FIG. 5.12: Ensemble mean of CTRL simulations, 3 month mean (DJF) of geopotential height at 500 hPa (thick lines, contour interval 100 gpm) and storm track (shaded, contour interval 10 gpm).

collocation of the southern part of the geopotential height difference with the increased storm track compares with the coupling of geopotential height and storm track patterns isolated by SVD analysis (Fig. 3.12). This suggests that the observed signals of both geopotential height and storm track are mutually consistent. The robustness of the above result is brought out by comparison of the ensemble of the three experiments (EXP 1, D1 and F1) and the CTRL simulation (Fig. 5.16). The difference of the EXP ensemble and the CTRL ensemble is similar (not shown). The CTRL ensemble spread is small and comparisons will be made with the CTRL run in the remainder of this Chapter.

The flow response in single months always shows a structure comparable to the whole winter signal, the strongest contribution occurs in December (Fig. 5.17) and January contributes least. Comparison of the storm track calculated based on nine 10-day periods for both the EXP 1 and CTRL simulations (not shown) indicates that the observed difference is highly recurrent.

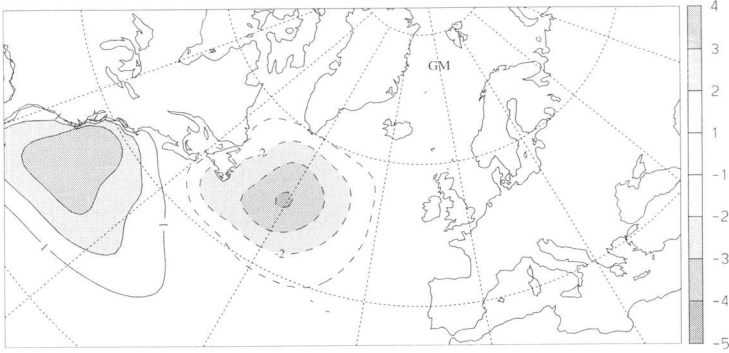


FIG. 5.13: The SST pattern imposed in the EXP 1 simulation, a smoothed version of the structure of Fig. 3.2. Contour interval 1 K, negative contours dashed and zero line omitted.

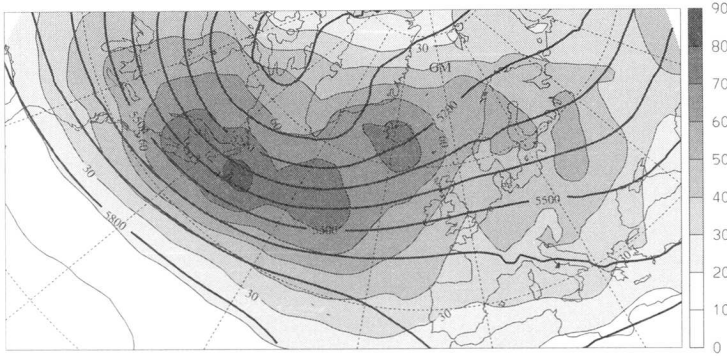


FIG. 5.14: EXP 1 simulation (imposition of SST anomaly shown in Fig. 5.13): 3 month mean (DJF) of geopotential height at 500 hPa (thick lines, contour interval 100 gpm) and storm track (shaded, contour interval 10 gpm).

SST warm and cold anomaly separately

To assess the question whether only the dipole as a whole (EXP 1) or either the warm or cold anomaly alone contribute most to the observed response, experiments with each part of the dipole anomaly have been performed separately. The experiments with the warm and cold anomaly alone will be referred to as EXP 2 and EXP 3, respectively. The response to the warm anomaly alone (Fig. 5.18) resembles more the total response (Fig. 5.15) than the cold anomaly alone (Fig. 5.19). The superposition of both the response to the warm and cold anomaly (Fig. 5.20) reproduces the response to the dipole anomaly (Fig. 5.15) quite well, so that the dipole can – to a first approximation – be interpreted as a superposition of a warm and cold anomaly.

The northern part of the SST dipole anomaly is more strongly forced by the atmosphere,

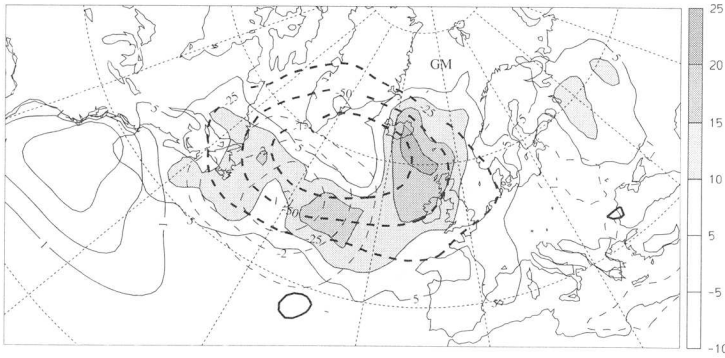


FIG. 5.15: Difference EXP 1 - CTRL. 3 month mean (DJF) geopotential height difference at 500 hPa (thick lines, contour interval 25 gpm, negative lines dashed and zero line omitted) and storm track difference (shaded, contour interval 5 gpm, negative lines dashed and zero line omitted). The SST anomaly is indicated by thin lines, contour interval 1 K.

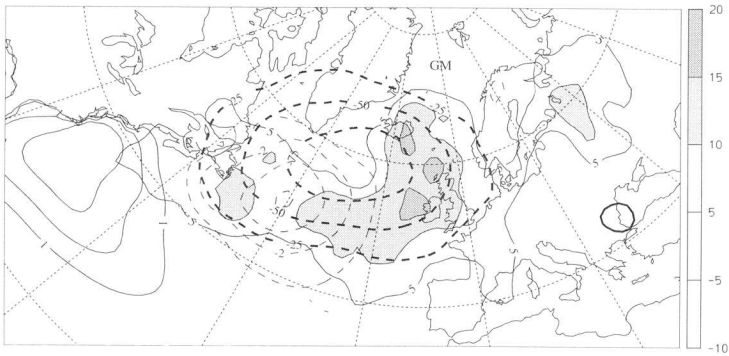


FIG. 5.16: As Fig. 5.15, but for the difference EXP 1 ensemble - CTRL simulation. Geopotential height differences larger than 25 gpm are significant at the 98% level.

since the mean surface flux of kinetic energy (not shown) has its maxima in the northern central North Atlantic, where it acts to advect the cold SST anomaly eastward. Recall further that the composite plots in Chapter 3 (Fig. 3.5) reveal that it is essentially the northern part of the SST anomaly which is linearly coupled to the first geopotential height mode. In contrast, the *variability* of the surface kinetic energy flux is largest over the warm anomaly, which helps to enhance the fluxes of latent and sensible heat (as discussed below) but does not lead to a displacement of the SST anomaly.

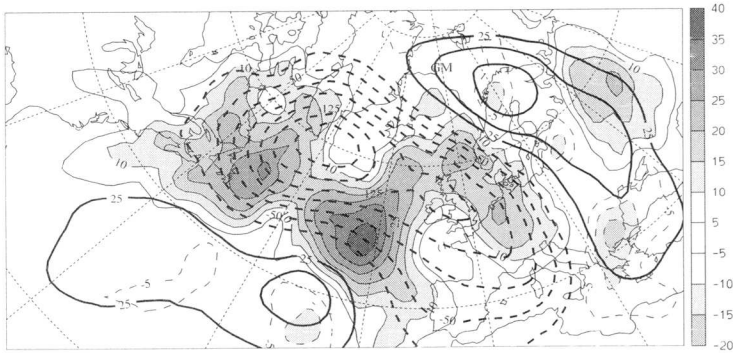


FIG. 5.17: As Fig. 5.15, but for December only (i.e. one month mean).

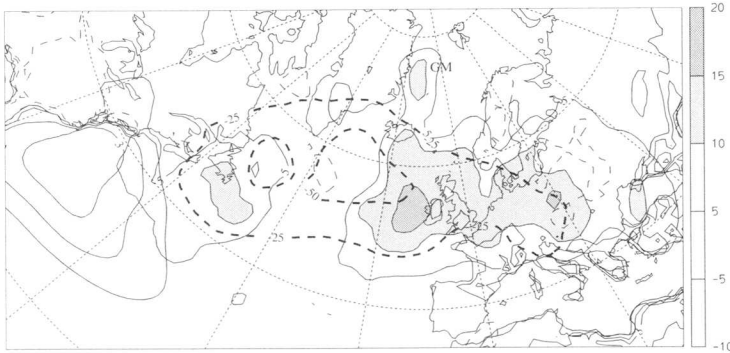


FIG. 5.18: As Fig. 5.15, but for the warm anomaly of Fig. 5.13 alone.

SST dipole of reversed sign

The linearity of the atmospheric response has been further tested by imposition of a SST anomaly with inverse sign (EXP 4). The atmospheric response (Fig. 5.21) does not show a reversed sign compared to Fig. 5.15, there is only a weak cyclonic anomaly over central Europe, but no noteworthy storm track difference. This non-linear response to the strengthening/weakening of the main SST gradient is in agreement with the findings of Lunkeit and van Detten (1997).

A further experiment with the SST anomaly as derived directly from statistical analysis (Fig. 3.2, i.e. with an amplitude equal to one standard deviation of the scores. The response (Fig. 5.22) is rather weak, a mere enhancement of internal variability. SST anomalies of 2 to 4 times the scores standard deviation (resulting in average amplitude around 1.5 K to 2.3 K) show a clear influence, comparable to the signal found in EXP 1.

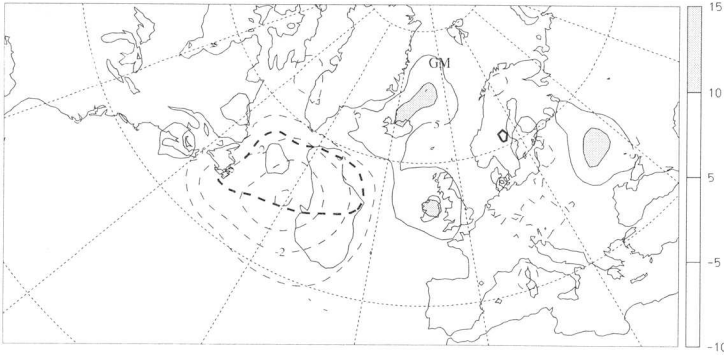


FIG. 5.19: As Fig. 5.15, but for the cold anomaly of Fig. 5.13 alone.

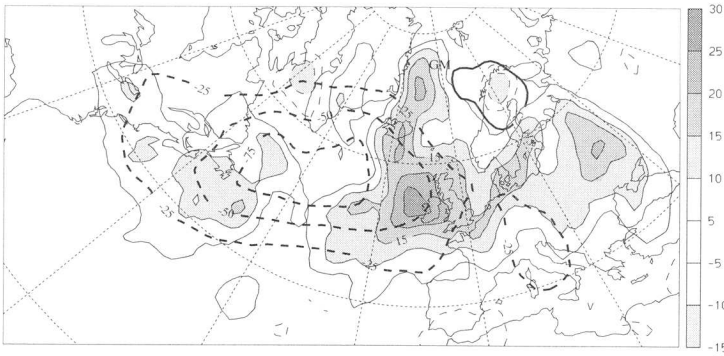


FIG. 5.20: As Fig. 5.15, but for the superposition of the responses to the warm (Fig. 5.18) and cold (Fig. 5.19) anomaly of Fig. 5.13 alone.

SST central monopole

In addition to the first SST mode, the effect of a smoothed version (Fig. 5.23) of the second SST (monopole) mode (Fig. 3.6) on the atmosphere has been assessed as well. These experiments consider the effect of an SST monopole in the central North Atlantic and the sensitivity of the atmospheric response to the position of the monopole anomaly (cf. previous experiments EXP 2 and EXP 3). They also provide a basis for direct comparison with the results of Palmer and Sun (1985) and Peng et al. (1995).

A negative SST monopole yields a considerable enhancement of the storm track and a decrease of geopotential height aloft and downstream of the anomaly (Fig. 5.24).

The inverse sign of the anomaly of Fig. 5.23 results in an opposite response (Fig. 5.25, with a slightly enhanced storm track to the north of a positive geopotential height anomaly. Since the main focus of this study lies on the first coupled mode and due to the good agreement with the results of Palmer and Sun (1985) and Peng et al. (1995), we did not run

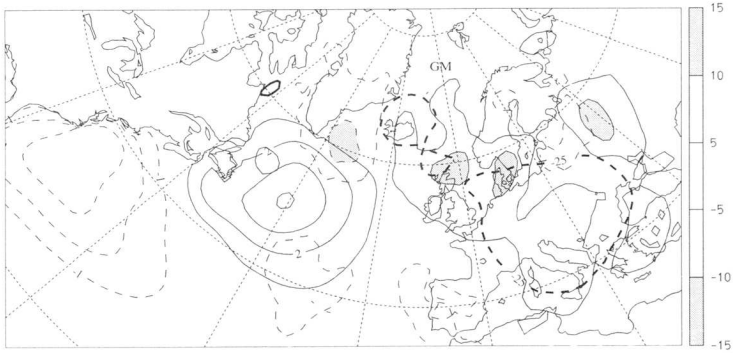


FIG. 5.21: As Fig. 5.15, but for the inverse sign of the SST anomaly of Fig. 5.13.



FIG. 5.22: As Fig. 5.15, but for the SST anomaly presented in Fig. 3.2. Note the smaller contour intervals for geopotential height (12.5 gpm) and the SST anomaly (0.5 K) compared to the other Figures of this Section.

the three-member ensemble for the simulations of the second mode. The general northward intensification of the storm track associated with a positive geopotential height anomaly in the warm SST case is comparable to the structure identified in Section 2.2.2 (Fig. 2.1) and has also been observed by Peng et al. (1995). It can be attributed to the northward deflection of the storm track in the presence of blocking. The simulations suggest that it is favoured by the warm SST anomaly – at least in this particular case.

The similarity of the response to a southern positive SST anomaly (EXP 2, Fig. 5.18) and a northern negative SST anomaly (Fig. 5.24) favours to the interpretation that both anomalies effectively enhance the main SST gradient, thus enhancing the low-level baroclinicity and affecting the growth rate of single cyclones in a similar way. The fact that the response to the northern cold anomaly of the dipole pattern alone (EXP 3) did not reveal a strong response points to a high sensitivity of the atmospheric response to the exact location (and shape) of the SST anomaly. The effect of prescribed SST anomalies appears therefore

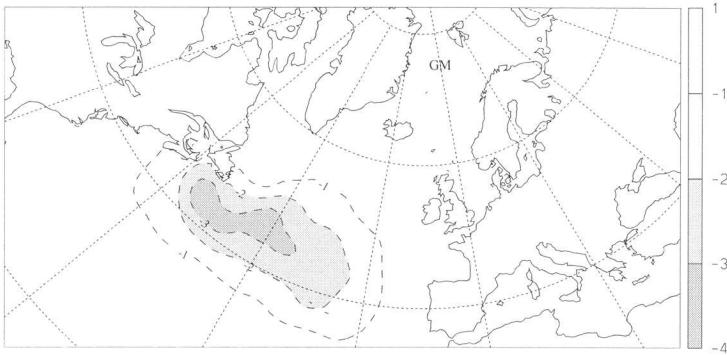


FIG. 5.23: The SST pattern imposed in the EXP 5 simulation, a smoothed version of the structure of Fig. 3.6. Contour interval 1 K, negative contours dashed and zero line omitted.

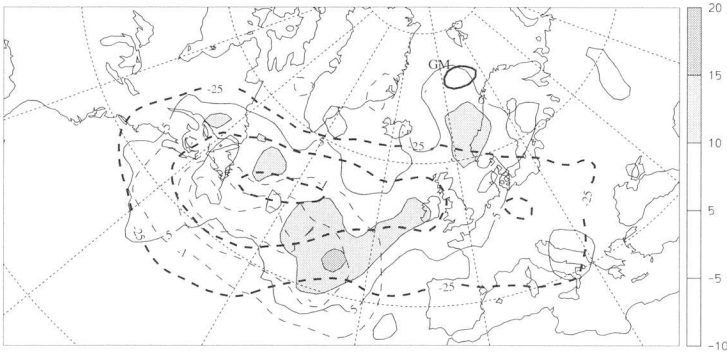


FIG. 5.24: As Fig. 5.15, but for the second SST pattern (Fig. 5.23).

to depend not only on the current atmospheric flow regime (Peng et al. 1995), but also on the position of the SST anomalies relative to this flow.

Note further that i) the geopotential height response resembles the central part of the statistically derived second coupled mode (Fig. 3.6) and ii) the storm track response to the positive (negative) sign of the SST anomaly matches more the central (northern) part of the climatological mode (Fig. 3.10). Therefore, we find a clear correspondence to the statistically derived patterns, different elements of them being related to specific SST configurations.

Peng and Fyfe (1996) hypothesised that the dipole mode can be related to an atmosphere driving the ocean process and the monopole mode to an ocean forcing the atmosphere process. The results of this study indicate that this might not be true at least for the specific winter simulated here, since an atmospheric response of comparable amplitude has been obtained for both dipole and monopole SST anomalies. Nevertheless, the response structure is different for the two types of forcing anomalies.

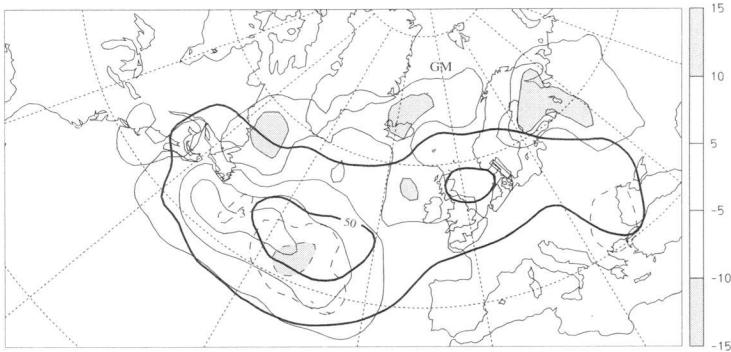


FIG. 5.25: As Fig. 5.24, but for the inverse sign of the imposed SST anomaly (depicted by thin lines, spacing 1 K).

5.2.3 Comparison of Surface Fluxes

A first approach to study the processes through which the SST anomaly influences the atmospheric flow evolution has been undertaken by comparing the surface fluxes between the EXP 1 and CTRL simulations, shown in Fig. 5.26. The structure and amplitude of the CTRL mean flux compares well with winter mean climatology (Fig. 1.5). By comparison of the flux anomalies with the atmospheric signals of the respective experiment (see Fig. 5.15), fluxes from the ocean into the atmosphere are observed to the southwest of the anomalous low pressure center (cf. Cayan 1992b; Alexander and Scott 1997). It is clearly apparent that i) the latent heat fluxes are much larger than those of sensible heat and ii) the fluxes into the atmosphere (over the positive SST anomaly) are important and significant. This is consistent with the warm anomaly part of the whole SST dipole being mainly responsible for the observed atmospheric response, as brought out by comparison with the latent heat flux of the experiment with the warm anomaly alone (Fig. 5.27, left panel). For the cold-only run (EXP 3), only weak positive flux anomalies as in Fig. 5.26 are observed (not shown). These weak fluxes are comparable to those obtained by forcing with a pattern similar to the negative anomaly alone in a 7 year AGCM experiment (Power et al. 1995). The experiment with the inverse sign of the SST dipole (EXP 4, Fig. 5.27, right panel) shows also reversal of the sign of the fluxes. The fluxes over the warm SST anomaly are again considerably larger than over the negative anomaly, but the latter are much larger than in EXP 1. It is hypothesised that these larger fluxes (where the atmosphere loses latent heat) counteract a possibly larger response to the northern warm anomaly, leading to the weak signal of EXP 4 (Fig. 5.21).

Note also the negative fluxes apparent in the eastern North Atlantic in Fig. 5.26 and – less pronounced – in Fig. 5.27 (left), where no SST-forcing occurred. It is hypothesised that these anomalies are related to cyclones intensified through the altered surface fluxes over the imposed SST anomalies. Hence the stronger low-level winds associated with these cyclones increase the vertical fluxes of latent and sensible heat.

The latent (Fig. 5.28) and sensible (not shown) heat flux differences EXP - CTRL are

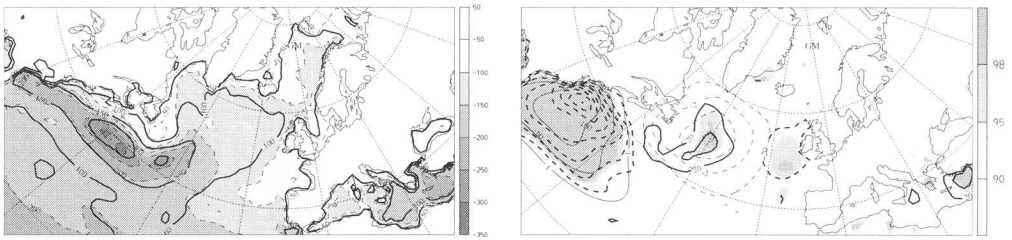


FIG. 5.26: Mean CTRL simulation latent heat flux (upper left panel) and difference EXP 1 ensemble - CTRL of latent (upper right panel, contour interval 20 Wm^{-2}) and sensible (right panel, contour interval 10 Wm^{-2}) heat flux. The t-test significance level of the difference is shaded and the SST anomaly is indicated by thin lines, contour interval 1 K.

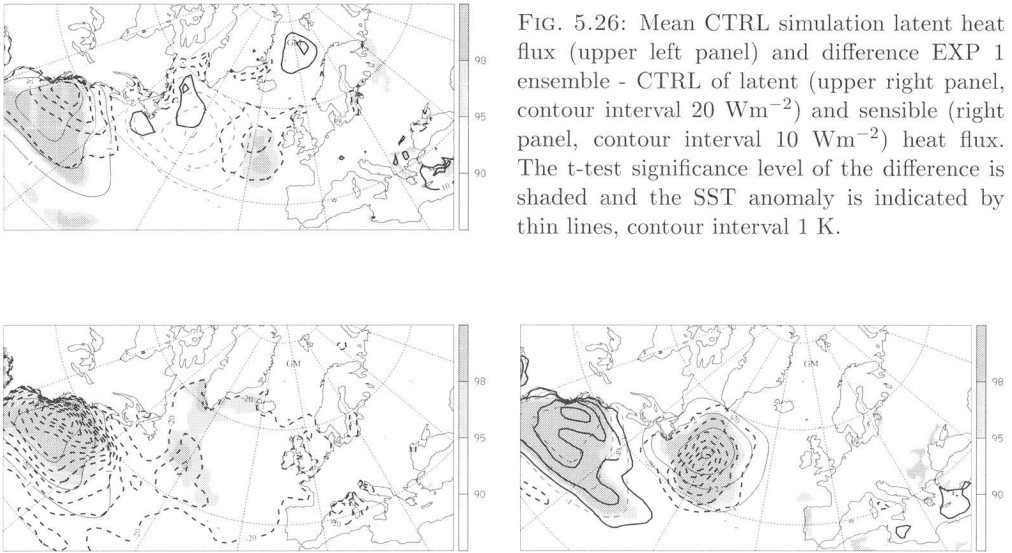


FIG. 5.27: Latent heat flux difference for EXP 2 - CTRL (left panel) and EXP 4 - CTRL (right panel), contour interval 20 Wm^{-2} . The t-test significance level of the difference is shaded and the SST anomaly is indicated by thin lines, contour interval 1 K.

much smaller for the monopole SST anomaly compared to the dipole anomaly. This indicates that different mechanisms might be involved in the generation of the respective responses. As in the dipole and warm anomaly only case, a region of fluxes from the ocean surface into the atmosphere to the east of the imposed cold anomaly is observed in the monopole cold anomaly case, underneath the positive storm track response.

Further insight into the processes related to the observed anomalous fluxes can be sought from an investigation of their time series. The time evolution of the difference EXP 1 - CTRL of latent and sensible heat flux averaged over the area of the positive SST anomaly of EXP 1 (Fig. 5.29) is mainly directed upward into the atmosphere and shows large variability in the 2-7 day band, clearly associated with midlatitude synoptic storms (cf. Alexander and Scott 1997). The fluxes averaged over the area of the negative SST anomaly exhibit the same variability structure but they do not show a clear polarity (lower panel). Therefore, the anomalous heat flux averaged over the whole North Atlantic ocean is dominated by

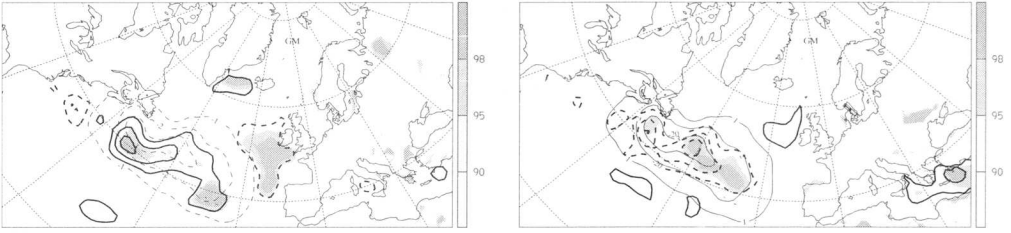


FIG. 5.28: As Fig. 5.27, but for the monopole SST anomaly (EXP 5 and EXP 6).

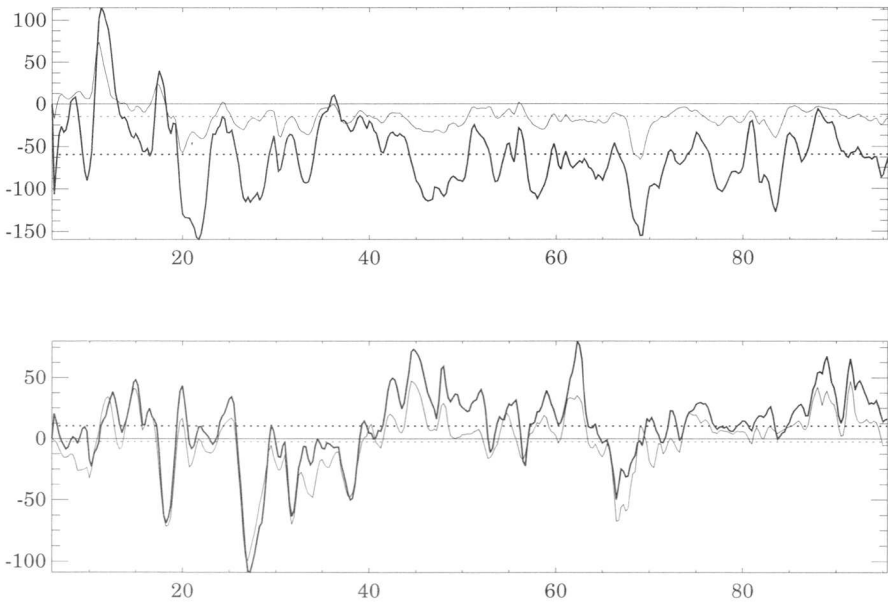


FIG. 5.29: Time evolution of the difference EXP 1 - CTRL of latent (bold) and sensible (thin) heat flux averaged over the area where $\Delta\text{SST} > +1$ K (upper panel) and $\Delta\text{SST} < -1$ K (lower panel). Vertical axis in Wm^{-2} , horizontal axis days since 1st of December. Dashed lines the respective time mean fluxes. Note that negative fluxes are directed from the ocean into the atmosphere.

the upward flux occurring over the positive SST anomaly, as confirmed by the experiment with the warm anomaly only (EXP 2). The time evolution of the anomalous fluxes reflects the passage of single synoptic systems. There is high evidence that these disturbances are affected by the anomalous fluxes of latent and sensible heat and lead to the storm track signal, which in turn contributes to the geopotential height response through forcing of the

slow transients by synoptic-scale eddies (cf. Sheng and Derome 1993).

5.2.4 Growth and Decay Rates of Synoptic Systems

Consideration of the growth and decay rates of cyclones (local changes in surface pressure of synoptic scale systems, see Section 2.2.2) illustrates further the effect of the imposed SST anomalies on single cyclones. Averaged over the North Atlantic ocean northward of 40°N the mean growth (decay) rate for EXP 1 was 15.04 (9.28) hPa/24h compared to 12.52 (8.16) hPa/24h for the CTRL experiment (the growth rate difference of 2.52 hPa/24h being significant at the 95% level). The largest region of enhanced growth (not shown) occurs in a belt off Newfoundland stretching over the western North Atlantic and might thus be attributed to the imposed SST anomalies. It is partly counteracted by the weak increase in the decay rate (about 40% of the growth rate difference), which reflects again the increased atmospheric variability. There appears also to be some tendency of an eastward shift of the region of high growth rates in the EXP simulations.

The attribution of the enhanced growth to mainly the warm SST anomaly (and the increased gradient effectuated by its imposition) is further elucidated by comparison of the surface pressure response to the SST dipole forcing (Fig. 5.30, left panel) with the simulation with the warm SST anomaly alone (right panel). In the EXP 2 simulation, the surface pressure pattern shows a pressure decrease starting near the center of the SST anomaly. In contrast, the surface pressure response of EXP 3 – cold anomaly only – appears to be rather weak with almost no difference in Murakami filtered surface pressure (not shown).

5.2.5 Moisture Distribution

To assess the effect of the changed SST configuration on the moisture budget, a Lagrangian trajectory analysis (Wernli and Davies 1997) was performed. The trajectories were started every 6 hours of simulation (for both the EXP 1 and CTRL simulations) on a coarse grid over the northern North Atlantic (Fig. 5.31, left panel) at the lowest model level⁷. Selected variables were traced along the particles' paths. The average *difference* between the EXP 1 and CTRL simulation of latent heat flux experienced by the trajectories is shown in Fig. 5.31, the average difference in moisture intake/depletion in Fig. 5.32. Note that only air parcels within 500 msl⁸ were subject to (latent heat) fluxes, while the moisture budget was calculated throughout the atmosphere. There is a clear collocation of moisture gain and negative (ocean to atmosphere) latent heat flux. The extension of the area of moisture depletion far to the east from the region where negative latent heat fluxes occurred can be attributed to diabatic processes taking place downstream of the source of the additional moisture (cf. Liniger 1998). This agrees with the growth rate increase observed in the previous Section. To further illustrate this, the precipitation difference EXP 1 minus CTRL simulation (and the CTRL totalised precipitation) is shown in Fig. 5.33. Two distinct features can be identified: i) the convective activity is enhanced over the warm SST anomaly and ii) the stratiform/convective

⁷Air parcels advected downward out of the lowest model level were re-placed into the lowest model level again.

⁸A rough measure of the thickness of the marine boundary layer where heat fluxes mainly take place.

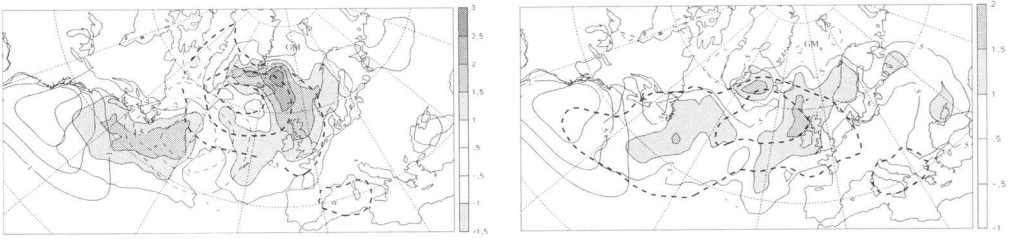


FIG. 5.30: Difference of mean (DJF) surface pressure (thick lines, contour interval 2.5 mb) and Murakami filtered surface pressure (shaded, contour interval 0.5 mb) for EXP 1 simulation - CTRL simulation (left panel) and EXP 2 simulation - CTRL simulation (right panel).

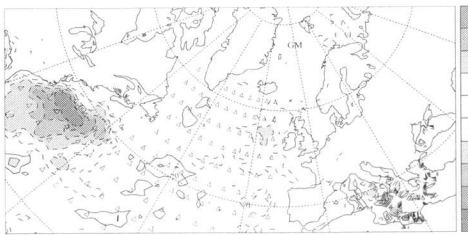


FIG. 5.31: Difference EXP 1 - CTRL simulation of average latent heat flux experienced by the trajectories along their path (negative values: air gaining heat, contour interval 20 Wm^{-2}). The starting points of the Lagrangian trajectories are indicated by triangles. See text about details.

precipitation is enhanced/decreased in the EXP 1 simulation in the central North Atlantic. Together with the consideration of the growth rate in the previous Section, it appears that the increased SST triggers local convection and influences the growth of synoptic scale systems by providing extra moisture which can contribute to stronger deepening through latent heat release reflected in stratiform precipitation, which in turn modifies – for example – the structure and dynamics of low-level PV-bands (Fehlmann and Davies 1997). In a case study, Reed et al. (1988) found that condensational heating accounted for 40%-50% of the deepening of three explosive cyclones and that most of the heating derived from stable, frontal rather than convective precipitation. Furthermore, the location of the moisture depletion suggests that secondary cyclogenesis on frontal systems (see Parker 1998 for a review) might be affected by these processes.

5.2.6 Vertical Structure

The changes to the vertical structure of the model response is illustrated by comparing the EXP 1 simulation with the CTRL run. The location of the vertical cross-section through the difference EXP 1 - CTRL is shown in Fig. 5.34. The vertical structure of the geopotential height response (Fig. 5.35, left panel) shows highly significant values from the surface up to the maximum amplitude at the tropopause level. The positive and negative anomalies of θ_e (Fig. 5.35, right panel), imply that the atmospheric stability is reduced/increased over the positive/negative SST anomaly. The stronger influence of the positive anomaly is illustrated by the pattern of the standard deviation difference of θ_e . There emanates a region

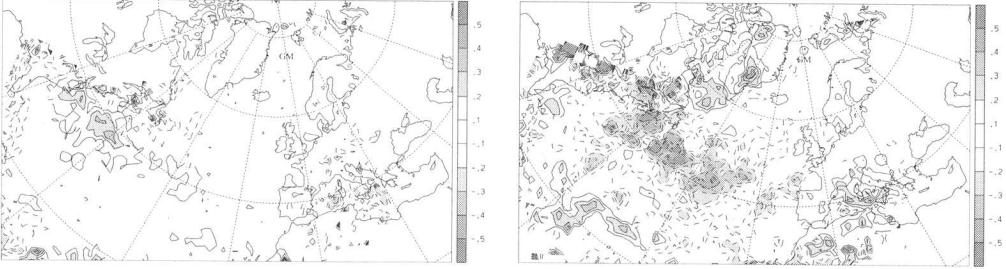


FIG. 5.32: Difference EXP 1 - CTRL of average moisture gain (left panel) and loss (right panel) of the trajectories along their path. Contour interval $0.1 \text{ g kg}^{-1} / 6 \text{ h}$. See text about details.

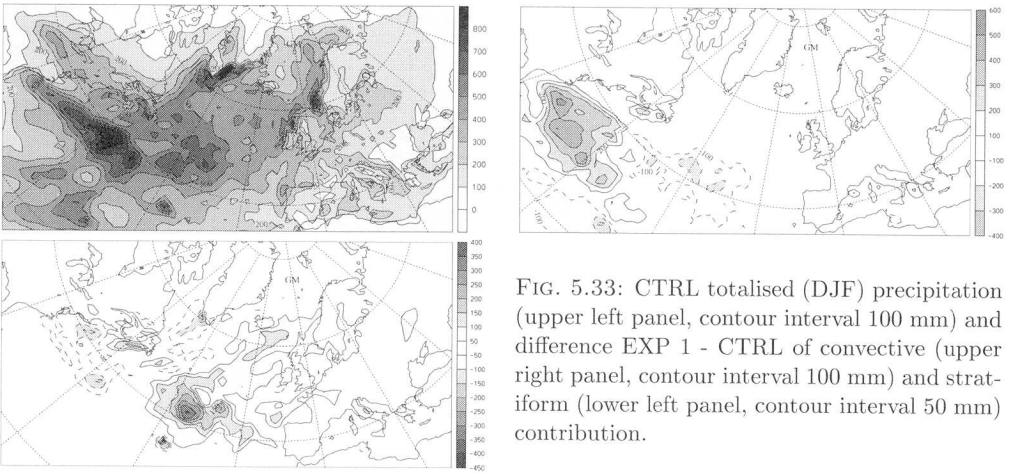


FIG. 5.33: CTRL totalised (DJF) precipitation (upper left panel, contour interval 100 mm) and difference EXP 1 - CTRL of convective (upper right panel, contour interval 100 mm) and stratiform (lower left panel, contour interval 50 mm) contribution.

of increased variability from the positive anomaly in a northeastward and upward direction, roughly collocated with the standard deviation difference in relative humidity (not shown). The positive relative humidity difference represents a 5% gain in the EXP 1 simulation (significant at 95%) and is separated from the region of high variability. This indicates a recurrent northeastward transport of moisture by the synoptic scale transients, while a large part of the additional moisture taken up over the warm SST anomaly is released downstream of the SST anomaly, temporarily reducing the stability by latent heat release, thus reflected in enhanced standard deviation of θ_e and relative humidity. This picture is consistent with the regional distribution of moisture loss as revealed by trajectory analysis in the previous Section (Fig. 5.32). Note further the higher values of θ_e in the upper atmosphere, indicative of increased stability as also revealed by the enhanced PV in this region (not shown). Together with the higher variability of the aforementioned variables at tropopause level, this indicates – in accordance with the geopotential height response – that the lowering of the mean tropopause can be attributed to intensified transients (consistent with the reduced relative humidity in the upper atmosphere, attributable to stratospheric intrusions).

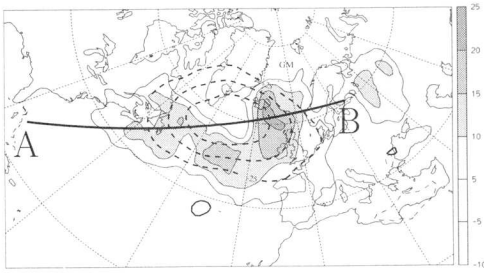


FIG. 5.34: Position of vertical cross-section discussed in Section 5.2.6 in relation to the model response to SST forcing (EXP 1 - CTRL simulation).

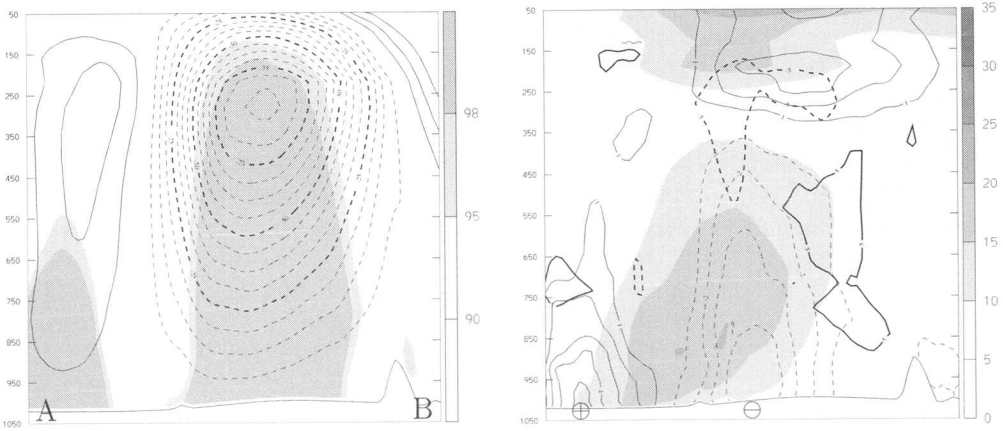


FIG. 5.35: Vertical cross-section through the model response to SST forcing as indicated in Fig. 5.34. Difference EXP 1 - CTRL of geopotential height (left panel, thick lines, contour interval 12.5 gpm) and its significance (shaded), θ_e (right panel, thin contours, interval 1 K), relative humidity (right panel, thick contours, interval 5% rel. hum.) and standard deviation of θ_e (right panel, shaded contours, contour interval 5 K). The orientation of the cross-section is indicated by letters A and B in the left and the center of the positive and negative SST anomalies by \oplus and \ominus in the right panel. Values larger than approximately 1 K in θ_e and 5% rel. hum. are significant at the 95%-level of Student's t-test.

5.2.7 Phase Space: Coupled Patterns

Several aspects of the model response to SST forcing have been covered by the previous Sections, shedding some light on the physical mechanisms. A direct comparison with the statistically derived patterns of Chapter 3 is undertaken here. First, the response will be analysed in terms of the model's own geopotential height EOFs (Fig. 5.36), as described in Section 2.3.3. The first model EOF resembles the first geopotential height pattern of Chapter 3 (Fig. 3.2). There is a close resemblance of the CTRL model EOFs to the patterns

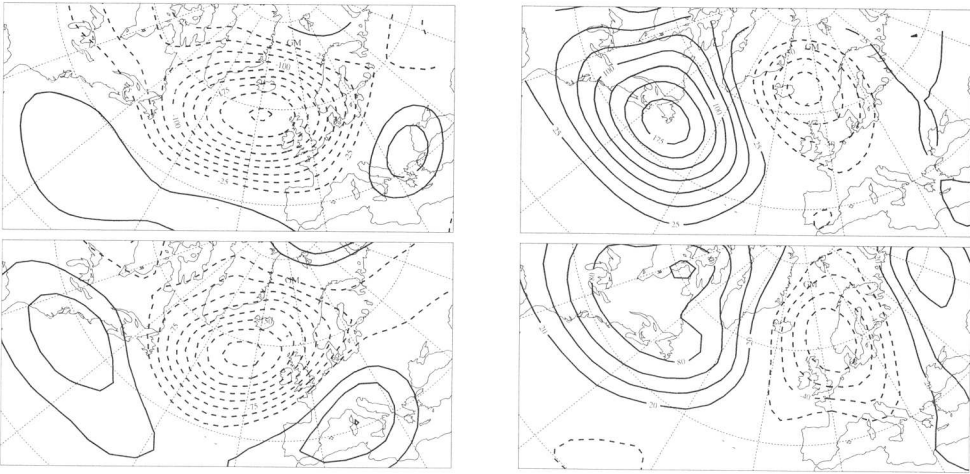


FIG. 5.36: First two geopotential height EOFs of CTRL simulation (upper panels), explaining 24% and 19% of the variance. First two geopotential height EOFs of PCA of twice daily NMC data December 1990 through February 1991 (lower panels), explaining 22% and 14% of the variance. The patterns depict one standard deviation of the scores.

derived from NMC twice daily data December 1990 through February 1991 (even explaining similar amounts of variance), and this indicates that the CTRL simulation reproduces the observed winter mean state (the NMC mean closely matches the CTRL mean) and the dominant mode of variability. The leading model EOF explains the maximal amount of model variance⁹, it represents a kind of optimal slice – in terms of the geopotential height field – through the model’s phase space, and provides a suitable measure of the model response to SST forcing. The projection of the various experiment’s responses onto the leading model EOF is presented in Fig. 5.37. The higher-order EOFs describe additional variability but may quickly degenerate into over fitting to noise, so the present study focuses on the first mode. The dependence of the strength of the first geopotential mode to SST forcing is clearly visible, since all statistically significant¹⁰ simulations lie in the upper right quadrant of the plot. The axes are labeled in units of the respective pattern scores, thus forcing with a SST anomaly 4 times the standard deviation of its scores leads to a change in the leading model geopotential height pattern of 35% of its scores’ standard deviation (EXP 1). The clustering of both the CTRL-simulation ensemble (D0, CTRL, F0) as well as the EXP 1 ensemble (D1, EXP1, F1) in clearly separated regions of the phase-space slice is evident. Note that the CTRL spread (i.e. vertical distance between D0, CTRL and F0) is considerably smaller than the experiment-spread, indicative of the fact that the imposition of SST anomalies affects the mean amplitude of the first geopotential height mode and its

⁹As mentioned in Section 2.3.3, we checked for the EOFs of the different simulations being similar.

¹⁰Prior to a two-tailed Student’s t-test, the six hourly model data has been filtered by application of a 3-day running mean to account for the characteristic time scale of synoptic-scale processes. It has to be noted that the test values based on unfiltered data were even better for all cases.

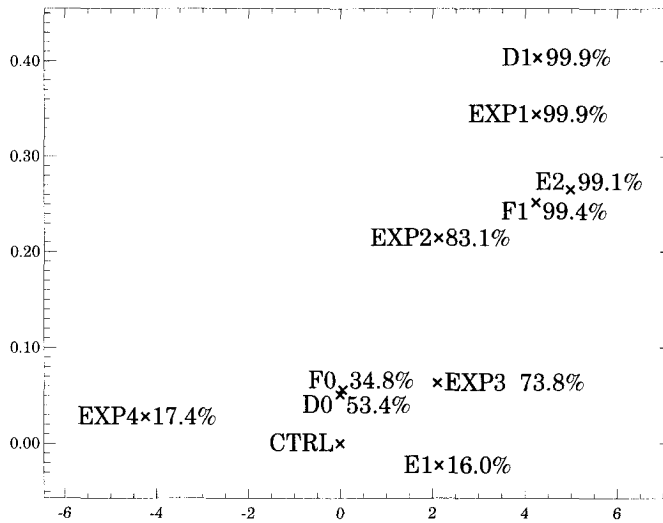


FIG. 5.37: Phase space: Position of the various experiments in a phase space slice spanned by the first SST pattern (the forcing, horizontal axis) and the first model geopotential height EOF of the CTRL simulation (the response, vertical axis). Axes are labeled in units of the pattern amplitude as shown in Fig. 3.2 and Fig. 5.36, respectively. The percentage numbers following the experiment names indicate the t-test significance level of the projection onto the first model EOF.

variability. EXP 2 (warm anomaly only) is contiguous to the EXP 1 ensemble, whereas EXP 3 (cold anomaly only) is not separated from the CTRL cluster. This is consistent with the warm anomaly being predominantly responsible for the atmospheric response. EXP 4 (inverse sign of the SST dipole anomaly) does not produce any significant change in the first model EOF, reflecting the non-linearity of the model response to SST forcing (cf. Lunkeit and van Detten 1997). Experiments E1 (two times the unsmoothed SST pattern) and E2 (as EXP 1, but with stronger negative anomaly) were not discussed in detail, but are included here. The projection of the experiments onto the second model geopotential height EOF indicates no highly significant amplification of this pattern (thus not shown), the CTRL ensemble spread being larger but still smaller than the EXP ensemble spread. (For the third model EOF, both CTRL and EXP ensembles are neither significantly separated nor spread out).

The comparison of the different simulations of the winter 1990/91 case will be concluded by considering the relation to the statistical patterns of Chapter 3. Note that the model NAO index (surface pressure difference between grid points near Iceland and the Azores) amounts to 25.7 mb for the CTRL and to 35.3 mb for the EXP 1 simulation, the imposition of the SST dipole thus raises the model NAO index by 41% of its standard deviation (significant at 95% level). This result is consistent with the forcing of the first (NAO) mode of geopotential height by the imposed SST anomaly.

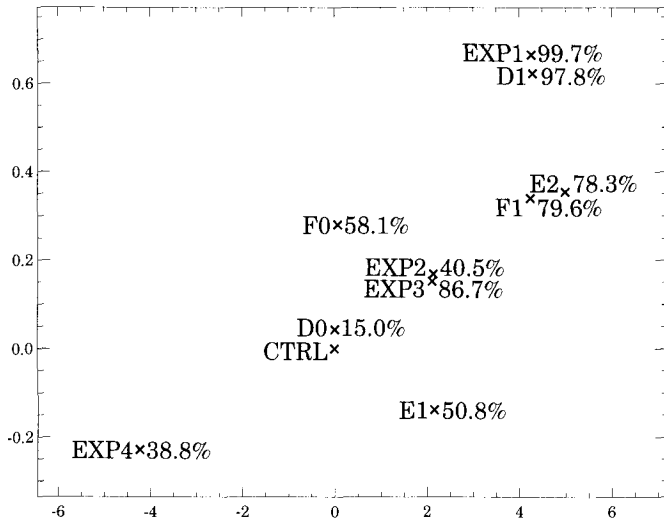


FIG. 5.38: As Fig. 5.37, but with the projection onto the leading climatological geopotential height pattern (Fig. 3.2) as vertical axis.

The phase space slice spanned by the first (statistically) coupled SST and geopotential height patterns (Fig. 5.38) is comparable to the picture obtained by projecting onto the first model EOF. Nevertheless, there are some remarkable differences. The separation of the CTRL and EXP 1 ensemble clusters is not as clear (but the significance of F1 being different from CTRL is much larger than for F0) and the experiment with reversed sign of the SST dipole (EXP 4) is at least placed in the right quadrant, but is still not really significantly different from the CTRL simulation. EXP 2 is less significant than EXP 3 (40% vs. 86%). This is linked to the difference of the model EOF and the first climatological pattern, especially to the fact that the model response does not show a positive response in the southern North Atlantic, as present in the statistically derived pattern.

The phase space slice spanned by the first coupled SST - storm track mode (Fig. 5.39) shows again a clear dependence of the storm track amplitude on SST forcing. We were not able to calculate any significance levels, since there are not enough storm track samples¹¹. Nevertheless, the high significance of the geopotential height response (Fig. 5.38) together with the fact that the storm track response pattern (for example Fig. 5.16) shows similar relations to the height response pattern as captured by the statistically coupled pattern(s) of the two fields (Fig. 3.12), show high evidence for the storm track response being clearly significant as well.

The different model simulations are best summarised by projecting the response patterns

¹¹We calculated nine 10-day storm tracks for the CTRL and EXP simulation as mentioned in Section 5.2.2, observing a similar structure of the difference as shown in Fig. 5.16, but there are too few samples for a statistical test.

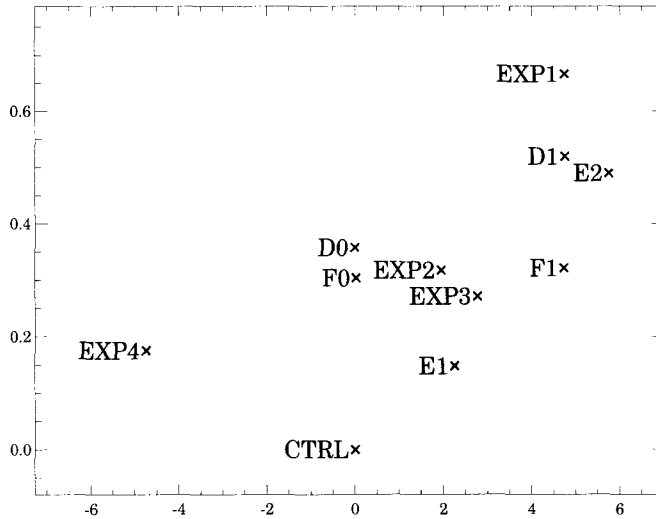


FIG. 5.39: As Fig. 5.38, but with the projection onto the leading climatological storm track pattern (Fig. 3.8) as vertical axis.

on the leading model EOF (Fig. 5.37), while the projection on the real coupled pattern captures at least the same general features, a significant forcing of the atmospheric flow in the direction of the leading geopotential height mode through imposition of the first SST pattern.

5.3 Summary and Discussion

In the present Chapter, the sensitivity of the atmospheric flow to SST configuration has been assessed for several cases using a limited area NWP model of the North Atlantic region. Two kinds of experiments have been performed which differ in the way the SST fields have been modified (either suppressing or imposing the dominant statistically derived SST mode). Note that the use of a limited area model prevents planetary-scale feedback and restricts the degrees of freedom of the simulations. Indeed the unperturbed (CTRL) flow incident at the lateral boundaries inhibits any (climate) ‘drift’. Therefore the modelled response provides a constrained estimate of the atmospheric signal.

The dominance of either the Pacific or Atlantic sector in a specific mode of midlatitude air-sea interaction was demonstrated in Chapter 3 (Fig. 3.1). The atmospheric response pattern to SST forcing in the North Atlantic obtained by simulations with a limited area model corresponds with GCM simulations of comparable resolution (Palmer and Sun 1985; Peng et al. 1995). Hence the use of a model limited to the North Atlantic sector is suited to study the effect of the lower boundary conditions on the atmospheric flow evolution.

For the case of a low NAO index (December 1981), the filtering out of the leading climatological SST pattern resulted in changes of geopotential height and storm track amplitude, but the EXP - CTRL differences do not project significantly on the difference patterns derived by statistical analysis. Enhanced fluxes of latent and sensible heat and higher growth rates over the northwestern North Atlantic were symptomatic of single cyclones contributing to the mean response. In December 1986 (high NAO index), the filtering out of the leading SST pattern did not produce significant results.

Thus month-long simulations with filtered SST patterns do not appear to be suited to assess the atmospheric response due to the small sample length. But the application of this approach to a large number of cases of several years might be appropriate to investigate the effect of a selected SST pattern on weather and climate (for example in the context of the ECMWF Reanalysis).

The second approach (imposition of SST anomalies) provided more reliable results, both due to the time-independent amplitude of the SST anomaly and the longer integration time. In the winter case 1990/91, it has been shown that the imposition of SST anomalies of considerable – but still realistic – amplitude results in a clear atmospheric flow response.

The response to a dipole SST anomaly consists of a strengthening of the trough in the geopotential height field at the southern tip of Greenland (with maximum amplitude at tropopause level) and a strengthening and zonal extension of the storm track¹². This result is in general agreement with the findings of Ferranti et al. (1994), where a geopotential height anomaly with the same sign as the northern component of the SST dipole anomaly has been observed to be a common element of the midlatitude atmospheric response. Furthermore, the observed amplitude in the cited study corresponds well with the values obtained in the present investigation, i.e. an SST anomaly of the order of 3 K produces a maximum downstream amplitude of about 75 gpm. Similar results for the winter 1980/81 case (not discussed in detail) suggest that these findings are not restricted to the winter 1990/91 case¹³. It has also been demonstrated that the warm anomaly of the SST dipole is responsible for a major part of the response. The effect of a monopole SST anomaly – a barotropic geopotential height response to the northeast with maximum amplitude at the tropopause level – is in general agreement with the results obtained by Palmer and Sun (1985) and Peng et al. (1995). The relative position of the geopotential height signal to the increased storm track observed in the model simulations compares with the large-scale coupling of geopotential height and storm track patterns isolated by SVD analysis (Chapter 3). In general, a negative geopotential height anomaly goes together with an enhanced storm track

¹²A repetition of the SST dipole experiments for winter 1980/81 reveals the same basic flow response is for the winter 1990/91 case, but the zonal intensification of the storm track is weaker, since the CTRL mean storm track of this particular winter appears to be already quite strong and latitudinally confined. The weakened response of the winter 1980/81 might thus be due to increased strength of the mean Atlantic jet stream, as proposed responsible for the difference of early and midwinter response by Ting and Peng (1995).

¹³Due to a stronger and more zonally extended storm track, the storm track response in winter 1980/81 is not as pronounced as in winter 90/91.

at its southern and eastern flanks, while a positive geopotential height anomaly is coupled to a northeastward deflection of the storm track.

The pattern of the geopotential height response projects significantly on the first *model* geopotential height EOF, and on the statistically derived leading *climatological* geopotential height pattern. The storm track signal projects on the dominant climatological storm track pattern (cf. Bresch et al. 1998). On average, the amplitude of the patterns was observed to be increased by about 30% of the respective scores' standard deviation (when forced with a SST anomaly representing 4 times the principal SST mode's scores standard deviation). The significance of the response has been further assessed with ensemble runs. The latter indicate that i) the control and experiment simulations are significantly different, ii) the dependence of the initial state is smaller than the response and iii) the ensemble spread of the control simulation (measured in terms of the leading geopotential height EOF) is smaller than the experiment ensemble spread. This indicates that the SST forcing not only affects the atmospheric mean flow, but also its variability. It has been shown that the imposed SST reinforces the dominant geopotential height pattern and probably influences its persistence (cf. Namias 1975; Barsugli 1995). The structure of the model response and its similarity to the observed teleconnection patterns suggests that the atmospheric response to SST anomalies might be interpreted as some type of normal mode response, rather than as a forced wave-train (Wallace and Jiang 1987).

The atmospheric response appears to be strongly dependent on the polarity, shape and precise location of the SST anomaly¹⁴ in relation to the mean flow. Furthermore, the results indicate that single elements of the statistically derived patterns are selectively excited by SST forcing. For example, only the Icelandic low but not the Azores high of the first geopotential height (NAO) mode is enhanced by the imposition of the SST dipole.

The strongest response was found in December, followed by February with the weakest signal in January (cf. Peng et al. 1995; Ting and Peng 1995). Additional simulations with the smoothed SST dipole for December 1981 and 1986 also exhibit an enhanced trough of geopotential height south of Greenland and latitudinal confinement and enhancement of the storm track (not shown). This betokens the reproducibility of the December response. However, no reversal of the sign of the response in January has been observed¹⁵ (cf. Peng et al. 1995).

It has been hypothesised earlier that in midlatitudes, the mean atmospheric response is caused by single cyclones influenced by the altered fluxes due to the imposition of SST anomalies. This is evidenced in the structure of the surface fluxes and their large temporal variability, the moisture transport revealed by trajectory analysis, considerations of the growth and decay rates, the structure of the response in terms of model EOFs and the strongly coherent storm track response. Both the similarity of the response in subsets of the data and the inspection of the mean and standard deviation of selected variables in a cross-section through the response reveal a comparable structure of the response in each of

¹⁴Note that smaller scale SST anomalies than those imposed in this study might also be effective in altering the atmospheric flow, since the largest fluxes were concentrated on an area smaller than the whole anomaly.

¹⁵The selected case was a winter with almost equally moderate NAO index, hence small month-to-month variability. This could explain why no midwinter reversal of the response has been observed.

the single events. Again, the warm part of the SST dipole proves to be more important than the cold part. It should be noted that the detailed structure of a given cyclone might also largely influence its sensitivity to the SST configuration due to the dependence of vertical fluxes of heat and momentum on air-mass properties and wind speed¹⁶.

Together with considerations about the limitations of methods like SVD in Section 3.5, it might be noted that the twofold approach followed in the present study is consistent with the following tentative hypothesis concerning the mutual relations of ocean and atmosphere in the North Atlantic sector: The large scale structure of the coupled system is set predominantly by the atmospheric circulation (cf. Saravanan 1998). The dipole-mode in geopotential height represents a kind of eigenmode of the North Atlantic sector and the SST pattern is shaped by atmospheric influence to the observed dipole structure. The anomalous SST configuration in turn affects the life cycle of single cyclones through the fluxes of latent and sensible heat. The sensible heating will occur predominantly in the flow of cold air off the continents over warm waters that occurs behind moving low pressure disturbances, and the latent heat release will be mostly in the warm moist air that is rising ahead of them. These recurrent effects on single cyclones in turn alter the storm track in position and intensity, which itself feeds back on the mean flow. Additional calculations of E-vectors (Hoskins et al. 1983) suggest that the feed-back of the transient eddies – i.e. the storm track – on the mean flow contributes substantially to the geopotential height response¹⁷. The effect is most pronounced at tropopause level. Since the atmospheric response projects on the initial atmospheric flow pattern, this feedback process can affect the statistics of the dominant mode of atmospheric variability in the North Atlantic sector.

¹⁶In this context, there is some suggestion that the detailed structure of the air-sea interface could be of substantial importance. If this is confirmed, then one should consider the inclusion of a wave model in coupled atmosphere-ocean models (Günther et al. 1992; Palmer and Anderson 1994).

¹⁷The divergence of the E-vectors is largest in the central and eastern North Atlantic and over northern Europe.

Chapter 6

Further Remarks

In this thesis, aspects of midlatitude air-sea interaction have been assessed using both statistical and modelling tools. A detailed discussion of the derived results has been presented in the concluding Sections of each Chapter. Here we provide only a brief overview summary, together with some further considerations.

The leading coupled modes of SST, geopotential height at 500 hPa and storm track of the wintertime circulation over the North Atlantic sector have been identified by SVD analysis of the monthly mean fields. The dipole signature of the first geopotential height pattern and the concomitant structure of the North Atlantic storm track is coupled to a dipole pattern in the SST field. This mode explains over 30% of the intraseasonal variability of the observed fields and reflects its two extremes strong and weak zonal flow regimes. Investigation of the last 30 years' trends in the aforementioned fields suggests that the dominant SVD modes do represent a significant part of both the intraseasonal variability and the decadal trends. The concomitant inference is that the strengthening phase of the NAO was characterised by changes in amplitude (and/or frequency) of recurrent weather modes rather than involving a transition towards a new regime. The analyses suggest that the atmosphere dominates the linear ocean - atmosphere coupling on monthly time scales, but a feedback of the ocean to the atmosphere can not be ruled out.

An examination of the possible effect of the distinctive SST patterns, identified by statistical analysis, formed the basis for a sequence of simulations with an idealised primitive equation model. The imposition of the SST dipole does not yield atmospheric anomalies that project on the corresponding statistically derived coupled patterns, but particular features of the idealised model results do relate to the overall structure of the first coupled mode. The intensification of the storm track and the concomitant strengthening of the trough in the geopotential height indicate that the SST dipole forces only limited features of the whole coupled atmospheric patterns. Furthermore, the modelled atmospheric response has been shown to be both nonlinear and highly sensitive to the precise location of the SST anomaly. In effect the atmosphere has been identified to dominate the linear coupling and the ocean configuration feeds back onto the atmosphere in a way difficult to isolate in the framework of linear statistical analysis.

To address the effect of SST anomalies in a more realistic set up, sensitivity experiments were conducted for selected months and seasons with a limited area NWP model of the North

Atlantic region. Two kinds of experiments were performed that differed in the way the SST fields were modified (either by suppressing or imposing the dominant statistically derived SST mode). The use of a limited area model prevents planetary-scale feedback and restricts the degrees of freedom of the simulations. The imposition of SST anomalies provided more reliable results than the simulations with filtered SST patterns. The response to a dipole SST anomaly consists of a strengthening of the trough in the geopotential height field over southern Greenland and a strengthening of the storm track. It was shown that the warm pole of the SST dipole is responsible for a major part of the response. The pattern of the geopotential height response projects significantly on the first *model* geopotential height EOF, and on the statistically derived leading *climatological* geopotential height pattern. In addition, the storm track signal projects on the dominant climatological storm track pattern. The atmospheric response appears to be strongly dependent on the polarity, shape and precise location of the SST anomaly and on the large-scale time-mean atmospheric flow itself.

The results of both the statistical analysis and model simulations are in harmony with the following hypothesis: The large scale structure of the coupled system is set predominantly by the atmospheric circulation. The dipole-mode in geopotential height replicates somewhat the eigenmode of the North Atlantic sector and the SST pattern is shaped by atmospheric influence to the observed dipole structure. The anomalous SST configuration in turn affects the life cycle of individual cyclones through the fluxes of latent and sensible heat. These recurrent effects on single cyclones in turn alter the storm track's position and intensity, and the latter effects feed back on the atmospheric mean flow.

These results suggest that midlatitude SST anomalies can induce weather regimes to be somewhat more persistent, but they do not fundamentally enhance the predictability of regime transitions (cf. Palmer 1993). For example, during a phase of prevailing zonal mean flow (e.g. positive NAO index), the results of the present study suggest that the flow statistics can be affected by the presence of a specific SST dipole anomaly – the dipole anomaly with a positive center off the North American east coast and a negative center to the North. In the context of extended range weather prediction, where the focus changes from deterministic to stochastic forecasting (Palmer 1996), it has been argued that the influence of the – slowly varying – boundary conditions can begin to dominate over the effect of the initial conditions. Thus it might not be sufficient merely to extend the length of integration of a weather prediction model, but the model must be dynamically coupled to the lower boundaries¹, *sic.* the oceans (Palmer and Anderson 1994). Furthermore, the correct representation of the air-sea interface through sufficient spatial model resolution (cf. Latif 1998) and adequate parametrisations (cf. Davis and Emanuel 1988) is of crucial importance.

For extended range weather prediction, the distinction between and the understanding of weather regimes with high/low predictability is central. For example, the variability in predictive skill over North America is strongly related to fluctuations in the Pacific/North American (PNA) mode of low frequency variability (Palmer 1988). For the North Atlantic region, the model results of the present study suggest that the sensitivity of the atmospheric

¹Note that even the medium range predictive skill might be improved if time-dependent (i.e. not fixed over one week or even month) SST is included (Ranelli et al. 1985).

flow evolution to lower boundary conditions depends on the prevailing sign and amplitude of the NAO.

Transitions between weather regimes do not necessarily require external forcing, and might be associated merely with the nonlinearity and internal instability of midlatitude atmospheric dynamics. These transitions tend to have small predictability, so that on time scales beyond the medium range period (i.e. about 10 days) but shorter than one month, about one to three regime transitions are likely to occur, but inherently difficult to predict. On the seasonal time scale, there could be many regime transitions which are not deterministically predictable. But a stochastic forecast is still possible instead, due to the slowly-varying boundary conditions, for example through the effect of the midlatitude SST anomalies, which bias the population statistics of the observed weather regimes. In the present study, both the modelling results and the fact that a significant portion of the long-term height and storm track trends can be statistically inferred from the changes in the SST configuration illustrate this perspective.

On even longer time scales, the feedback from ocean to atmosphere in midlatitudes has been identified to play a significant role in North Atlantic variability. Low frequency responses of the ocean to atmospheric forcing could feed back on the atmosphere through processes such as those addressed in the present study, resulting in oscillatory behaviour on decadal time scales (cf. Latif and Barnett 1996; Griffies and Bryan 1997).

Hence a better understanding of the feedback processes between ocean and atmosphere in midlatitudes is necessary for the assessment of climate variability and predictability and for extended/seasonal range forecasting. These important and open issues merit considerable further attention.

Leer - Vide - Empty

Appendix A

Another Application of PCA

There are a myriad of applications of multivariate statistical analysis methods in meteorology and other fields. A simple illustration that captures the essence of the procedure is given here, and relates to image processing. Given a series of images with somewhat similar structure, e.g. passport photographs, PCA allows considerable data compression. Consider the application of PCA to thirty members of the Institute for Atmospheric Science at the Swiss Federal Institute of Technology (ETH) in Zurich. The mean and leading EOFs carry with them recognizable physical characteristics and can provide a rudimentary classification of human appearance (Fig. A.1). The short haircut of the 'mean' member of the institute can be interpreted as a reflection of either the minority of female members or the general lack of long-haired individuals among the people employed at the institute. Note further the beard-type EOF 1. The reconstruction capability of the PCA approach for people of the Institute

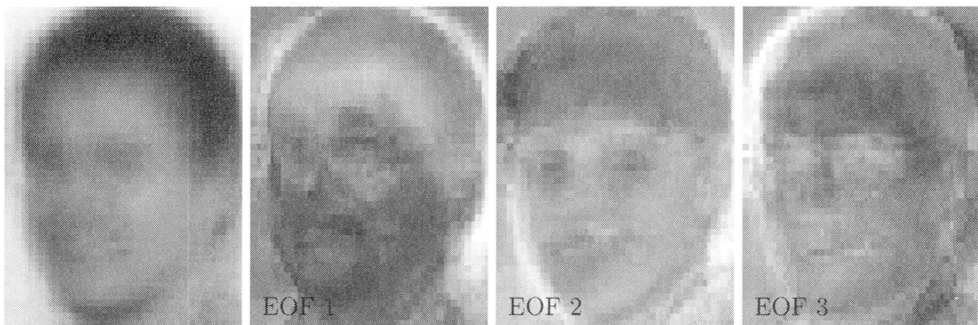


FIG. A.1: Mean (leftmost panel) and leading three EOFs of the people at the Institute for Atmospheric Science at ETH in Zürich.

is shown for selected individuals in Fig. A.2. A distinction between individuals can not be made based upon the reconstruction with the leading 6 EOFs, whereas 12 EOFs already resolve the principal differences. A reconstruction with 24 EOFs is capable of reproducing small features (like glasses) and reflects the facial expression, possibly even the psychological condition? Any further speculation is left to the reader.



FIG. A.2: Sample images of four selected people, namely Huw C. Davies, Klaus Fraedrich, Christoph Schär and David N. Bresch (from top to bottom). Leftmost panel the original scanned image the PCA is based upon. Middle and right panels reconstruction with 6, 12 and 24 EOFs, respectively.

Appendix B

Overview of Model Experiments

Experiment	Name	Description	Figure(s)
Control simulation	CTRL	Section 4.1	4.1, 4.2, 4.3, 4.4, 4.5, 4.15
dipole anomaly	EXP 1	Section 4.2.1	4.7, 4.8, 4.9, 4.15, 4.16
- double amplitude		Section 4.2.1	4.10
warm anomaly only	EXP 2	Section 4.2.2	4.11, 4.15
cold anomaly only	EXP 3	Section 4.2.2	4.12, 4.15
NE shifted warm anomaly	EXP 2b	Section 4.2.2	4.13, 4.15
reversed dipole anomaly		Section 4.2.2	4.14, 4.15

TABLE B.1: List of all idealised model experiments discussed in Chapter 4.

Experiment	Name	Description	Figure(s)
Dec 81 control simulation	CTRL	Section 5.1.1	5.1
filtered SST	EXP	Section 5.1.1	5.2, 5.3, 5.4, 5.5, 5.6
Dec 86 control simulation	CTRL	Section 5.1.2	5.7
filtered SST	EXP	Section 5.1.2	5.8, 5.9, 5.10
Winter 90/91 control simulation	CTRL	Section 5.2.1	5.11,5.12,5.39
dipole anomaly	EXP 1	Section 5.2.2	5.13-5.17, 5.26,5.29-5.39
unsmoothed dipole anomaly	E 1	Section 5.2.2	5.22,5.39
warm anomaly only	EXP 2	Section 5.2.2	5.18, 5.20,5.27,5.30,5.39
unsmoothed warm anomaly	E 2	Section 5.2.7	5.39
cold anomaly only	EXP 3	Section 5.2.2	5.19, 5.20,5.39
reversed dipole anomaly	EXP 4	Section 5.2.2	5.21,5.39
central monopole	EXP 5	Section 5.2.2	5.23,5.24,5.28,5.39
inverse sign	EXP 6	Section 5.2.2	5.25,5.28,5.39

TABLE B.2: List of all experiments discussed in Chapter 5.

Leer - Vide - Empty

References

- Alexander, M. A., and J. D. Scott. 1997. Surface flux variability over the North Pacific and North Atlantic oceans. *J. Climate* **10**, 2963–2978.
- Appenzeller, C., and H. C. Davies. 1992. Structure of stratospheric intrusions into the troposphere. *Nature* **358**, 570–572.
- Appenzeller, C., J. Schwander, S. Sommer, and T. F. Stocker. 1998. The North Atlantic Oscillation and its imprint on precipitation and ice accumulation in Greenland. *Geophysical Research Letters* **25**, 1939–1942.
- Bacon, S., and D. J. T. Carter. 1993. A connection between mean wave height and atmospheric pressure gradient in the North Atlantic. *Int. J. Climatol.* **13**, 423–436.
- Barnett, T. P., and R. W. Preisendorfer. 1987. Origins and levels of monthly and seasonal forecast skill for United States surface air temperatures determined by canonical correlation analysis. *Mon. Wea. Rev.* **115**, 1825–1850.
- Barnston, A., and R. E. Livezey. 1987. Classification, seasonality and persistence of low-frequency atmospheric circulation patterns. *Mon. Wea. Rev.* **115**, 1083–1126.
- Barsugli, J. J. 1995. *Idealized models of intrinsic midlatitude atmosphere-ocean interaction*. PhD thesis. Department of Atmospheric Sciences, University of Washington. [Available on-line from: <http://www.cdc.noaa.gov/jbb/thesis.html>].
- Bergot, T., S. Malardel, and A. Joly. 1996. Sensitivity and singular vectors calculation in the operational context of FASTEX. *Proc. 7th Conf. on Mesoscale Processes, Reading*.
- Bjerknes, J. 1964. Atlantic air-sea interaction. *Advances in Geophysics* **10**, 1–82.
- Blackmon, M. L. 1976. A climatological spectral study of the 500 mb geopotential height of the Northern Hemisphere. *J. Atmos. Sci.* **33**, 1607–1623.
- Blackmon, M. L., J. M. Wallace, N.-C. Lau, and S. L. Mullen. 1977. An observational study of the Northern Hemisphere wintertime circulation. *J. Atmos. Sci.* **34**, 1040–1053.
- Blackmon, M. L., Y.-H. Lee, and J. M. Wallace. 1984. Horizontal structure of 500 mb height fluctuations with long, intermediate and short time scales. *J. Atmos. Sci.* **41**, 961–979.

- Blender, R., K. Fraedrich, and F. Lunkeit. 1997. Identification of cyclone track regimes in the North Atlantic. *Quart. J. Roy. Meteor. Soc.* **123**, 727–741.
- Boer, G. J., K. Arpe, M. Blackburn, M. Deque, W. L. Gates, L. T. Hart, H. Le Treut, E. Roeckner, D. A. Sheinin, I. Simmonds, R. N. B. Smith, T. Tokioka, R. T. Wetherald, and D. Williamson. 1992. Some results from an intercomparison of the climates simulated by 14 atmospheric general circulation models. *J. Geophys. Res.* **97**, 12771–12786.
- Branstator, G. 1992. The maintenance of low-frequency atmospheric anomalies. *J. Atmos. Sci.* **49**, 1924–1945.
- Branstator, G. 1995. Organization of storm track anomalies by recurring low-frequency circulation anomalies. *J. Atmos. Sci.* **52**, 207–226.
- Bresch, D. N. 1995. *Die mittlere Zirkulation der Nordhemisphäre und deren Variabilität*. Diplomarbeit, Institut für Atmosphärenphysik, ETH Zürich.
- Bresch, D. N., and H. C. Davies. 1996. A SVD analysis of the North Atlantic sea surface temperature and geopotential fields. *Annales Geophysicae, suppl. II to Vol. 14. EGS General Assembly*. Den Haag.
- Bresch, D. N., and H. C. Davies. 1998a. Recent co-variations and trends of the SST and mid-troposphere flow signatures in the extratropical North Atlantic. *J. Climate*, submitted.
- Bresch, D. N., and H. C. Davies. 1998b. Sensitivity studies of NAO variability. In *Proceedings of 9th Conference on Interaction of the Sea and Atmosphere*. American Meteorological Society (ed.). Phoenix, Arizona. Pp. 65–68.
- Bresch, D. N., R. Fehlmann, and H. C. Davies. 1998. Simulations of North Atlantic storm track variability. *Annales Geophysicae, suppl. II to Vol. 16. EGS General Assembly*. Nice, France.
- Bretherton, C., C. Smith, and J. M. Wallace. 1992. An intercomparison of methods for finding coupled patterns in climate data. *J. Climate* **5**, 541–560.
- Buell, C. E. 1979. On the physical interpretation of EOFs.. In *Preprint 6th Conf. Statistics in Atm. Sc.*. American Meteorological Society (ed.). Banff. Pp. 112–117.
- Carleton, A. M. 1988. Meridional transport of eddy sensible heat in winters marked by extremes of the North Atlantic Oscillation, 1948/49–1979/80. *J. Climate* **1**, 212–223.
- Cayan, D. R. 1992a. Latent and sensible heat flux anomalies over the northern oceans: Driving the sea surface temperature. *J. Phys. Oceanogr.* **22**, 859–881.
- Cayan, D. R. 1992b. Latent and sensible heat flux anomalies over the northern oceans: The connection to monthly atmospheric circulation. *J. Climate* **5**, 354–369.

- Cayan, D. R. 1992c. Variability of latent and sensible heat fluxes estimated using bulk formulae. *Atmos.-Ocean*. **30**, 1-42.
- Chang, E. K. M., and I. Orlanski. 1993. On the dynamics of a storm track. *J. Atmos. Sci.* **50**, 999-1015.
- Cheng, X. H., and T. J. Dunkerton. 1995. Orthogonal rotation of spatial patterns derived from singular value decomposition analysis. *J. Climate* **8**, 2631-2643.
- Cherry, S. 1996. Singular value decomposition analysis and canonical correlation analysis. *J. Climate* **9**, 2003-2009.
- Cherry, S. 1997. Some comments on singular value decomposition analysis. *J. Climate* **10**, 1759-1761.
- Christoph, M., U. Ulbrich, and U. Haak. 1995. Faster determination of the intraseasonal variability of storm tracks using Murakami's recursive filter.. *Mon. Wea. Rev.* **123**, 578-581.
- CLIVAR Science Plan 1995. A study of climate variability and predictability. *Technical report*. WCRP-89, WMO/TD-No. 690.
- Cook, E. R., R. D. D'Arrigo, and K. R. Briffa. 1998. A reconstruction of the North Atlantic Oscillation using tree-ring chronologies from North America and Europe. *Holocene* **8**, 9-17.
- Craddock, J. M., and C. R. Flood. 1969. Eigenvectors for representing the 500 mb geopotential surface over the Northern Hemisphere. *Quart. J. Roy. Meteor. Soc.* **95**, 570-593.
- Cress, A., D. Majewski, R. Podzun, and V. Renner. 1995. Simulation of European climate with a limited area model. Part I: Observed boundary conditions. *Contr. Atmos. Phys.* **68**, 161-178.
- Davies, H. C. 1976. A lateral boundary formulation for multi-level prediction models. *Quart. J. Roy. Meteor. Soc.* **102**, 405-418.
- Davies, H. C. 1997. Emergence of the mainstream cyclogenesis theories. *Meteorol. Zeitschrift* **6**, 261-274.
- Davies, H. C., and H. Wernli. 1997. On studying the structure of synoptic systems. *Meteorol. Appl.* **4**, 365-374.
- Davies, H. C., C. Schär, and H. Wernli. 1991. The palette of fronts and cyclones within a baroclinic wave development. *J. Atmos. Sci.* **48**, 1666-1689.
- Davis, C. A., and K. A. Emanuel. 1988. Observational evidence for the influence of surface heat fluxes on rapid maritime cyclogenesis. *Mon. Wea. Rev.* **116**, 2649-2659.

- Davis, R. 1976. Predictability of sea surface temperature and sea-level pressure anomalies over the Northern Hemisphere. *J. Phys. Oceanogr.* **6**, 249–266.
- Delworth, T. L. 1996. North Atlantic interannual variability in a coupled ocean-atmosphere model. *J. Climate* **9**, 2356–2375.
- Deser, C., and M. Blackmon. 1993. Surface climate variations over the North Atlantic during winter 1900–1989. *J. Climate* **6**, 1743–1753.
- Deser, C., and M. S. Timlin. 1997. Atmosphere-ocean interaction on weekly timescales in the North Atlantic and Pacific. *J. Climate* **10**, 393–408.
- Dickson, R., J. Lazier, J. Meincke, P. Rhines, and J. Swift. 1996. Long-term coordinated changes in the convective activity of the North Atlantic. *Prog. Oceanogr.* **38**, 241–295.
- Dickson, R. R., J. Maincke, S.-A. Malmberg, and A. J. Lee. 1988. The "Great Salinity Anomaly" in the northern North Atlantic 1968–1982. *Prog. Oceanogr.* **20**, 103–151.
- Eckert, P., D. Cattani, and J. Ambühl. 1996. Classification of ensemble forecasts by means of an artificial neural network. *Meteorol. Appl.* **3**, 169–178.
- Esbensen, S. K., and Y. Kushnir. 1981. The heat budget of the global ocean: An atlas based on estimates from surface marine observations. *Technical report*. Rep. No. 29, Climate Research Institute, Oregon State University, Corvallis, Ore., 244 pp.
- Fang, Z. F., and J. M. Wallace. 1994. Arctic sea ice variability on a time scale of weeks and its relation to atmospheric forcing. *J. Climate* **7**, 1897–1914.
- Fehlmann, R. 1997. *Dynamics of seminal PV elements*. PhD thesis. Swiss Federal Institute of Technology (ETH). Dissertation Nr. 12229.
- Fehlmann, R., and H. C. Davies. 1997. Misforecasts of synoptic systems: Diagnosis via PV retrodiction. *Mon. Wea. Rev.* **125**, 2247–2264.
- Ferranti, L., F. Molteni, and T. N. Palmer. 1994. Impact of localized tropical and extratropical SST anomalies in ensembles of seasonal GCM integrations. *Quart. J. Roy. Meteor. Soc.* **120**, 1613–1645.
- Fraedrich, K., and H. Böttger. 1978. A wavenumber-frequency analysis of the 500 mb geopotential at 50°N. *J. Atmos. Sci.* **35**, 745–750.
- Fraedrich, K., and K. Müller. 1992. Climate anomalies in Europe associated with ENSO extremes. *Int. J. Climatol.* **12**, 25–31.
- Fraedrich, K., C. Bantzer, and U. Burckhardt. 1993. Winter climate anomalies in Europe and their associated circulation at 500 hpa. *Climate Dynamics* **8**, 161–175.
- Fraedrich, K., R. Grotjahn, and L. M. Leslie. 1990. Estimates of cyclone track predictability. II. Fractal analysis of mid-latitude cyclones. *Quart. J. Roy. Meteor. Soc.* **116**, 317–335.

- Frankignoul, C. 1985. Sea-surface temperature anomalies, planetary waves, and air-sea feedbacks in the middle latitudes. *Rev. Geophys.* **23**, 357–390.
- Friedland, K. D., D. G. Reddin, and J. F. Kocik. 1993. Marine survival of North American and European salmon: effects of growth and environment. *ICES J. Mar. Sci.* **50**, 481–492.
- Frisius, T., F. Lunkeit, K. Fraedrich, and I. N. James. 1998. Storm-track organization and variability in a simplified atmospheric global circulation model. *Quart. J. Roy. Meteor. Soc.* **124**, 1019–1043.
- Fromentin, J., and B. Planque. 1996. Calanus and environment in the eastern North Atlantic: Influence of the North Atlantic Oscillation on *C. finmarchicus* and *C. helgolandicus*. *Mar. Ecol. Prog. Ser.* **134**, 111–118.
- Gibson, R., P. Kallberg, and S. Uppala. 1996. The ECMWF Re-Analysis (ERA) project. *ECMWF Newsletter* **73**, 7–17.
- Giorgi, F. 1990. Simulation of regional climate using a limited area model nested in a general circulation model. *J. Climate* **3**, 941–963.
- Glowienka-Hense, R. 1990. The North Atlantic Oscillation in the Atlantic-European SLP. *Tellus* **42A**, 497–507.
- Griffies, S., and K. Bryan. 1997. Predictability of North Atlantic multidecadal climate variability. *Science* **275**, 181–184.
- Grötzner, A., M. Latif, and T. P. Barnett. 1998. A decadal climate cycle in the North Atlantic ocean as simulated by the ECHO coupled GCM. *J. Climate* **11**, 831–847.
- Günther, M., P. Lionello, P. A. E. M. Janssen, L. Bertotti, C. Brüning, J. C. Carretero, L. Cavaleri, A. Guillaume, B. Hansen, S. Hasselmann, K. Hasselmann, M. de la Heras, A. Hollingsworth, M. Holt, J. M. Lefevre, and R. Portz. 1992. Implementation of a third generation ocean wave model at the European Centre for Medium-range Weather Forecasts. *Technical report*. ECMWF No. 68, ECMWF, Reading, UK.
- Hall, N. M. J., B. J. Hoskins, P. J. Valdes, and C. A. Senior. 1994. Storm tracks in a high-resolution CGM with doubled carbon dioxide. *Quart. J. Roy. Meteor. Soc.* **120**, 1209–1230.
- Halpert, M. S., and G. D. Bell. 1997. Climate assesment for 1996. *Bull. Amer. Meteor. Soc.* **78**, S1–S49.
- Hasselmann, K. 1976. Stochastic climate models, Part I: Theory. *Tellus* **28**, 473–485.
- Hastenrath, S. 1991. *Climate Dynamics of the Tropics*, Kluwer Academic Publishers, 488pp.
- Held, I. M., and P. J. Phillips. 1993. Sensitivity of the eddy momentum flux to meridional resolution in atmospheric GCMs. *J. Climate* **6**, 499–507.

- Held, I. M., S. W. Lyons, and S. Nigam. 1989. Transients and the extratropical response to El Niño. *J. Atmos. Sci.* **46**, 163–174.
- Hendon, H. H., and D. L. Hartmann. 1982. Stationary waves on a sphere: Sensitivity to thermal feedback. *J. Atmos. Sci.* **39**, 1906–1920.
- Hendon, H. H., and D. L. Hartmann. 1985. Variability in a nonlinear model of the atmosphere with zonally symmetric forcing. *J. Atmos. Sci.* **42**, 2783–2797.
- Hoskins, B. J., and D. J. Karoly. 1981. The steady linear response of a spherical atmosphere to thermal and orographic forcing. *J. Atmos. Sci.* **38**, 1179–1196.
- Hoskins, B. J., and P. J. Valdes. 1990. On the existence of storm-tracks. *J. Atmos. Sci.* **47**, 1854–1864.
- Hoskins, B. J., H. H. Hsu, I. N. James, M. Masutani, P. D. Sardeshmukh, and G. H. White. 1989. Diagnostics of the global atmospheric circulation based on ECMWF analyses 1979–1989. *Technical report*. WCRP-27, WMO/TD-No. 326, 219 pp.
- Hoskins, B. J., I. N. James, and G. H. White. 1983. The shape, propagation and mean-flow interaction of large-scale weather systems. *J. Atmos. Sci.* **40**, 1595–1612.
- Hoskins, B. J., M. E. McIntyre, and A. W. Robertson. 1985. On the use and significance of isentropic potential vorticity maps. *Quart. J. Roy. Meteor. Soc.* **111**, 877–946.
- Houghton, J., L. G. Meiro Filho, B. A. Callender, N. Harris, A. Kattenbur, and Maskell. 1996. *Climate change. The science of climate change. The second Assessment of the Intergovernmental Panel on Climate Change*, Cambridge Univ. Press, 527pp.
- Hu, Q. 1997. On the uniqueness of the singular value decomposition in meteorological applications. *J. Climate* **10**, 1762–1766.
- Hurrell, J. W. 1995a. Decadal trends in the North Atlantic Oscillation: Regional temperatures and precipitation. *Science* **269**, 676–679.
- Hurrell, J. W. 1995b. Transient eddy forcing of the rotational flow during northern winter. *J. Atmos. Sci.* **52**, 2286–2301.
- Hurrell, J. W. 1996. Influence of variations in extratropical wintertime teleconnections on Northern Hemispheric temperature. *Geophysical Research Letters* **23**, 665–668.
- Iwasaka, N., and J. M. Wallace. 1995. Large scale air-sea interaction in the Northern Hemisphere from a view point of variations of surface heat flux by SVD analysis. *J. Met. Soc. Japan.* **73**, 781–794.
- James, I. N., and P. N. James. 1989. Ultra-low frequency variability in a simple atmospheric model. *Nature* **342**, 53–55.

- Johansson, A., A. Bernston, S. Saha, and H. van den Dool. 1998. On the level and origin of seasonal forecast skill in northern Europe. *J. Atmos. Sci.* **55**, 103–127.
- Joly, A., D. Jorgensen, M. A. Shapiro, A. Thorpe, P. Bessemoulin, K. A. Browning, J. P. Cammas, J. P. Chalon, S. A. Clough, K. A. Emmanuel, L. Eymard, R. Gall, P. H. Hildebrand, R. H. Langland, Y. Lemaitre, P. Lynch, J. A. Moore, P. O. G. Persson, C. Snyder, and R. M. Wakimoto. 1997. Definition of the Fronts and Atlantic Storm-Track Experiment (FASTEX). *Bull. Amer. Meteor. Soc.* **78**, 1917–1940.
- Kaurola, J. 1997. Some diagnostics of the northern winter climate simulated by the ECHAM3 model. *J. Climate* **10**, 201–222.
- Kendall, M. G. 1970. *Rank correlation methods*, Griffin, 4th ed., London, 258pp.
- Kharin, V. V. 1995. The relationship between sea surface temperature anomalies and atmospheric circulation in GCM experiments. *Clim. Dyn.* **11**, 359–375.
- Knig, W., R. Sausen, and F. Sielmann. 1993. Objective identification of cyclones in GCM simulations. *J. Climate* **6**, 2217–2231.
- Kodera, K., and H. Koide. 1997. Spatial and seasonal characteristics of recent decadal trends in the Northern Hemispheric troposphere and stratosphere. *J. Geophys. Res.* **102**, 19433–19447.
- Köppen, W. 1881. Die Zugstrassen der barometrischen Minima in Europa und auf dem nordatlantischen Ocean und ihr Einfluss auf Wind und Wetter bei uns. *Mittheilungen der Geographischen Gesellschaft in Hamburg* **1**, 76–97.
- Kraus, E. B., and J. A. Businger. 1994. *Atmosphere-Ocean Interaction*, 2nd ed., Oxford University Press, New York, 275pp.
- Kushnir, Y., and I. M. Held. 1996. Equilibrium atmospheric response to North Atlantic SST anomalies. *J. Climate* **9**, 1208–1220.
- Kushnir, Y., and J. M. Wallace. 1989. Low-frequency variability in the Northern Hemisphere winter: Geographical distribution, structure and time-scale. *J. Atmos. Sci.* **46**, 3122–3142.
- Kushnir, Y., and N.-C. Lau. 1992. The general circulation model response to a North Pacific SST anomaly: Dependence of time scale and pattern polarity. *J. Climate* **5**, 271–283.
- Kushnir, Y., V. J. Cardone, J. G. Greenwood, and M. A. Cane. 1997. The recent increase in North Atlantic wave heights. *J. Climate* **10**, 2107–2113.
- Kutzbach, J. E. 1970. Large scale features of monthly mean Northern Hemisphere anomaly maps of sea-level pressure. *Mon. Wea. Rev.* **98**, 708–716.
- Lamb, P. J., and R. A. Pepler. 1987. North Atlantic Oscillation: Concept and application. *Bull. Amer. Meteor. Soc.* **68**, 1218–1225.

- Lambert, S. J., and G. J. Boer. 1989. Atmosphere ocean heat fluxes and stresses in general circulation models. *Atmos. Ocean* **27**, 692–715.
- Langland, R. H., and G. D. Rohaly. 1996. Adjoint-based targeting of observations for FASTEX cyclones. *Proc. 7th Conf. on Mesoscale Processes, Reading*.
- Lanzante, J. R. 1984. A rotated eigenanalysis of the correlation between 700 mb heights and sea surface temperatures in the Pacific and Atlantic. *Mon. Wea. Rev.* **112**, 2270–2280.
- Latif, M. 1998. Dynamics of interdecadal variability in coupled ocean-atmosphere models. *J. Climate* **11**, 602–624.
- Latif, M., and T. P. Barnett. 1996. Decadal variability over the North Pacific and North America: Dynamics and predictability. *J. Climate* **9**, 2407–2423.
- Latif, M., and T. P. Barnett. 1994. Causes of decadal climate variability over the North Pacific and North America. *Science* **266**, 634–637.
- Lau, N.-C. 1981. A diagnostic study of recurrent meteorological anomalies appearing in a 15-year simulation with a GFDL general circulation model. *Mon. Wea. Rev.* **109**, 2287–2311.
- Lau, N.-C. 1988. Variability of the observed midlatitude storm tracks in relation to low frequency changes in the circulation pattern. *J. Atmos. Sci.* **45**, 2718–2743.
- Lau, N.-C. 1997. Interactions between global SST anomalies and the midlatitude atmospheric circulation. *Bull. Amer. Meteor. Soc.* **78**, 21–33.
- Lee, S., and J. L. Anderson. 1996. A simulation of atmospheric storm tracks with a forced barotropic model. *J. Atmos. Sci.* **53**, 2113–2128.
- Levitus, S., J. I. Antonov, and T. P. Boyer. 1994. Interannual variability of temperature at a depth of 125 meters in the North Atlantic Ocean. *Science* **266**, 96–99.
- Liang, X.-Z., W.-C. Wang, and M. P. Dudek. 1996. Northern Hemispheric interannual teleconnection patterns and their changes due to the greenhouse effect. *J. Climate* **9**, 465–479.
- Lin, H., and J. Derome. 1997. On the modification of the high- and low-frequency eddies associated with the PNA anomaly: An observational study. *Tellus* **49 A**, 87–99.
- Liniger, M. 1998. *Direct Impact of Sea Surface Temperature South of Newfoundland on the General Circulation: A Trajectory Analysis*. Diplomarbeit, Institut für Atmosphärenphysik, ETH Zürich.
- Lorenz, E. N. 1969. Three approaches to atmospheric predictability. *Bull. Amer. Meteor. Soc.* **50**, 345–349.

- Lunkeit, F., and Y. van Detten. 1997. The linearity of the atmospheric response to North Atlantic sea surface temperature anomalies. *J. Climate* **10**, 3003–3014.
- Majewski, D. 1991. The Europa Modell of the Deutscher Wetterdienst. *Numerical methods in atmospheric models*. Vol. 2, European Centre for Medium Range Weather Forecasts, Reading, GB.
- Malberg, H., and G. Frattesi. 1995. Changes of the North Atlantic sea surface temperature related to the atmospheric circulation in the period 1973 to 1992. *Meteorol. Zeitschrift* **4**, 37–42.
- Marshall, J., and F. Molteni. 1993. Toward a dynamical understanding of planetary-scale flow regimes. *J. Atmos. Sci.* **50**, 1792–1881.
- Mitchell, J. F. B., and T. C. Johns. 1997. On modification of global warming by sulfate aerosols. *J. Climate* **10**, 245–267.
- Mo, K., and R. E. Livezey. 1986. Tropical-extratropical geopotential height teleconnections during the Northern Hemisphere winter. *Mon. Wea. Rev.* **114**, 2488–2515.
- Mo, K. C., and M. Ghil. 1988. Cluster analysis of multiple planetary flow regimes. *J. Geophys. Res.* **93D**, 10927–10952.
- Mullen, S. L. 1989. Model experiments on the impact of Pacific sea surface temperature anomalies on blocking frequency. *J. Climate* **2**, 997–1013.
- Murakami, M. 1979. Large-scale aspects of deep convective activity over the GATE area. *Mon. Wea. Rev.* **107**, 994–1013.
- Nakamura, H. 1992. Midwinter suppression of baroclinic wave activity in the Pacific. *J. Atmos. Sci.* **49**, 1629–1642.
- Nakamura, H., and J. M. Wallace. 1990. Observed changes in baroclinic wave activity during the life cycles of low-frequency circulation anomalies. *J. Atmos. Sci.* **47**, 1100–1116.
- Namias, J. 1964. Seasonal persistence and recurrence of European blocking during 1958–1960. *Tellus* **16**, 394–407.
- Namias, J. 1975. Stabilization of atmosphere circulation patterns by SST. *J. Mar. Res.* **33**, suppl., 53–60.
- Namias, J., X. Yuan, and D. R. Cayan. 1988. Persistence of sea-surface temperature and atmospheric flow patterns. *J. Climate* **1**, 682–703.
- Newman, M., and P. D. Sardeshmukh. 1995. A caveat concerning singular value decomposition. *J. Climate* **8**, 352–360.
- North, G. R., T. L. Bell, R. F. Cahalan, and M. F. J.. 1982. Sampling errors in the estimation of EOFs. *Mon. Wea. Rev.* **110**, 699–706.

- O'Brien, E. W., and E. P. Chassignet. 1995. Extratropical large-scale air-sea interaction in a coupled and uncoupled ocean-atmosphere model. *Clim. Dyn.* **12**, 53–65.
- Oerlemans, J. 1980. An observational study of the upward sensible heat flux by synoptic-scale transients. *Tellus* **32**, 6–14.
- Palmer, T. N. 1988. Medium and extended range predictability and stability of the Pacific/North American mode. *Quart. J. Roy. Meteor. Soc.* **114**, 691–713.
- Palmer, T. N. 1993. A nonlinear dynamical perspective on climate change. *Weather* **48**, 314–326.
- Palmer, T. N. 1995. The influence of north-west Atlantic sea surface temperature: An unplanned experiment. *Weather* **50**, 413–419.
- Palmer, T. N. 1996. Predictability of the atmosphere and oceans: From days to decades. Pp. 84–155. *Decadal Climate Variability: Dynamics and Predictability*. Vol. 44. NATO ASI series, Series I: Global Environmental Change, Springer.
- Palmer, T. N. 1998. Nonlinear dynamics and climate change: Rossby's legacy. *Bull. Amer. Meteor. Soc.* **79**, 1411–1423.
- Palmer, T. N., and D. Anderson. 1994. The prospects for seasonal forecasting - a review. *Quart. J. Roy. Meteor. Soc.* **120**, 755–793.
- Palmer, T. N., and Z. Sun. 1985. A modelling and observational study of the relationship between sea surface temperature anomalies in the north-west Atlantic and the atmospheric circulation. *Quart. J. Roy. Meteor. Soc.* **111**, 947–975.
- Palmer, T. N., G. J. Shutts, and R. Swinbank. 1986. Alleviation of a systematic westerly bias in general circulation and weather prediction models through an orographic gravity wave drag parametrization. *Quart. J. Roy. Meteor. Soc.* **112**, 1001–1039.
- Parker, D. J. 1998. Secondary frontal waves in the North Atlantic region: A dynamical perspective of current ideas. *Quart. J. Roy. Meteor. Soc.* **124**, 829–856.
- Peixoto, J. P., and A. Oort. 1992. *Physics of Climate*, American Institute of Physics, New York, 520pp.
- Peng, S., and J. Fyfe. 1996. The coupled patterns between sea level pressure and sea surface temperature in the midlatitude North Atlantic. *J. Climate* **9**, 1824–1839.
- Peng, S., L. Mysak, H. Ritchie, J. Derome, and B. Dugas. 1995. The difference between early and midwinter atmospheric responses to sea surface temperature anomalies in the northwest Atlantic. *J. Climate* **8**, 137–157.
- Perlwitz, J., and H. Graf. 1995. The statistical connection between tropospheric and stratospheric circulation of the Northern Hemisphere winter. *J. Climate* **8**, 2281–2295.

- Petterssen, S. 1956. *Weather analysis and Forecasting*. Motion and motion systems, Vol 1, 2nd ed., McGraw-Hill, 428pp.
- Philander, G. S. 1990. *El Niño, La Niña, and the Southern Oscillation*, Academic Press, San Diego, 293pp.
- Pierrehumbert, R. T. 1984. Local and global baroclinic instability of zonally varying flow. *J. Atmos. Sci.* **41**, 2141–2162.
- Pitcher, E. J., M. L. Blackmon, G. T. Bates, and S. Munoz. 1988. The effect of North Pacific sea surface temperature anomalies on the January climate of a general circulation model. *J. Atmos. Sci.* **45**, 173–188.
- Podzun, R., A. Cress, D. Majewski, and V. Renner. 1995. Simulation of European climate with a limited area model. Part II: AGCM boundary conditions. *Contr. Atmos. Phys.* **68**, 205–225.
- Power, S. B., R. Kleeman, and R. A. Colman. 1995. Modeling the surface heat flux response to long-lived SST anomalies in the North Atlantic. *J. Climate* **8(9)**, 2161–2180.
- Ranelli, P. H., R. L. Elsberry, C.-S. Liou, and S. A. Sandgathe. 1985. Effects of varying sea-surface temperature on 10-day atmospheric model forecasts. Pp. 675–695. In *Coupled Ocean-atmosphere models*. J. Nihoul (ed.). Elsevier Oceanography series, 40.
- Ratcliffe, R. A. S., and R. Murray. 1970. New lag associations between North American sea temperatures and European pressure, applied to long-range weather forecasting. *Quart. J. Roy. Meteor. Soc.* **96**, 226–246.
- Reed, R. J., A. J. Simmons, M. D. Albright, and P. Uden. 1988. The role of latent heat release in explosive cyclogenesis: Three examples based on ECMWF operational forecasts. *Wea. Forecasting* **3**, 217–229.
- Reed, R. J., G. A. Grell, and Y. H. Kuo. 1993. The ERICA IOP 5 storm. Part II: Sensitivity tests and further diagnosis based on model output. *Mon. Wea. Rev.* **121**, 1595–1612.
- Renwick, J. A., and J. M. Wallace. 1995. Predictable anomaly patterns and the forecast skill of Northern Hemisphere wintertime 500-mb height fields. *Mon. Wea. Rev.* **123**, 2114–2131.
- Renwick, J. A., and J. M. Wallace. 1996. Relationships between North Pacific wintertime blocking, El Niño, and the PNA pattern. *Mon. Wea. Rev.* **124**, 2071–2076.
- Reynolds, R., and T. M. Smith. 1995. A high-resolution global sea surface temperature climatology. *J. Climate* **6**, 1571–1583.
- Robertson, A. W., and W. Metz. 1990. An investigation of the storm-track eddies in a low-resolution climate model using linear theory. *Cont. to Atmos. Phys.* **63**, 177–188.

- Robinson, W. A. 1991. The dynamics of low-frequency variability in a simple model of the global atmosphere. *J. Atmos. Sci.* **48**, 429–441.
- Rogers, J. 1984. The association between the North Atlantic Oscillation and the Southern Oscillation in the Northern Hemisphere. *Mon. Wea. Rev.* **112**, 1999–2015.
- Rogers, J. 1990. Patterns of low-frequency monthly sea level pressure variability (1899–1986) and associated wave cyclone frequencies. *J. Climate* **3**, 1364–1379.
- Rogers, J. C. 1997. North Atlantic storm track variability and its association to the North Atlantic Oscillation and climate variability of northern Europe. *J. Climate* **10**, 1635–1647.
- Rogers, J. C., and H. van Loon. 1979. The seasaw in winter temperatures between Greenland and northern Europe. Part II: Some oceanic and atmospheric effects in middle and high latitudes. *Mon. Wea. Rev.* **107**, 509–519.
- Rowell, D. P. 1998. Assessing potential seasonal predictability with an ensemble of multi-decadal GCM simulations. *J. Climate* **11**, 109–120.
- Saravanan, R. 1998. Atmospheric low-frequency variability and its relationship to midlatitude SST variability: Studies using the NCAR climate system model. *J. Climate* **11**, 1386–1404.
- Saravanan, R., and J. C. McWilliams. 1998. Advective ocean-atmosphere interaction: An analytical stochastic model with implications for decadal variability. *J. Climate* **11**, 165–188.
- Schär, C., C. Frei, D. Lüthi, and H. C. Davies. 1996. Surrogate climate-change scenarios for regional climate models. *Geophysical Research Letters* **23**, 669–672.
- Sciremammano, J. 1979. A suggestion for the presentation of correlations and their significance levels. *J. Phys. Oceanogr.* **9**, 1273–1276.
- Serreze, M. C., F. Carse, R. G. Barry, and J. C. Rogers. 1997. Icelandic low cyclone activity: Climatological features, linkages with the NAO, and relationships with recent changes in the northern hemisphere circulation. *J. Climate* **10**, 453–464.
- Sheng, J., and J. Derome. 1993. The dynamic forcing of the slow transients by the synoptic-scale eddies: An observational study. *J. Atmos. Sci.* **50**, 757–771.
- Sheng, J., J. Derome, and M. Klasa. 1998. The role of transient disturbances in the dynamics of the Pacific-North American pattern. *J. Climate* **11**, 523–536.
- Shutts, G. 1987. Some comments on the concept of thermal forcing. *Quart. J. Roy. Meteor. Soc.* **113**, 1387–1394.
- Simmons, A. J., and B. J. Hoskins. 1979. The downstream and upstream development of unstable baroclinic waves. *J. Atmos. Sci.* **36**, 1239–1254.

- Simmons, A. J., and D. M. Burridge. 1981. An energy and angular momentum conserving vertical finite difference scheme and hybrid vertical coordinates. *Mon. Wea. Rev.* **109**, 758–766.
- Stephenson, D. B., and I. M. Held. 1993. GCM response of northern winter stationary waves and storm tracks to increasing amounts of carbon dioxide. *J. Climate* **6**, 1859–1870.
- Sutcliffe, R. C. 1951. Mean upper contour patterns of the Northern Hemisphere – the thermal-synoptic view pattern. *Quart. J. Roy. Meteor. Soc.* **77**, 435–440.
- Taylor, A. H. 1996. North-south shifts of the Gulf Stream: Ocean-atmosphere interactions in the North Atlantic.. *Int. J. Climatol.* **16**, 559–583.
- Thompson, D. W., and J. M. Wallace. 1998. The Arctic oscillation signature in the wintertime geopotential height and temperature fields. *Geophysical Research Letters* **25**, 1297–1300.
- Ting, M. 1991. The stationary wave response to a midlatitude SST anomaly in an idealized GCM. *J. Atmos. Sci.* **48**, 1249–1275.
- Ting, M., and N.-C. Lau. 1993. A diagnostic and modelling study of the monthly mean wintertime anomalies appearing in a 100-year GCM experiment. *J. Atmos. Sci.* **50**, 2845–2867.
- Ting, M., and S. Peng. 1995. Dynamics of the early and middle winter atmospheric response to the northwest Atlantic SST anomalies. *J. Climate* **8**, 2239–2254.
- Trenberth, K. E., and D. A. Paolino. 1981. Characteristic patterns of variability of sea-level pressure in the Northern Hemisphere. *Mon. Wea. Rev.* **109**, 1169–1189.
- van Loon, H., and J. C. Rogers. 1978. The seasaw in winter temperatures between Greenland and northern Europe. Part I: General description. *Mon. Wea. Rev.* **106**, 296–310.
- Venegas, S. A., L. A. Mysak, and D. N. Straub. 1997. Atmosphere ocean coupled variability in the South Atlantic. *J. Climate* **10**, 2904–2920.
- von Storch, H., and A. Navarra. 1995. *Analysis of Climate Variability*, Springer Verlag, 334pp.
- Walker, G. T., and E. W. Bliss. 1932. World weather V. *Memoirs of the Royal Met. Soc.* **4**, 53–84.
- Wallace, J. M., and D. S. Gutzler. 1981. Teleconnections in the geopotential height field during the Northern Hemisphere winter. *Mon. Wea. Rev.* **109**, 784–812.
- Wallace, J. M., and Q. Jiang. 1987. On the observed structure of the interannual variability of the atmosphere/ocean climate system. Pp. 17–43. In *Atmospheric and Oceanic Variability*. H. Cattle (ed.). R. Met. Soc.

- Wallace, J. M., C. Smith, and C. S. Bretherton. 1992. Singular value decomposition of sea-surface temperature and 500 mb height anomalies. *J. Climate* **5**, 561–576.
- Wallace, J. M., C. Smith, and Q. Jiang. 1990. Spatial patterns of atmosphere-ocean interaction in the northern winter. *J. Climate* **3**, 990–998.
- Wallace, J. M., G.-H. Lim, and M. L. Blackmon. 1988. Relationship between cyclone tracks, anticyclone tracks and baroclinic waveguides. *J. Atmos. Sci.* **45**, 439–462.
- Wanner, H., R. Rickli, E. Salvisberg, C. Schmutz, and M. Schüepp. 1997. Global climate change and variability and its influence on Alpine climate - concepts and observations. *Theor. Appl. Climatol.* **58**, 221–243.
- Ward, M. N., and A. Navarra. 1997. Pattern analysis of SST-forced variability in ensemble GCM simulations: Examples over Europe and the Tropical Pacific. *J. Climate* **10**, 2210–2220.
- WASA Group 1998. Changing waves and storms in the Northeast Atlantic ?. *Bull. Amer. Meteor. Soc.* **79**, 741–760.
- Webster, P. J. 1981. Mechanisms determining the atmospheric response to sea surface temperature anomalies. *J. Atmos. Sci.* **38**, 554–571.
- Webster, P. J. 1982. Seasonality in the local and remote atmospheric response to sea surface temperature anomalies. *J. Atmos. Sci.* **39**, 41–52.
- Wernli, H., and D. N. Bresch. 1997. An objective climatology of Northern Hemisphere cyclones and anticyclones. *Annales Geophysicae, suppl. II to Vol. 15. EGS General Assembly*. Vienna.
- Wernli, H., and H. C. Davies. 1997. A lagrangian-based analysis of extratropical cyclones. I: The method and some applications. *Quart. J. Roy. Meteor. Soc.* **123**, 467–489.
- Whitaker, J. S., and R. M. Dole. 1995. Organization of storm tracks in zonally varying flows. *J. Atmos. Sci.* **52**, 1178–1191.
- Widmann, M. 1996. *Mesoscale variability and long-term trends of Alpine precipitation and their relation to the synoptic-scale flow*. PhD thesis. Swiss Federal Institute of Technology (ETH). Dissertation No. 11769.
- Widmann, M., and C. Schär. 1997. A principal component and long-term trend analysis of daily precipitation in Switzerland. *Int. J. Climatol.* **17**, 1333–1356.
- Widmann, M., D. N. Bresch, C. Frei, and C. Schär. 1995. Daily Alpine precipitation and its relation to the synoptic scale flow - a principal component and singular value decomposition approach. *Proc. 6th Int. Meeting on Stat. Climatol.*. Galway. Pp. 381–384.
- Xie, S.-P., and Y. Tanimoto. 1998. A pan-Atlantic decadal climate oscillation. *Geophysical Research Letters* **25**, 2185–2188.

-
- Zorita, E., V. V. Kharin, and H. von Storch. 1992. The atmospheric circulation and sea surface temperature in the North Atlantic area in winter: Their interaction and relevance for Iberian precipitation. *J. Climate* **5**, 1097–1108.

Leer - Vide - Empty

Acknowledgments

Working in science is like wandering through a mountained landscape, every hill providing a view over uncharted land and unseen valleys – but at the same time bringing into sight new hilltops, impeding further view and posing new challenges¹. Such a journey would not have been possible without the help of many persons to whom I am indebted. I would like to express my gratitude to

Huw Davies who supported me through many valuable discussions full of wit and invested a lot of time to share his knowledge with me. His art of talking and writing will be a (I fear everlasting) challenge for me. His critical comments were always inspiring and substantially contributed to this thesis. He also gave me the opportunity to present my work at international conferences.

My external co-examiner Klaus Fraedrich who reviewed carefully the present thesis.

Christoph Schär, who guided my diploma thesis and reviewed the present work. He introduced me into the world of climate research and stimulated my interest in storm track dynamics.

I am very grateful to all my colleagues, who made the Institute for Atmospheric Science a friendly place of intensive communication:

Heini Wernli for his friendship and for patiently answering a vast number of questions. His support far outreached the issues concerning data processing and trajectory analysis.

René Fehlmann for his collaboration, which led to the idealised model study and many stimulating discussions (including sailing matters).

Martin Widmann for the numerous discussions on statistical methods and dozens of other issues.

Dani Lüthi for his support with the EM model and handling the ECMWF data transfer. In this context, my thanks should include the German Weather Service (DWD), the Swiss Meteorological Institute (SMI) and Uwe Christoph for providing the routine for Murakami-filtering.

Marc Liniger for his enthusiasm during his diploma thesis and the collaboration on ARGOS

¹“Eine Entwicklung der Wissenschaft ist wie eine Wanderung durch eine gebirgige Landschaft, bei welcher von jeder Kuppe neue unerforschte Täler unserem Blick sich öffnen und neue Bergspitzen erkennbar werden, welche die weitere Aussicht hemmen und neue Aufgaben stellen” (Köppen, 1881).

(interActive thRee-dimensional Graphics ObServatory²). What an “Ironie des Schicksals”³ that there are no three dimensional visualisations in the present thesis.

Coni Schwierz for many discussions – most of them not lacking a sense of humour – and for even improving further the friendly atmosphere in our quite crowded office.

I also thank Urs Aebischer, Dominik Brunner, Chrigel Frei, Pamela Heck, Dominique Jeker, Alexia Massacand, Joachim Orb, Christian Quadri, Andrea Rossa, Jürg Schmidli, Michael Sprenger and all the other (former) members of our institute for many interesting discussions and the good time we spent together. Special thanks to Ruedi Lüthi and Peter Isler for maintaining the excellent computer facilities and the technical support at our institute and to Eva Choffat for assistance concerning travel organisation and all administrative matters.

Finally I would like to thank all my friends, my parents, my brother and – last but not least – Sarah who encouraged me to go my way and always gave me the support I needed.

David N. Bresch, September 1998

²<http://grieg.ethz.ch/argos/argos.html>

³Lit. “irony of the destiny”

Curriculum Vitae

David Niklaus Bresch, born on April 9 1970 in Zürich (ZH), Switzerland

EDUCATION AND PROFESSIONAL TRAINING

1983 – 89 Kantonsschule Wiedikon, Zürich

Matura Type B

1989 – 95 University study in Physics at the Swiss Federal Institute of Technology (ETH) Zürich. Specialisation in the fields *Atmospheric Science* and *Scientific Computing*. Diploma thesis “Mean northern hemispheric circulation and its variability” under the guidance of Prof. C. Schär

Dipl. Phys. ETH

1995 – 98 Ph.D. student at the Institute for Atmospheric Science, ETH Zürich, in the group for Theoretical Meteorology of Prof. H. C. Davies

INTERNATIONAL CONFERENCES AND WORKSHOPS

EGS General Assembly, Den Haag 1996; 12th Int. Conf. on Clouds and Precipitation, Zürich 1996; 7th Conf. on Mesoscale Processes, Reading 1996; 10th Meeting DWD/SMA, Bad Säckingen 1997; 9th Conf. on Interaction of the Sea and Atmosphere, Phoenix, AZ 1998; EGS General Assembly, Nice 1998; FASTEX Workshop, Toulouse 1998.

SPECIAL TRAINING COURSES AND FIELD EXPERIMENTS

ECMWF annual seminar, Reading 1997; Meteorology teacher at Crossair pilot training, Basel 1996; FASTEX, one month aboard French research vessel 'Le Suroit', North Atlantic, February 1997.

CURRENT ADDRESS

David N. Bresch
Irchelstr. 8
CH – 8057 Zürich

e-mail: bresch@atmos.umnw.ethz.ch